



Development of nanocomposite membranes for dairy wastewater treatment

PH.D. thesis

by

Elias Jigar Sisay

Supervisor

Professor László Zsuzsanna

Doctoral School of Environmental Sciences

Department of Biosystems Engineering

Faculty of Science and Informatics

University of Szeged

Szeged, 2023

Abstract

A novel photocatalytic nanocomposite membrane was prepared successfully by blending poly(vinylidene-fluoride) (PVDF) with TiO_2 , and/or carbon nanotube (CNT), and/or BiVO_4 at various ratios in the membrane material via phase inversion method. The prepared membranes were evaluated for model or real dairy wastewater treatment. The membranes were characterized by several surface characterization methods as SEM, AFM, XRD, and EDX. XRD and SEM measurements revealed that the nanoparticles were present as 200–300 nm-sized aggregates in the membrane, which increased the roughness of composite blended membranes (AFM results). EDX measurements exhibited that the proteins have covered a relatively large area of the pristine PVDF membrane, resulting in a relatively high N/F ratio. Addition of TiO_2 , and/or carbon nanotube (CNT), and/or BiVO_4 nanoparticles into the PVDF membrane material decreased the contact angle of membrane surface, thus increased the hydrophilicity of modified blended membranes. In dead end cell BSA filtration experiment, PVDF/ TiO_2 /CNT/ BiVO_4 nanocomposite blended membrane exhibited a pure water flux up to $150.52 \text{ L m}^{-2} \text{ h}^{-1}$ which is two-fold higher than virgin membrane and a higher bovine serum albumin (BSA) rejection of about 97 %. Based on flux recovery ratio and flux the optimal CNT ratio in the PVDF/ TiO_2 /CNT and BiVO_4 in PVDF/ TiO_2 / BiVO_4 nanocomposite membrane was 2 % and 50 % respectively. More importantly, the PVDF/ TiO_2 /CNT- BiVO_4 -50 (PTCB50) (containing 0.48 wt % TiO_2 , 0.02 wt % CNT and 0.5 wt % BiVO_4) and PVDF/ TiO_2 / BiVO_4 -50 (PTB50) (containing 0.5 wt % TiO_2 and 0.5 wt % BiVO_4 in PVDF) membrane exhibited a smaller irreversible fouling and a higher flux recovery ratio, revealing that blending with TiO_2 , and/or CNT, and/or BiVO_4 could improve the self-cleaning under visible irradiation and the antifouling properties of PVDF membrane. The application of B-PTB50 and B-PTCB50 membranes to treat real dairy wastewater were promising. They exhibited better antifouling and foulant degradation performance as compared to pristine membrane. However, the lower rejection performances of the membranes were due to ability of lactose to pass through the membranes which requires further treatment. Overall, the incorporation of nanoparticles in the polymer matrix enhanced the antifouling and foulant degradation performance of the photocatalytic nanocomposite membrane to a remarkable extent.

Keywords: PVDF, photocatalytic membranes, fouling control, antifouling, visible light, bismuth vanadate, carbon nanotube

Table of Contents

Abstract	1
Table of Contents	2
List of Figures	5
List of Tables	7
Nomenclature/ Abbreviations	8
1. Introduction	10
2. Theoretical background	12
2.1. Membrane filtration in dairy industry	12
2.2. Characterization of dairy industry wastewater	14
2.3. Membrane filtration in dairy industrial wastewater treatment	15
2.4. Factors affecting membrane fouling	17
2.4.1. Membrane properties: hydrophilicity, roughness, functional groups, and surface charge... 17	
2.4.1.1. Hydrophilicity of membrane	18
2.4.1.2. Membrane surface roughness	18
2.4.1.3. Functional groups	18
2.4.1.4. Surface charge	18
2.4.2. Composition of the wastewater: foulant type, concentration, pH, ionic strength	19
2.4.2.1. Ionic strength	19
2.4.2.2. Solution pH	20
2.4.2.3. Solution concentration	20
2.4.2.4. Salinity	20
2.4.3. Hydrodynamic operating condition: trans-membrane pressure (TMP), flow velocity, temperature	21
2.4.3.1. Trans-membrane pressure (TMP)	21
2.4.3.2. Flow velocities	21
2.4.3.3. Temperature	21
2.5. Fouling control and mitigating strategies	22
2.5.1. Pretreatment of feed solution	22
2.5.2. Physical membrane cleaning	23
2.5.3. Chemical membrane cleaning	24
2.5.4. Physicochemical membrane cleaning	25
2.5.5. Membrane modification	25
2.5.5.1. Membrane modification by semiconductor heterogeneous photo-catalysts	26

2.5.5.1.1. Heterogeneous photo-catalysts and mechanism of heterogeneous photocatalysis	26
2.5.5.2. General and structural properties of BiVO_4	28
2.5.5.3. Photocatalytic activity of BiVO_4	28
2.5.5.4. Methods of synthesis for BiVO_4	29
2.5.5.5. Role of BiVO_4 in improving the performance of TiO_2 -based photocatalysts	29
2.5.5.6. General and structural properties of Carbon nanotubes (CNTs)	29
5.5.5.7. Role of CNTs and mechanisms of photocatalysis in TiO_2/CNT composite.....	30
2.6. Catalytic membrane reactors	32
3. Aims	35
4. Materials and methods	36
4.1 Materials.....	36
4.1.1. Chemicals and materials used	36
4.1.2. BSA model solution	36
4.1.3. Synthetic dairy wastewater.....	36
4.1.3.1. Characterization of synthetic dairy wastewater	37
4.1.4. Dairy wastewater	39
4.2. Synthesis and characterizing methods for bismuth vanadate	40
4.3. Membrane filtration experiments	41
4.4. Photocatalyst-coated membrane preparation by physical deposition.....	41
4.5. Photocatalyst blended membrane preparation by phase inversion method.....	43
4.6. Membrane characterization methods	45
4.6.1. Porosity of the prepared membranes	45
4.6.2. Membrane hydrophilicity	45
4.6.3. Membrane surface characterization.....	46
4.6.4. Filtration performance of the membranes	47
4.6.5. Data analysis	48
5. Results and discussion.....	49
5.1. Photocatalytic activities of bismuth vanadate and nanoparticle mixtures.....	49
5.2. Performance of physically coated membranes	51
5.2.1. Investigation of stability of nanoparticle-coated membranes	51
5.2.2. Characterization of nanoparticle-coated membranes	52
5.2.2.1. Water contact angle measurements	52
5.2.2.2. Zeta potential of nanoparticle-coated PVDF membranes	53
5.2.3. Filtration performance of pristine and physically coated PVDF membranes	53

5.2.3.1. Effects of nanoparticle coating on flux and filtration resistances during filtration of model wastewaters	54
5.2.3.2. Effects of nanoparticle coating on rejection of BSA.....	56
5.2.3.3. Regeneration of physically modified fouled membranes	57
5.3. Photo-catalytic blended ultrafiltration membranes	59
5.3.1. Effects of TiO ₂ concentration on the performance of PVDF-TiO ₂ photocatalytic blended ultrafiltration membranes	59
5.3.1.1. Contact angle, water flux and rejection performance	59
5.3.1.2. Filtration resistances for blended PVDF-TiO ₂ photocatalytic UF membranes	60
5.3.1.3. Regeneration of BSA fouled blended PVDF-TiO ₂ photocatalytic UF membranes	61
5.3.2. Characterization of blended PVDF-TiO ₂ -CNT-BiVO ₄ photocatalytic membranes.....	63
5.3.2.1. Crystalline and morphological structure of blended membranes (XRD, SEM and AFM).....	63
5.3.2.2. Porosity and pore size estimation	65
5.3.2.3. Wettability	67
5.3.2.4. Zeta potential of fabricated PVDF and blended photocatalytic PVDF membranes	67
5.3.2.5. Rejection and extent of fouling	68
5.3.3. Fouling mitigation and photocatalytic regeneration of nanocomposite membranes.....	69
5.4. Application of best performing fabricated photocatalytic blended UF PVDF membranes for synthetic and real dairy wastewater treatment	73
5.4.1. Synthetic dairy wastewater treatment	73
5.4.1.1. Effects of salinity on fouling and retention	73
5.4.1.2. Effects of lactose on fouling and retention.....	74
5.4.1.3. Effects of pH on fouling and rejection	74
5.4.2. Real dairy wastewater treatment	75
5.4.2.1. Filtration resistances	75
5.4.2.2. Rejection.....	76
5.4.2.3. Membrane regeneration.....	77
6. Conclusions	78
7. Summary	80
8. Összefoglalás.....	82
9. New scientific results	84
10. Publications	86
ACKNOWLEDGEMENTS	89
References	90
Appendices	109

List of Figures

Figure 1. Fouling mechanisms of skim milk

Figure 2. Main factors influencing membrane fouling

Figure 3. Solute-solute and membrane-solute interactions

Figure 4. Mechanism of heterogeneous photocatalysis

Figure 5. Structures of SWCNTs, DWCNTs, and MWCNTs

Figure 6 Role of CNTs and mechanisms of photocatalysis in TiO₂/CNT composite

Figure 7. Visible light driven photocatalytic test

Figure 8. Graphical illustration of the dead-end filtration setup

Figure 9. Graphical representation of membrane preparation by physical deposition

Figure 10. Graphical illustration of membrane fabrication by phase inversion method

Figure 11. Photocatalytic activity of nanoparticles, described by the absorbance reduction of methylene blue or BSA during 30 min dark adsorption, followed by 120 min VIS irradiation.

Figure 12. pH dependence of Zeta potential for pristine and TiO₂ coating PVDF membrane

Figure 13. Filtration resistances of TiO₂-CNT coated PVDF membranes (a) and TiO₂-BiVO₄ coated PVDF membranes (b)

Figure 14. BSA and COD rejection performance of TiO₂-CNT coated PVDF membranes (a) and TiO₂-BiVO₄ coated PVDF membranes (b)

Figure 15. Regeneration of BSA fouled TiO₂-CNT coated PVDF membranes (a) and TiO₂-BiVO₄ coated PVDF membranes (b)

Figure. 16. Filtration resistances of TiO₂/PVDF photocatalytic blended UF membranes of different TiO₂ concentrations

Figure. 17. Regeneration of BSA fouled PVDF and TiO₂/PVDF photocatalytic blended UF membranes of various TiO₂ concentrations

Figure 18. Zeta potential of unused PVDF, B-PT, B-PB, B-PTB and B-PTCB blended membranes as a function of pH at 10⁻³ M KCl

Figure 19. Pore size distributions of neat PVDF, B-PT100 and B-PB100 membranes by the BJH approach

Figure 20. Surface roughness of unused blended membranes

Figure 21. N/F ratio of fouled blended membranes

Figure 22. Filtration resistances of (a) PVDF, PVDF-TiO₂, and PVDF-TiO₂/CNT-membranes, (b) PVDF, PVDF-TiO₂ and PVDF-TiO₂/BiVO₄ membranes, and(c) different PVDF-TiO₂/CNT/BiVO₄

Figure 20. FRRs of BSA-fouled (a) PVDF, PVDF-TiO₂ and PVDF-TiO₂/CNT membranes, (b)

PVDF, PVDF-TiO₂ and PVDF-TiO₂/BiVO₄ membranes, and (c) different PVDF-TiO₂/CNT/BiVO₄ membranes with 2% CNT content.

Figure 23. FRRs of BSA-fouled (a) PVDF, PVDF-TiO₂ and PVDF-TiO₂/CNT membranes, (b) PVDF, PVDF-TiO₂ and PVDF-TiO₂/BiVO₄ membranes, and(c) different PVDF-TiO₂/CNT/BiVO₄ membranes with 2% CNT content.

Figure 24. Effect of salinity during synthetic dairy waste water membrane filtration on membrane fouling (a) or COD and turbidity rejection (b)

Figure 25. Effect of lactose during synthetic dairy wastewater (SW-BSA-L) membrane filtration on membrane fouling (a) or COD and turbidity rejection (b)

Figure 26. Effect of pH during synthetic dairy wastewater (SW-BSA) membrane filtration on membrane fouling (a) or COD and turbidity rejection (b)

Figure 27. Filtration resistances of PVDF, B-PTB50 and B-PTCB50 membranes for real dairy waste water, unfiltered (a) or pre-filtered (0.2μm filter paper) (b)

Figure 28. Rejection performance of pristine PVDF, B-PTB50 and B-PTCB50 membranes during real dairy waste water filtration, unfiltered(a) or pre-filtered (0.2μm filter paper) (b)

Figure 29. Regeneration performance of fouled PVDF, B-PTB50 and B-PTCB50 membranes of real dairy waste water, unfiltered (a) or pre-filtered (0.2μm filter paper) (b)

List of Tables

Table 1. Characteristics of the milk proteins related to membrane fouling propensities

Table 2. Characteristics of dairy industry wastewaters

Table 3. Composition of synthetic dairy wastewater (SW-BSA)

Table 4. Characteristics of synthetic dairy wastewater (SW-BSA) with various level of salinity

Table 5. Characteristics of SW-BSA and SW-BSA-L

Table 6. Physico-chemical characteristics of real influent industrial dairy wastewater

Table 7. Loading and ratio of TiO_2 and CNT

Table 8. Loading composition and abbreviation of hybrid membranes

Table 9. Filtration resistance formulas

Table 10. Turbidity of distilled water containing TiO_2 Coated membrane and various concentration of TiO_2

Table 11. Contact angle of C- TiO_2 /CNT and C- TiO_2 / BiVO_4 coated membranes

Table 12. Characteristics of B- TiO_2 /PVDF photo-catalytic blended ultrafiltration membranes

Table 13. Characteristics of fabricated PVDF and photocatalytic blended UF membranes

Table 14. Specific surface area of neat PVDF, B-PT100 and B-PB100 membranes by BET method

Table 15. AFM and SEM micrographs of the surface of the membranes

Nomenclature/ Abbreviations

A: Effective surface area of the membrane (m^2)
AFM: Atomic force microscope
BET: Brunauer–Emmett–Teller model
BOD: Biological oxygen demand (mgL^{-1})
BJH: Barrett–Joyner–Halenda method
BSA: Bovine serum albumin
 c_1 : Concentration of feed before filtration (gL^{-1})
 c_2 : Concentration of feed after filtration (gL^{-1})
 c : Concentration of MB (mgL^{-1})
 c_0 : Concentration of MB (mgL^{-1})
CNTs: Carbon nanotubes
COD: Chemical oxygen demand (mg L^{-1})
EDX: Energy dispersive X-ray
EC: Electrical conductivity (mS)
FRR: flux recovery ratio (%)
 J_w : Water flux of clean membrane ($\text{Lm}^{-2} \text{h}^{-1}$)
 J_c : Water flux of used membrane after rinsing ($\text{Lm}^{-2}\text{h}^{-1}$)
 J : Flux ($\text{Lm}^{-2} \text{h}^{-1}$)
 L : Membrane thickness (μm)
MB: Methylene blue
NMP: N-Methyl-2-pyrrolidone
PVDF: Poly (vinylidene fluoride)
 Δp : Transmembrane pressure (Pa)
 Q : Volume flow (m^3s^{-1})
PB: PVDF-BiVO₄ composite membranes
PT: PVDF-TiO₂ composite membranes
PTB: PVDF-TiO₂-BiVO₄ composite membranes
PTC: PVDF-TiO₂-CNT composite membranes
PTCB: PVDF-TiO₂-CNT-BiVO₄ composite membranes
RM: Membrane resistance (m^{-1})
 R_{rev} : Reversible resistance (m^{-1})
 R_{irr} : Irreversible resistance (m^{-1})
 R_T : Total resistance (m^{-1})
 S_{BET} : Specific surface area (m^2)
SDS: Sodium dodecylsulfate

SEM: Scanning electron microscope

t: Time (h)

TDS: Total dissolved solid (gL^{-1})

VRR: Volume reduction ratio (m^3)

V_F : Volume of the feed (m^3)

V_P : Volume permeate (m^3)

V: Pore volume (m^3)

VT: Volume of the membrane in the wet state (m^3)

W_i : Initial weight of membrane to be coated (kg)

W_f : Final weight of coated membrane (kg)

W: Weight of permeate (kg)

W_1 : weight of wet membrane (kg)

W_2 : weight of dry membrane (kg)

XRD: X-ray diffraction

ϵ : Porosity (%)

η_w : Dynamic viscosity of water (Pa s)

η_{ww} : Dynamic viscosity of wastewater (Pa s)

ρ_w : density of water (kg m^{-3})

ρ_{md} : Density of PVDF membrane in the dry state (kg m^{-3})

ζ : Apparent zeta potential (mV)

ϵ_{rel} : Dielectric coefficient of water (-)

ϵ_0 : Permittivity of vacuum (Fm^{-1})

1. Introduction

Water pollution by industries is becoming a critical problem worldwide as it leads to water scarcity and other water related problems. Food production requires large amount of water and large volumes of waste water is generated (Mancosu et al., 2015), and dairy industry is among the food production industries that generates the largest volume of waste water (6–10 L of wastewater per liter of processed milk) and huge pollution load of wastewater (Deshannavar et al., 2012; Shete, 2013; Bustillo-Lecompte and Mehrvar, 2015). Dairy wastewaters generally contain organic matter (proteins, carbohydrates, and lipids), nutrients (nitrogen and phosphorous), salts and cleaning agents (Shete et al., 2013). In many countries, dairy industry wastewaters are treated by physico-chemical and biological methods (Ahmad et al., 2019; Wang and Serveti, 2019). However, these methods have high cost of reagents and high energy demand or operational difficulties (Xie et al., 2016).

In recent years, the application of membrane filtration in dairy waste water treatment is growing (Galvão, 2018 and Velpula et al, 2017), especially integrating membrane filtration with other systems, is becoming a one of the promising technologies applied to meet the environmental waste water discharge limit (Bixio et al., 2006; Lakra, et al., 2021, Das et al., 2016; Abdelkader et al., 2019; Sarkar et al., 2006; Bortoluzzi et al., 2017; Mehta et al., 2015; Gong et al., 2012; Farahani and Vatanpour., 2018; Pal., 2020; Chen et al., 2019; Li et al., 2021; Catenacci et al., 2020). Among them, ultrafilter membranes have received more attention due to their capability to efficiently reject macromolecules, colloids, bacteria, and particles (Ayyaru and Ahn, 2017; Al Aani et al., 2020). However, these processes are susceptible for fouling, limit the broader application of the technology (Chang et al., 2019) in water treatment. Recent publications (Anis et al., 2022; He et al., 2022) have focused on fouling reduction by offering innovative cleaning processes, optimizing the existing techniques, or integrating devices to the membrane set-up.

Poly (vinylidene fluoride) (PVDF) is a widely applied polymeric membrane material commonly used in ultrafiltration (Schulze et al., 2016). This is due to its superior physical, chemical, and mechanical properties (Ji et al., 2015). However, PVDF membranes are easily fouled by wastewaters containing proteins, oils, and natural organic matter due to their hydrophobic nature. Chemical backwashing is commonly applied conventional method for flux recovery, this method requires high cost for chemicals and producing large amounts of sludge leading to disposal problems (Anis et al., 2022).

This problem may be overcome by using the recently developed photocatalytic membranes characterized by superior antifouling properties, high flux, and excellent shelf life (Farahani and Vatanpour, 2018; Riaz and Park, 2020). Many heterogeneous photocatalysts have been applied in the photodegradation of pollutants under UV light, among them, **titanium dioxide** is used predominantly in wastewater treatment applications, as it is cheap, chemically stable, highly

photoactive, hydrophilic, and a nontoxic material (Leong et al., 2014). However, TiO₂ has two main limitations that hinder its wider practical application. Firstly, the high recombination ratio of photocatalytically-generated electron-hole pairs reduce photocatalytic activity. Secondly, TiO₂ has a wide bandgap of ~3.15eV, its photocatalytic activity can only be efficiently activated under UV light ($\lambda < 390$ nm), excluding visible light (Akhavan, 2009; Zouzelka et al., 2016).

Nanocomposite TiO₂ help in faster photocatalytic reaction and photo degradation (Gao et al., 2014), enhancing membrane antifouling property (Trapalis et al., 2016; Selvaraj et al., 2020; Moslehyani et al., 2015; Ayyaru et al., 2019). and enabling photocatalytic performance under visible light irradiation (Malathi et al., 2018; Ratova et al., 2018). These include combination of TiO₂ and materials with a narrower band gap (Malathi et al., 2018; Ratova et al., 2018), such as sulphur, transitional metal ions, noble metals or nitrogen (Malato, et al., 2009); or photosensitizer (Yogarathinam, et al., 2018). In recent years, **bismuth-based oxides** have gained attention in photo-catalytic technology because of its superior band gap and efficient visible light absorption performance, however, their relatively low surface area and activity hinders their broader application (Malathi et al., 2018; Ratova et al., 2018; Orimolade and Arotiba, 2020; Kunduz and Soylu, 2015; Lin et al., 2012; Hou et al., 2011; Wang et al., 2017; Abazari et al., 2019; Li et al., 2012).

Carbon nanotubes (CNTs) are semiconductor materials that also have received considerable attention due to their outstanding properties, such as unique mechanical (stiffness and flexibility), large specific surface area, high thermal and electrical conductivities. They are broadly used as electron acceptors and reduce the recombination rate (Trapalis et al., 2016; Selvaraj et al., 2020). It can also enhance membrane antifouling property, water flux and BSA rejection (Moslehyani et al., 2015; Ayyaru et al., 2019).

To overcome their drawback and taking advantage of their benefits, the aim of this work was to develop a novel photocatalytic composite PVDF membrane containing TiO₂/CNT/BiVO₄ nanoparticles and examine their applicability for the treatment of a model and real dairy wastewater. My aim was to characterize membrane surface properties, using several up-to date surface characterization method as AFM (determining surface roughness), SEM, zeta potential measurements and surface contact angle measurements. These results were used to explain the improved antifouling properties of the developed membranes. Moreover, the visible light driven photocatalytic cleanability of nanocomposite membranes also was investigated.

2. Theoretical background

2.1. Membrane filtration in dairy industry

Polymeric membranes are widely used as compared to other membrane materials, e.g. ceramic membranes (Zoubeik et al., 2017). This is due to their low cost, possibility to integrate with other methods and low environmental footprint (Ng et al., 2013). However, polymeric membranes are susceptible to fouling by proteins (Madaeni and Mansourpanah, 2004).

Ultrafilter membranes are gaining attention in membrane separation processes because of their effectiveness in rejecting macromolecules, colloids, bacteria, and particles (Ayyaru and Ahn, 2017; Al Aani et al., 2020). Poly(vinylidene fluoride) (PVDF) is a commonly used polymeric membrane material in ultrafiltration because of its good physical, chemical, and mechanical properties (Ji et al., 2015). However, the hydrophobic nature of PVDF membranes makes them prone to fouling by wastewaters containing proteins, oils, and natural organic compounds (e.g. humic materials), which can deteriorate filtration efficiency by decreasing the flux, shelf life, and increasing operating costs of the operation (Chang et al., 2019). There are commonly used conventional methods for flux recovery (e.g. chemical backwashing) (Anis et al., 2022), but they are generally expensive due to the cost of chemicals and the production of large amounts of sludge, which leads to disposal problems.

Recent research has focused on photocatalytic membranes, which are characterized by their superior antifouling properties, high flux, and excellent shelf life in the field of membrane separation (Farahani and Vatanpour, 2018; Riaz and Park, 2020).

Ultrafiltration has been used for protein or carbohydrate recovery in dairy industry for a long time (Atra et. al., 2005; Lakra et al., 2021). In addition to this, membrane filtration has been applied for separation of milk components (Kumar et.al. 2013). The main two protein components of milk are caseins and whey proteins and are mainly found in skim milk and whey respectively. Characteristics of the milk proteins are indicated in the Table 1.

Table 1. Characteristics of the milk proteins related to membrane fouling propensities (Schulze et.al, 2016)

Proteins/Membrane material	Concentration in milk (g/L)	Size (kDa)	Size (nm)	IEP	Charge in neutral pH
Caseins					
α_{s1} -casein (α_{s1} -CN)	12–15	23.6	form casein micelles (50-300 nm)	4.96	negative
α_{s2} -casein (α_{s2} -CN)	3–4	25.2		5.27	negative
β -casein (β -CN)	9–11	24.0		5.2	negative
κ -casein (κ -CN)	2–4	19.0		5.54	negative
Whey proteins					
β -lactoglobulin (β -LG)	2–4	18.3	3-8 nm	4.6	negative
α -lactalbumin (α -LA)	0.6–	14.2		5.35	negative
bovine serum albumine	1.7	66.4		4.7	negative
BSA	0.4	150–1000		6.1-8.5	negative/
Immunoglobulin G IgG	0.4				positive
Membrane material					
Poly (vinylidene fluoride)(PVDF)				3.5	negative

The former milk proteins are the major group of milk proteins with small size micelles attached together by calcium phosphate bridges to make large size micelles in milk (McMahon & Oommen, 2008). These proteins are grouped as β -casein, κ -casein, α_{s1} -casein, and α_{s2} -casein and are the highest, moderate, and lowest hydrophobic respectively (Farrell et al., 2004).

The later milk proteins are called as whey proteins. These proteins are found mainly in the whey which is the main by-product of dairy industry formed after cheese and caseins making. The three main components of whey proteins include: Bovine serum albumin (BSA), α -lactalbumin (α -LA), and β -lactoglobulin (β -LG) (Ng et al., 2017). In addition to proteins, milk whey contains carbohydrate, lipids, vitamins, and minerals. From the total whey solids, lactose account about 75% (Ahmad, et al., 2019).

2.2. Characterization of dairy industry wastewater

In dairy industry there are many unit operations (cooling, heating, cleaning and washing (Slavov, 2017; Hung et al., 2005)). Each sections discharge wastewater (Shete, 2013; Hung et al., 2005). The characteristics of the wastewater from each unit varies based on its products and the operational circumstances. The characteristics of dairy wastewater as reported by authors are given in Table 2.

Table 2. Characteristics of dairy industry wastewaters

Wastewater description	Parameters in mg/L except pH							References
	COD	BOD	pH	TSS	TS	NH ₃	PO ₄ ³⁻	
Dairy waste water	80–95000	40–48000	4.7 to 11	-	-	-	-	Ahmad, et al., 2019
Dairy effluent	190 - 2700	120 - 1800	7.2-8.8	500 – 740	900-1350	-	-	Deshannavar et.al., 2012
Dairy wastewater	890 ± 14	216.17 ± 4.17	6.035 ± 0.065	-	938 ± 6	69.96 ± 1.16	69.96 ± 1.16	Krishan & Srivastava, 2015
whey	71526	20000	4.1	22050	56782	-	-	Deshpande et al., 2012
Dairy wastewater	2500-3000	1300-1600	7.2- 7.5	72000-80000	800-10000	-	-	Qazi et.al., 2011

In wastewater treatment, the choice of the methods depends on the size of pollutants in the effluents. Generally, the typical strategy for wastewater treatment includes the following methods (Slavov, 2017):

- Mechanical treatment involves in eliminating suspended solids, in this method the organic content may not be treated efficiently.
- Physical methods: aimed to eliminate milk fat and colloidal proteins
- Chemical treatment: remove majority of colloids and soluble pollutants through reaction with FeSO₄ and H₂O₂ or other coagulants.
- Biological treatment: can be applied for highly biodegradable product under aerobic or anaerobic conditions. The aerobic processes are effective for wastewater containing low organic content (BOD < 0.3 kgm⁻³) and can easily remove ammonia, but P removal is not effective. The anaerobic processes are more suitable for concentrated wastewaters, and appropriate for biogas production, but unable to remove ammonia and P.

2.3. Membrane filtration in dairy industrial wastewater treatment

Several studies reported that there are possibilities to reuse the treated dairy industrial wastewater by membrane filtrations. This involve use of microfiltration (MF) (Steinhauer et al., 2015a), ultrafiltration (UF) (Silva et al., 2019), nanofiltration (NF) (Andrade, et. al., 2014), reverse osmosis (RO) (Vourch et. al., 2008) or two-stage filtration (UF+NF) (Gong et al., 2012). Membrane separation can be considered as a promising newly developed technology to treat dairy industry wastewater. It is simple and has wastewater zero emissions. It can also be effective at treating dairy industry wastewater with high salinity. Previous studies have also shown that membrane separation processes have got considerable attention for dairy wastewater treatment (Das et al., 2016; Abdelkader et al., 2019; Sarkar et al., 2006; Bortoluzzi et al., 2017). These processes are more energy-efficient, environmentally friendly, and economical, excellent contaminant rejection, and can be integrated with other processes (Gong et al., 2012; Farahani and Vatanpour., 2018; Pal., 2020; Chen et al., 2019; Li et al., 2021; Catenacci et al., 2020). Various physical, chemical, and biological processes have been developed and utilized for nutrient recovery. However, the common objective of all these processes is to separate nutrients from other wastewater pollutants. The prevailing technique for N and P recovery is currently struvite formation through crystallization and precipitation (Mehta et al., 2015). Despite its effectiveness, this process presents several challenges. Therefore, utilizing membrane separation to concentrate or isolate nutrients could prove advantageous.

Membrane filtration offers many benefits in dairy wastewater treatment. These include best contaminant removal, low cost, easily operated, and can be easily integrated with other systems. However, the membrane can easily be fouled and reduce its life span and productivity (Madaeni & Mansourpanah, 2004). There are many strategies to tackle such problem and will be discussed in much more detail in the next section.

Fouling in membrane filtration is undesired accumulations of solutes in all parts of the membrane (Geise et al., 2010). Membrane filtration application in dairy industry wastewater treatment is growing however the problem of fouling is becoming the main obstacles for its widespread application. It reduces the productivity of the membrane through reducing flux, reducing separation efficiency of membranes, increasing maintenance and operation costs, shortening the shelf life of the membrane and increase energy use of the system (Yang et al., 2006; Chang et al., 2019).

Fouling could be grouped based on three criterion, these are composition, reversibility and location (Wang et al., 2014). Based on the *composition* of pollutants, fouling could be grouped into

biofouling, organic fouling, and inorganic fouling. Using fouling *reversibility* as criteria, fouling could be classified as reversible and irreversible.

By considering fouling *location* criteria, fouling could be grouped into concentration polarization, internal fouling, and external fouling. In membrane filtration, avoiding irreversible fouling is much more important because it can only be cleaned by chemical cleaning. Backwashing is the most common method applied in UF and MF to remove this type of fouling, which is not possible in NF and RO membranes (Nguyen, 2012).

Understanding fouling *mechanisms* is an important step to develop mitigation strategies to the problems of fouling. The commonly existing fouling mechanisms in membrane filtration can be classified pore blocking, scaling, gel layer, cake layer, adsorption, biofilm and concentration polarization (Nguyen, 2012; Wang et al., 2014).

In membrane filtration of dairy wastewater, protein component of the wastewater is the most severe foulant for UF membranes (Madaeni & Mansourpanah, 2006; Ng et al., 2017). The fouling mechanism of milk proteins is presented in Fig. 1.

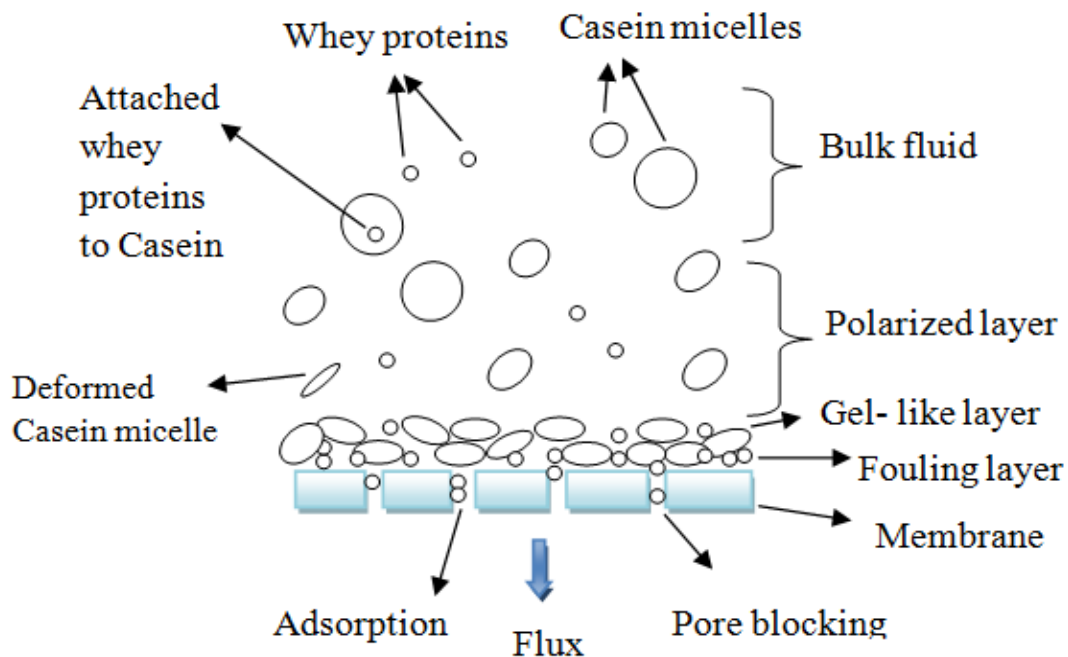


Figure 1. Fouling mechanisms of skim milk UF (modified from Ng, et al., 2017).

Fig. 1 indicates that casein micelles (CMs) are larger in size as compared to whey proteins (WPs). This size difference determines the composition of the concentration polarization (CP) layer (Ng et al., 2017).

In general, foulants such as proteins, humic materials, emulsified oils and microorganisms have a higher tendency of fouling to hydrophobic membranes as compared to hydrophilic membranes (Chang et al., 2018). For this reason, fouling hydrophobic-foulants on hydrophobic membranes can be mitigated by modification of the membrane by hydrophilic materials. This is due to the tendency of hydrophilic surfaces of the membrane to form a layer of water, which prevent the build-up of hydrophobic foulants on the surface (Elimelech & Phillip, 2011). However, some hydrophilic fraction of natural organic matter (Zularisam et al., 2006) are having tendency of easily fouling hydrophilic membranes. Contact angle measurement is commonly used to characterize the hydrophilicity of the membrane, even though contact angle depends upon other factors, such as surface roughness, pore size, porosity, and time.

2.4. Factors affecting membrane fouling

In membrane filtration, membrane flux performance depends on solution composition, hydrodynamic operating condition and membrane properties. These factors are considered as the main factors affecting membrane fouling (Tang et al., 2011). These factors are illustrated in Fig. 2.

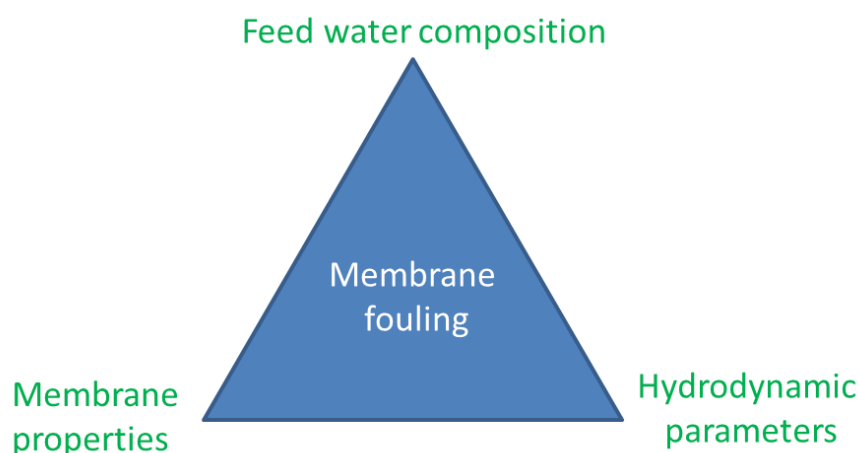


Figure 2. Main factors influencing membrane fouling

2.4.1. Membrane properties: hydrophilicity, roughness, functional groups, and surface charge

Membrane surface can be characterized by hydrophilicity, roughness, and surface charge. These are an important membrane surface properties that need to be taken into account in membrane fouling (Louie et al., 2006).

2.4.1.1. Hydrophilicity of membrane

Membrane hydrophilicity is the tendency of membrane towards water. Generally, water contact angles (WCA) has been applied to explain membrane hydrophilicity. CA of the membrane is determined by the surface energy and surface roughness. WCA is decreased with increase in surface energy and decrease surface roughness (Ravi et al., 2021). The hydrophilicity of the membrane surface has been considered as a crucial factor to explain antifoul in property of membrane (Du et al., 2020a)

2.4.1.2. Membrane surface roughness

Membrane surface roughness is considered as a structural property of membranes and has been studied for its influence on fouling. Ravi et al. (2021) revealed that all nanocomposite PVDF membranes that have higher roughness have showed higher water permeate fluxes than the neat membrane. Al-Gharabli et al., (2022) have also shown that carbon based nanocomposite with higher roughness exhibited better antifouling than the pristine PVDF membrane. Similar results have obtained by other groups of researchers (Goodyer et al., 2012; Chew et al., 2017, Yang et al., 2021; Lin et al., 2022). However, these results are different from the result obtained by other researchers in that, nanocomposite PVDF membranes showed a smoother surface than pristine PVDF membrane (Du et al., 2020a;).

2.4.1.3. Functional groups

Functional groups are one of the factors determine fouling condition of membrane surface (Tong et al., 2017). Wang et al., (2020) revealed that membranes with negatively charged functional groups (-COOH) or acrylic acid (AA) repelled negatively charged dissolved silica species and exhibit better antifouling property as compared to the pristine membrane.

A study by Guan et al., 2020 investigated the effect of functional groups on membrane fouling and found that functionalized membrane surface by negative surface charge of sulfonic group (vinyl sulfonic acid) mitigates not only negatively charged silica scaling but also organic foulants.

Another research by Farahani & Vatanpour, 2018 studied the effect of carboxyl- functionalized PVDF membrane performance and revealed that the modified membranes exhibited better antifouling performance and BSA rejection as compared to pristine PVDF membrane.

2.4.1.4. Surface charge

Generally, repelling and attracting forces between membrane and foulant increase and decrease fouling respectively (Yu et al., 2010). These two forces are mainly affected by the charge and hydrophobicity the membrane (Xiao et al., 2011). Many authors argue that proteins are neutral charge and hydrophobic at their isoelectric point (pH 4.7) that their fouling is sever due to hydrophobic interaction or aggregation as a result of reduced electrostatic repulsion (Huisman

et.al., 2000). At this isoelectric point, proteins are small in size and tend to form densely packed fouling layer that result in lower permeability. The solute-solute and membrane-solute interactions are summarized in Fig.3.

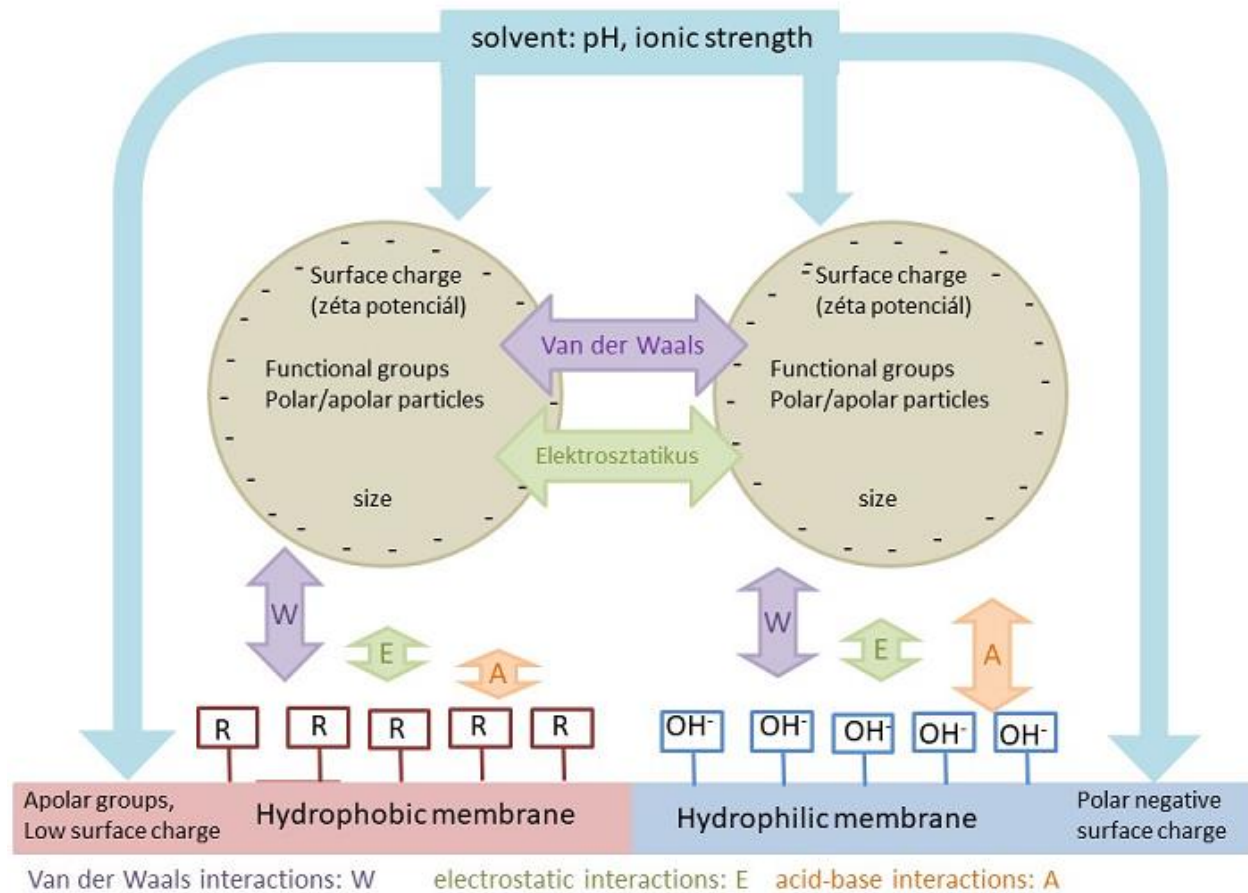


Figure 3. Solute-solute and membrane-solute interactions

2.4.2. Composition of the wastewater: foulant type, concentration, pH, ionic strength

Wastewater composition is considered as one of the factors affecting fouling. For example, in membrane filtration of dairy wastewater, the protein component behaves as amphoteric or hydrophobic and can easily fouled to hydrophobic membranes, however the severity of the fouling is still relay on many factors such as ionic concentration, pH, nature of dairy proteins, protein type, and calcium phosphate (Hausmann et al., 2013).

2.4.2.1. Ionic strength

Ionic strength affects fouling through shielding effect. This effect occurred at high concentration ions in a solution. In dairy wastewater this effect keeps charged protein molecules apart from each other and makes the molecules small in size. In this case the rejection efficiency of membranes is

low (Persson et al., 2003; Miao et al., 2015). Besides, at high ionic strength, the electrical double layer (EDL) of protein molecules is compressed. As a result of the effect, protein molecules become small and tend to aggregate to form dense fouling layer (Ding et al., 2019; Navarro et al., 2016; Miao et al., 2015). She et al., (2009) showed that the impact of ionic strength (1, 10 and 100 mM NaCl) on fouling varies with pH (3, 4.7, 5.8 and 7) As the ionic concentration increase from 1 to 100 mM, the fouling was increase at pH 3.0, decreased at 5.8 and no considerable effect at pH 4.7 and 7. For all ionic strength the lowest flux was observed at pH 4.7, isoelectric point of BSA. The negative effect of high ionic strength, high ionic concentration directly affects osmotic pressure and filtration resistance by reducing the cake layer porosity.

2.4.2.2. Solution pH

Changing solution pH plays an important role in altering the zeta-potential colloidal of protein particles like BSA and thereby affects fouling. BSA molecules are neutral charge at pH 4.7, isoelectric points (IEP) of BSA. At this pH or close to IEP, BSA molecules have low repulsion force and tend to aggregate which results in fouling. On the other hand, at higher pH a repulsion force is formed between negatively charged membrane and BSA molecules, however a gradually cake layer formation is developed (Ding et al., 2019; Navarro et al., 2016).

2.4.2.3. Solution concentration

Akamatsu et al., 2020 studied the effect of BSA feed concentration of 10 ppm, 50 ppm, 300 ppm, 500 ppm, 1000 ppm and 5000 ppm on fouling. The authors found out that the fouling severity increased as the concentration increased from 1 ppm to 500 ppm.

2.4.2.4. Salinity

Dairy industry salt waste water is originated from cheese manufacturing and whey processing. The salinity, EC and sodium load of dairy industry effluent is 1800–2700 mg·L⁻¹ TDS, more than 4000 µm EC and 532–600 mg·L⁻¹ Na respectively (Chen et al., 2018). Salts mostly contains Na⁺, Ca²⁺, Fe³⁺, Al³⁺ and Mg²⁺ etc. Generally, the salt content of high-salinity organic wastewater is more than 1% (Cai et al., 2021). Some authors argued that high salinity increased the severity of fouling. Sim, et al., (2014) investigated the effects of salinity using aqueous solution containing 0.4 g·L⁻¹ of silica and 1 to 8 g·L⁻¹ sodium chloride (NaCl) on membrane fouling. They found that, the severity of fouling was increased with increasing the salinity.

Jang, et al., 2013 investigated the effects of various NaCl (0, 5, 10, 20 g·L⁻¹) concentration on fouling using synthetic wastewater and revealed that the irreversible fouling enhanced with increasing salinity. Lin et al., (2022) studied the effects of salinity (EC from 250 to 10,000 µs cm⁻¹) on fouling using humic acid (HA) and sodium alginate (SA). They found a decreased trend for both flux and rejection (Du, et al., 2020b). However, Cai et al., (2021) found that high salinity sodium

chloride (NaCl) with the concentration higher than 10 gL^{-1} increased HA fouling, while decreased BSA fouling formation.

Cai et al., (2022) investigated the effects of high-concentration of Na^+ , Ca^{2+} and Al^{3+} (2 M Na^+ and $0.5 - 1.0 \text{ M Ca}^{2+}$ or Al^{3+}) using bovine serum albumin (BSA) and humic acid (HA) solution on UF fouling characteristics. They revealed that Na^+ alone decreased fouling formation during the ultrafiltration of BSA solution but increased the severity of fouling on the ultrafiltration of HA solution. Addition of Ca^{2+} or Al^{3+} on Na^+ was found to pose adverse effect the development of BSA fouling.

2.4.3. Hydrodynamic operating condition: trans-membrane pressure (TMP), flow velocity, temperature

In membrane filtration hydrodynamic operating conditions include trans-membrane pressure (TMP), velocity and temperature.

2.4.3.1. Trans-membrane pressure (TMP)

Many studies revealed that higher trans-membrane pressure (TMP) results sever fouling and lower flux as a result of more compact protein layer built up on the membrane surface, as compared to lower trans-membrane pressure. Jiang et al., (2018) obtained to only 28.5% flux reduction at 20 kPa as compared to 70.4%, 81.6%, and 92.2% at 100 kPa, 200 kPa, and 500 kPa.

2.4.3.2. Flow velocities

Flow velocity is another factor that needs to take into account during fouling mitigation. She et al., 2009 obtained higher flux performance ($137.4 \text{ Lm}^{-2}\text{h}^{-1}$) at higher velocity $41.7 \text{ cm}\cdot\text{s}^{-1}$ as compared with the flux $51.0 \text{ L}\cdot\text{m}^{-2}\text{h}^{-1}$ at $13.9 \text{ cm}\cdot\text{s}^{-1}$ and $74.7 \text{ Lm}^{-2}\text{h}^{-1}$ at $27.8 \text{ cm}\cdot\text{s}^{-1}$. Besides, higher velocity offers lower concentration polarization and possibility of improved back transport.

Flow velocity that leads to above critical flux and too low flow cause severe fouling (Tang et al., 2007) while below critical flux is negligible (Bacchin et al., 2006).

2.4.3.3. Temperature

Fouling can be significantly affected by temperature. According to Ding et al., 2019 the effect of temperature on fouling was proved by flux decline. The authors found that the flux of BSA solution during ultrafiltration membrane filtration were declined from $0.68 \text{ L}\cdot\text{m}^{-2}\text{h}^{-1}$ at 20°C to $0.43 \text{ L}\cdot\text{m}^{-2}\text{h}^{-1}$ at 27°C , to $0.30 \text{ L}\cdot\text{m}^{-2}\text{h}^{-1}$ at 34°C and then to $0.28 \text{ L}\cdot\text{m}^{-2}\text{h}^{-1}$ at 80°C . Fouling of whey protein is much sever at lower (less than 10°C) and higher temperatures (higher than 35°C) (Steinhauer et al., 2015b), as both extreme temperatures denatured protein structures which can aggregate and foul easily on the membrane surface (Thereza et al., 2019; Pelegrine and Gasparetto, 2006)

2.5. Fouling control and mitigating strategies

In recent years, several methods have been used to control. These methods include pre-treatment of feed solution, optimizing operating condition, physical cleaning, chemical cleaning and membrane modification (Zhao and Yu, 2014).

2.5.1. Pretreatment of feed solution

This fouling prevention method reduces the risk of membrane fouling. The fouling risk reduction efficiency depends on the type of pre-treatment method. Coagulation is widely applied method for removing particles and dissolved contaminants, but it is not effective to remove low molecular weight fractions and neutral hydrophilic (Carroll, 2000).

Coagulation/flocculation along with oxidation method has been used as physicochemical pre-treatment method to reduce contaminants from wastewater. However, its wider application is limited by high cost and ineffective contaminant removal (Sharma, 2014). Besides, it generates huge amounts of chemical sludge that requires further treatment (Mehta and Chavan, 2009).

Advanced oxidation processes can be applied alone or in a combination. In recent years, ozone, *ultraviolet (UV)* radiation with *hydrogen peroxide* (H_2O_2) and *ultraviolet (UV)* radiation with persulfate (PS) were applied as pre-treatments for UF process. From the above oxidation pre-treatment methods, *ultraviolet (UV)* and persulfate (PS) combination offered an excellent contaminant removal and membrane fouling mitigation result. Li et al., (2019) associated outstanding result with the ability of PS, a powerful oxidant, to generate sulphate radicals ($\text{SO}_4^{\cdot-}$). Li et al., (2020) studied the effects of combination of ferrous ion (Fe(II)) and sodium per carbonate (SPC) on fouling reduction and found that a combination of Fe(II) and SPC were superior membrane fouling control than using them separately, is due to activation of SPC oxidation by catalyst, Fe(II) .

Chang et al., (2020) investigated the effects of combinations of advanced oxidation processes on fouling control and revealed that the outstanding performance was shown by combination of ultraviolet light, ferrous ion and persulfate followed by ferrous ion and persulfate, while the worst performance was shown by combination of ultraviolet pre-oxidation together with ferrous ion pre-coagulation, as Fe(II) has high tendency to reduce its catalytic effect at neutral pH and oxidize rapidly to Fe(III) in a reaction (Yang et al., 2015).

The most widely used effective pre-treatment combination methods for reverse osmosis (RO) involves use of disinfection (destroy microorganisms), scale inhibitor (acid) (remove inorganic molecules), activated carbon (remove dissolved organic carbon (DOC)), coagulation/flocculation (removes colloidal particles and dissolved organic carbon (DOC)), and membrane filtration (UF/MF) (removes colloids, particles, and microorganism) (Jiang et al., 2017).

2.5.2. Physical membrane cleaning

Membrane fouling can be prevented by changing the hydrodynamics nature of a given solution. In recent times hydraulic flushing, cross-flow, shearing, field (electric, ultrasonic, magnetic), and adding activated carbon are widely applied physical cleaning approaches (Zhao and Yu, 2014). The most commonly used cleaning methods are backflush and backwash. However, these technologies are time consuming (Muthukumaran et al., 2005). Better shear rate can be obtained from vibration, in this way improved flux can be obtained by mitigating membrane fouling (Li et al., 2014; Kola et al., 2014). The cleaning mechanism involves generating of high turbulence and shear forces on the membrane surface, that help to destroy and remove foulant deposits from membrane surface (Altaee et al., 2010). They studied that the effect of vibration on cleaning of membrane and found that cleaning efficiency was improved with increased vibration. They obtained a flux of 15, 27 and 56 L·m⁻²h⁻¹ for vibration frequency of 0, 1.67 and 8.35 Hz respectively. Li et al, (2013) has also obtained more than 90 % membrane cleaning efficiency at 8 Hz.

Ultrasound is also one of commonly applied physical cleaning method, and it offers strong convective currents, micro mixing, pressure shockwaves, and micro jetting. These strong mixing waves agitate the aqueous medium which in turn acts on the foulants adhering to the membrane surface for reducing concentration polarization and removing cake layers (Muthukumaran et al., 2004; Luján-Facundo et al., 2017; Muthukumaran et al., 2005; Muthukumaran et al., 2007; Ahmad et al., 2012; Aktij et al., 2020). Camara et al., (2020) found best PVDF membrane fouling cleaning performance at 20–28 kHz. Many researchers showed ultrasound as a promising fouling cleaning technology as compared with membrane cleaning without ultrasound (Lee et. al., 2017; Yu et al., 2017). Integrating ultrasound with surfactant has also showed a superior performance than ultrasound alone (Muthukumaran et al., 2004; Maskooki et al., 2010). Ultrasonication can overcome the limitation of backwashing or chemical cleaning in that, it can be integrated in the filtration process without stopping the filtration. It avoids using chemicals and backwashing water. It does not have much concern of chemical cost, waste disposal and the environment as compared to backwashing or chemical cleaning (Muthukumaran et al., 2004). Fouling mechanisms of ultrasonication involves four processes; firstly, by promoting the agglomeration of small particles. This reduces pore blockage and cake compaction. Secondly, providing mechanical vibrational energy, particles are suspended. Thirdly, by generating small vapour-filled cavities that scour the membrane surface and can reach areas not accessible to conventional cleaning methods. Fourthly by generating turbulence and more intense mixing, which will result bulk fluid movement toward and away from the membrane cake layer (Muthukumaran et al., 2005).

2.5.3. Chemical membrane cleaning

Chemicals such as acids, alkaline or oxidants may undergo reactions such as hydrolysis, dissolution or dispersion and are used to degrade mainly the irreversible foulant or minimize the attractive bonding between the membrane and the foulants of the solution ([Kazemimoghadam and Mohammadi, 2007](#)). Nowadays sodium hypochlorite, sodium hydroxide, hydrochloric acid, sulfuric acid, nitric acid, ethylene domain tetra acetic acid and sodium dodecylsulphate are the commonly applied chemicals used for chemical cleaning in membrane filtration. [Kazemimoghadam and Mohammadi, \(2007\)](#) compared cleaning performance of alkaline and acid, and they obtained superior cleaning performance by alkaline chemicals as compared to acids for dairy wastewaters. Integrating alkaline chemicals with surfactant (sodium dodecylsulfate (SDS)) or chelating agent (Ethylenediaminetetraacetic acid (EDTA)) has also showed a superior performance than alkaline alone ([Shi et al., 2014](#); [Guan et al., 2018](#)).

Chemical cleaning can be applied in four ways. Both cleaning-in-place (CIP) and cleaning out of place (COP) involves cleaning of membrane using chemical solution within and outside the membrane reactor respectively. The other two, involves adding chemicals in the feed stream and use of combination of physical chemical method ([Lin et al., 2010](#)).

A study of [Souza and Mawson, \(2005\)](#) showed an excellent cleaning performance of alkaline solutions for proteins and polysaccharides removal and acids for elimination of inorganic salts and metal oxides or hydroxides.

Chemical cleaning is advantageous from membrane cleaning efficiency point of view however it has some drawbacks. This includes high cost for chemicals, high effluent generation and possibility of damaging the membrane, generate effluents and are expensive ([Shi et al., 2014](#)).

2.5.4. Physicochemical membrane cleaning

Nowadays, chemically enhanced backwashing (CEB) is the most widely applied integrated physical and chemical membrane cleaning method in membrane cleaning processes. This method involves use of chemicals during backwashing (Lin et al., 2010).

Wang et al., (2014) obtained fouling rate reduction of 63–77% using chlorine ($0.2\text{--}0.5\text{ mgL}^{-1}$) and backwash at flux of $8.33\text{ L}\cdot\text{m}^{-2}\text{h}^{-1}$ compared to normal water back flushing. Zhou et al., (2014) achieved a fouling rate reduction of 50 % using $0.01\text{ mol}\cdot\text{L}^{-1}$ NaOH and backwash at flux of $8.33\text{ Lm}^{-2}\text{h}^{-1}$ (Zhou et al., 2014).

2.5.5. Membrane modification

In recent years, fouling control and mitigation using modified membrane is a promising development in membrane technology and can be done by integrating membrane with hydrophilic polymers or semiconductor heterogeneous photo-catalysts (Liu et al., 2011). Many researchers come up with modified membranes that have better in surface charge, hydrophobicity and morphology, and offer antifouling and photocatalytic degradation benefits (Louie et al., 2006; Tang and Li, 2013; Zhou et al., 2014; Chew et al., 2017; Du et al., 2020a; Lin et al., 2022).

Some researchers studied the effect of polyvinylpyrrolidone (PVP), polyethylene glycol (PEG) or poly (methyl methacrylate) (PMMA) on fouling control and mitigation and found that with the addition of hydrophilic polymers increased the antifouling property of the membrane (Liu et al., 2011; Vatsha, et al., 2014; Chang, et al., 2014; Du et al., 2021; Lin, et al., 2021). .

Membrane fouling prevention and cleaning are the two main challenges in membrane filtration application. Regular chemical cleaning is expensive and environmentally unfriendly (McCartney et al., 2017; Zhao et al., 2019). Membrane modification using nanocatalysts are a recent development that offers both antifouling and catalytic degradation benefits. The sources of activation energy of the nanocatalyst could be light, electrical and Fenton. Therefore, based on these sources of activation energy, the nanocatalysts may be classified as photocatalysts and electrocatalysts (Dutta et al., 2014), and Fenton based catalysts (Kurian and Nair, 2015) respectively. The nanocatalyst aimed to degrade contaminants of wastewater such as organic contaminants (Han et al., 2018) and microbial agents (Natarajan et al., 2018).

2.5.5.1. Membrane modification by semiconductor heterogeneous photo-catalysts

In recent years, the application of membrane filtration in dairy waste water treatment is growing (Galvão, 2018 and Velpula et al., 2017), especially integrating membrane filtration with other systems is becoming a one of the promising technologies applied to meet the environmental wastewater discharge limit (Bixio et al., 2006; Lakra, et al., 2021). However, these processes are susceptible for fouling, which may occur as a result of hydrophobicity of the membrane leads to a decline flux and raise energy use. These effects may limit the broader application of the technology (Chang et al., 2019) in water treatment.

Nowadays, several novel and emerging techniques have developed to tackle the constraint of membrane separation processes. Besides, recent publications (Anis et al., 2022; Ruigómez et al., 2022; He et al., 2022) have focused on fouling reduction by offering innovative cleaning processes, optimizing the existing techniques, or integrating devices to the membrane set-up. As a result of the above activities, the membrane separation becomes a viable alternative for dairy industry wastewater treatment.

2.5.5.1.1. Heterogeneous photo-catalysts and mechanism of heterogeneous photocatalysis

Heterogeneous photocatalysis is a process of converting light energy into chemical energy by semiconductor heterogeneous photocatalysts, which can be used to degrade wastewater contaminants (Di Mauro et al., 2017). The processes of heterogeneous photocatalysis are illustrated in Fig. 4.

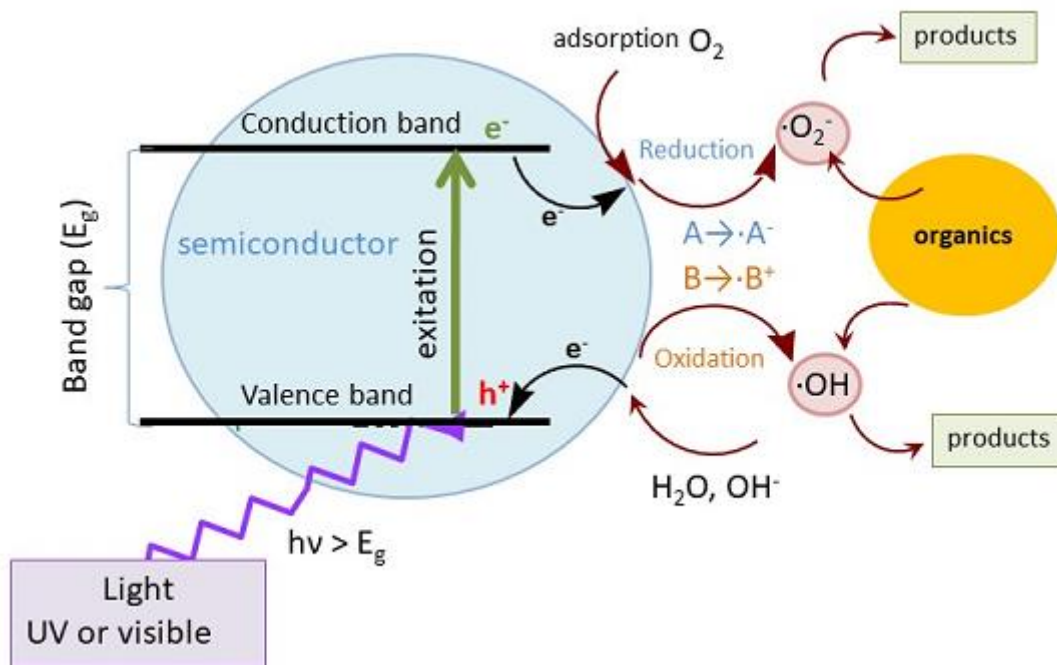


Figure 4. Mechanism of heterogeneous photocatalysis

Many heterogeneous photo-catalysts have been widely applied in the photodegradation of pollutants under UV light. These include; tungsten-oxide (WO_3) (Peyravi et al., 2017), titania (TiO_2) (Kovács et al., 2017; Yogarathinam et al., 2018), zinc-oxide (ZnO) (Thebo et al., 2018), graphene oxide (GO) (Bottino et al., 2002), zirconia (ZrO_2) (Yan et al., 2006; Yogarathinam et al., 2018), alumina (Al_2O_3) (Yan et al., 2006) and silica (SiO_2) (Yu et al., 2009).

Among the above mentioned photocatalyst titanium dioxide (TiO_2) is the most widely applied photocatalyst. Previous studies mentioned that the hybrid TiO_2 blended PVDF membranes has excellent photocatalytic activity, outstanding physical and chemical property, superior hydrophilic and antifouling properties, nontoxic effect, excellent stability, and low cost (Leong et al., 2014; Akhavan, 2009; Kumar and Bansal, 2013). Similar results exhibited that incorporation of TiO_2 in the membrane matrix have contributed to improve flux and antifouling of UF PVDF membrane (Farahani and Vatanpour, 2018). TiO_2 offers both antifouling and photocatalytic degradation benefits.

However, as it was mentioned earlier, TiO_2 has two main limitations that hinder its wider practical application. Firstly, the high recombination ratio of photocatalytically generated electron-hole pairs reduce photocatalytic activity. Secondly, TiO_2 has a wide bandgap of 3.15 eV, its photocatalytic activity can only be efficiently activated under UV light ($\lambda < 390$ nm), excluding visible light (Akhavan, 2009; Zouzelka et al., 2016). The former leads to waste of energy and result in low degradation efficiency under UV light while the later result in a low photocatalytic

performance under visible light illumination (Zouzelka et al., 2016). These two drawbacks limit its wider practical application in membrane separation processes.

Several strategies have been applied to enhance the low photo-efficiency and high recombination rate of TiO_2 . Anatase is one of three structure polymorphs of titania that have lowest recombination rate of electron-hole pairs and highest photocatalytic reactivity as compared to rutile and brookite (Fujishima et al., 2008). Another possibility is integrating of TiO_2 with semiconductor that has narrower band gap (Malathi et al., 2018; Ratova et al., 2018) or with nitrogen, sulphur, noble metals transitional metal ions or photosensitizer (Yogarathinam, et al., 2018) and electron acceptor semiconductors (Selvaraj et al., 2020).

In recent years, bismuth-based oxides have gained attention in photo-catalytic technology because of their superior band gap and efficient visible light absorption performance, however, their relatively low surface area and activity hinders their broader application (Malathi et al., 2018; Ratova et al., 2018; Orimolade and Arotiba, 2020; Kunduz and Soylu, 2015; Lin et al., 2012; Hou et al., 2011; Wang et al., 2017; Abazari et al., 2019; Li et al., 2012).

2.5.5.2. General and structural properties of BiVO_4

BiVO_4 has a narrow band gap of 2.4 eV in the monoclinic phase and an excellent light absorption property (Sadeghzadeh-Attar, 2020). It has also other outstanding properties such non-toxicity, corrosion resistance, good dispensability, superior chemical stability (Huang et al., 2022)

BiVO_4 can be found as orthorhombic structure of vanadium bismuth ore in nature. Whereas the structure of synthesized BiVO_4 can be monoclinic scheelite structure (m- BiVO_4), tetragonal zirconium silicate structure (tz- BiVO_4) and tetragonal scheelite structure (ts- BiVO_4) (Zhao et al., 2017). Among the above-mentioned structures of BiVO_4 , m- BiVO_4 has the most efficient photocatalytic activity (Srinivasan et al., 2022).

2.5.5.3. Photocatalytic activity of BiVO_4

Bismuth vanadate (BiVO_4) is an n-type semiconductor with a narrow band gap (2.3–2.5 eV) and show excellence in visible light absorption (Phuruangrat et al., 2023). BiVO_4 has recently been proved to be a potential candidate for organic decontamination. This is because of its low cost, excellent photocatalytic stability, narrow band gap of 2.4 eV in the monoclinic phase (Sadeghzadeh-Attar, 2020).

Degradation efficiency of 98.79 % over the methylene blue (MB) was observed within 60 min of light irradiation (Srinivasan et al., 2022). However, the wider practical application of BiVO_4 in organic pollutants in wastewater was limited due to the small specific surface area and the lower separation efficiency of photogenerated electrons and holes (Guo et al., 2022).

2.5.5.4. Methods of synthesis for BiVO₄

BiVO₄ can be synthesized by precipitation method (Yalçın and Dükkancı, 2022), solvothermal method (Ma et al., 2014; He et al., 2018), hydrothermal method (Srinivasan et al., 2022), and microemulsion method (Huang et al., 2022). From the above-mentioned methods, the hydrothermal method is widely used to synthesize smaller particle size, better crystalline nature, and controlled shape of the BiVO₄ nanostructures (Srinivasan et al., 2022).

2.5.5.5. Role of BiVO₄ in improving the performance of TiO₂-based photocatalysts

The wide band gap of TiO₂ limits their applications under visible-light and rapid charge recombination rate reduces their photocatalytic efficiencies (Zouzelka et al., 2016). Considerable efforts have been applied to enhance the low photo-efficiency and high recombination rate of TiO₂. These include integrating of TiO₂ with narrow band gap semiconductors such nanocubes of silver-chloride (AgCl) (Yang et al., 2017), Bismuth vanadate (BiVO₄) (Sadeghzadeh-Attar, 2020), cadmium sulphide (CdS) (Yue et al., 2017), iron (Fe (III) and active carbon (Lavand and Malghe, 2018), copper sulphide nanostructures (CuS NSs) (Nezar et al., 2019), Ag₂O, graphene and graphene oxide (Barakat et al., 2020).

Integration of TiO₂ with other low-band gap semiconductors not only can enhance the light absorption phenomenon broadening the spectral responsive range, but also promote the charge carriers' separation (Barakat et al., 2020). Bismuth-based oxides have received great attention and been applied widely (Das et al., 2017; Žerjav et al., 2018; Angelo and Filice, 2019).

2.5.5.6. General and structural properties of Carbon nanotubes (CNTs)

Carbonaceous nanomaterials are semiconductor materials that have received considerable attention for design of new photocatalytic applications because of their superior properties, such as large specific surface area, unique mechanical (stiffness and flexibility), high electrical and thermal conductivities (Trapalis et al., 2016; Gupta et al., 2019; Selvaraj et al., 2020). They have also excellent electronic properties, chemical stability, conductivity, thermal stability, pore structure and high surface area.

Carbon nano-tubes (CNTs) are the most common carbonaceous materials used to combine with semiconductors (Isari, et al., 2020; Huang et al., 2018). Depending on the number of walls, CNT can be classified into single-walled carbon nanotubes (SWCNTs), double-walled carbon nanotubes (DWCNTs), and multi-walled carbon nanotubes (MWCNTs) (Fig. 5). SWCNTs, MWCNTs and DWCNTs consist of one, two and many nanotubes respectively. SWNT is much thinner and are

more vulnerable to structural change which can easily affect their electrical and mechanical properties (Gupta et al., 2019).

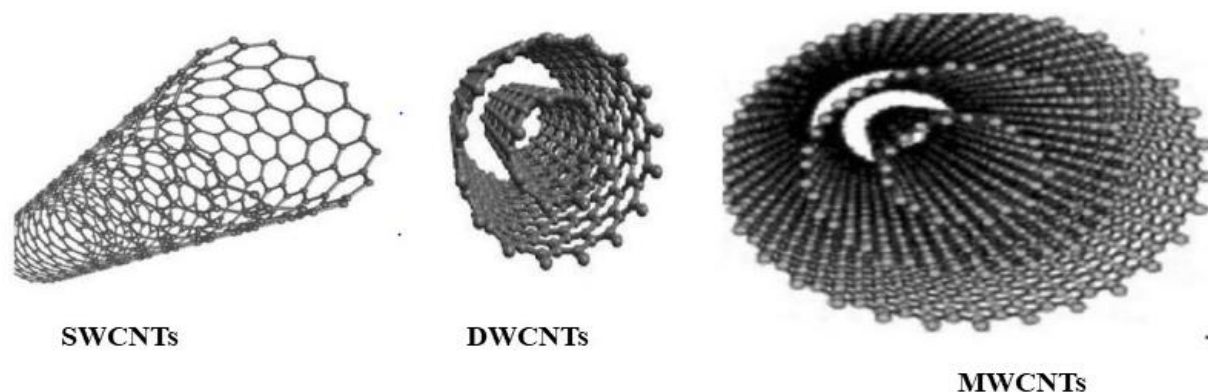


Figure 5. Structures of SWCNTs, DWCNTs, and MWCNTs (Gupta et al., 2019)

5.5.5.7. Role of CNTs and mechanisms of photocatalysis in TiO₂/CNT composite

Various carbon-based materials, such as activated carbon, graphite, carbon nanotubes, and graphene oxide, or other porous carbon derivatives, are potential candidates for composites due to their high absorbance of visible light and efficient electron-hole separation (Barakat et al., 2020). One study found that the Ni(OH)₂/GO/TiO₂ composite is a highly effective catalyst for the removal, disinfection, and degradation of complex wastewater constituents (Barakat et al., 2020)..

Additional research have shown that the incorporation of GO with metal-semiconductors reduces the recombination rate of electron-hole pairs by acting as an electron acceptor. This extends light absorption to the visible range and enhances the mobility of charge carriers, resulting in improved photocatalytic performance in visible light (Gong et al., 2017; Nadimi et al., 2019; Khan et al., 2019).

Carbon nanotubes (CNTs) are semiconductor materials that have received considerable attention due to their outstanding properties, such as unique mechanical (stiffness and flexibility), large specific surface area, high thermal and electrical conductivities. They are broadly used as electron acceptors and reduce the recombination rate (Trapalis et al., 2016; Selvaraj et al., 2020). They also may enhance membrane antifouling property, water flux and BSA rejection (Moslehyani et al., 2015; Ayyaru et al., 2019).

Photocatalytic performance of a photocatalyst is affected by the e/h recombination time (Cao et al., 2013). This problem is common during single semiconductor application. Several methods have been studied to increase the e-h recombination time, the catalysts with nano dimension, combining two or more semiconductors, adding supporting materials to semiconductors (such as CNTs, silica,

g-C₃N₄, graphene oxide, alumina, zeolites etc., and doping of metals or nonmetals into the semiconductors etc. (Hemmatpour et al., 2022). Catalysts with Nano dimension have lower e/h recombination rate than single dimension due to short path length to the surface. Thus, the photoexcited electrons and hole pairs can quickly travel to the surface before they recombine. Combination of two or more semiconductors creates a chance for the electron transfer between the CB positions, and the photoinduced holes between the VB positions which result in lower e/h recombination.

One simple method to reduce e–h recombination is to add electron scavengers such as CNT into the photocatalysis system (Cao et al., 2013). Carbon nanotubes have large electron storage capacity which hinders electron-hole recombination. Moreover, the high sp²-ordered structures of CNTs made CNT to have an excellent metallic conductivity, which form a Schottky barrier junction between the semiconductors and CNTs (Isari, et al., 2020; Sharma et al., 2021). The role of CNT and photocatalysis mechanism of TiO₂/CNT composite is presented in Fig. 6. Fig. 6a. shows the role of CNT as electron scavenger (the electron acceptor), in this figure the. excited electrons from the conduction band of TiO₂ is flowed to CNTs. However, Fig. 6b shows the role of CNTs as photosensitizer (electron donor), where excited electrons from the conduction band of CNTs is flowed to TiO₂. Fig. 6c shows the presence of Ti–O–C bonds, this extends the light absorption to longer wave lengths, leading to the improvement of the photocatalytic activity.

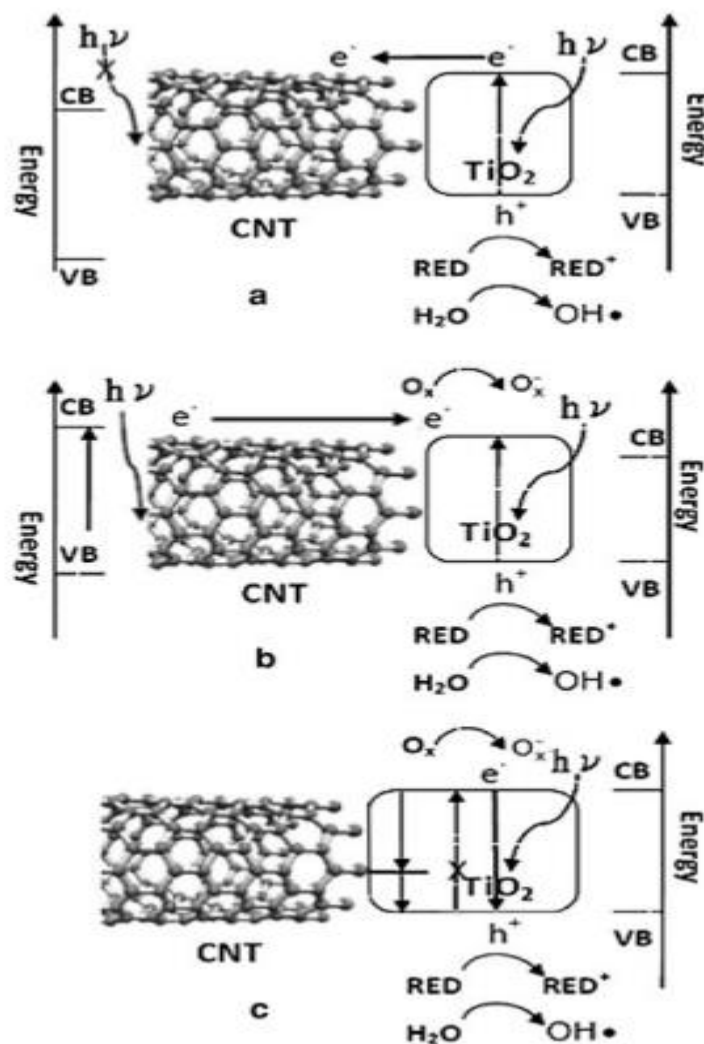


Figure 6. Role of CNTs and mechanisms of photocatalysis in TiO₂/CNT composite (Cao et al., 2013).

2.6. Catalytic membrane reactors

A catalytic membrane reactor (CMR) is an integrated unit of membrane and catalyst. Catalytic membrane reactors currently used for wastewater treatment can be classified in to four.

- 1) photo-catalytic membrane reactors (PMRs), which are prepared by combining photocatalysis with membrane technology (Bellardita et al., 2018).
- 2) enzymatic membrane reactors, which are prepared by combining electrocatalytic reactions and processes of membrane separation into one processing stage (Vanangamudi et al., 2018).
- 3) electro-catalysts, which integrate electrocatalytic reactions and the process of membrane separation into one processing stage (Kokko et al., 2017), and
- 4) Fenton-based chemical reactors (Kurian and Nair, 2015). The reactors mentioned above help improve chemical oxidation of organic pollutants (Han et al., 2018) and antimicrobial action

(Natarajan et al., 2018). Among the above membrane reactors, the PMRs are promising for the treatment of contaminants due to the potential use of suitable light irradiation to degrade compounds in wastewater into less or nontoxic minerals, such carbon dioxide, ammonia, and water (Das et al., 2017).

Based on three methods of preparation used photocatalytic membrane reactors can be, grouped into (1) photocatalyst-coated membranes (Li et al., 2013), (2) photocatalyst-blended membranes (Ngang et al., 2012; Song et al., 2012; Shaban et al., 2018), and (3) self-photocatalytic membranes (Li Menglin et al., 2013).

Firstly, physical coating, there are several physical coating methods available to prepare photocatalyst-coated membrane. The most common methods are dip-coating (Hou et al., 2014), electrospinning (Ramasundaram et al., 2015), electrospraying (Ramasundaram et al., 2015; Ramasundaram et al., 2016), advanced atomic layer deposition (Wang et al., 2013), and physical deposition (Kovács et al., 2018). **Dip-coating** ensures uniform coating of the nanomaterials on the surface of the membrane. However, the process involves complex steps and requires high heat resistance support material (Hou et al., 2014). **Electrospinning** is a simple method of preparing membranes that have a uniform distribution of pores and better interconnectivity. However, the method is not suitable to use at commercial level (Ramasundaram et al., 2015). **Electrospraying** is an electro hydrodynamic atomization method that offers easy control of film thickness, low cost, and high deposition efficiency (Ramasundaram et al., 2016). **Atomic layer deposition** (ALD) is a process of coating the membrane at low temperature by easily control film thickness (Wang et al., 2013). **Physical deposition** is a process of filtering the ultrasonicated solution of photocatalyst and propanol through a membrane in a dead-end cell and dries the membrane at room temperature (Kovács et al., 2018). This method is advantage in terms of simplicity and reproducibility, and offers higher hydrophilicity, improved anti-fouling properties, and help protect UV sensitive membranes (Nady et al., 2011).

Secondly, blended (phase inversion) method is a process of converting of a uniform solution of polymer and nanoscales into a solid phase membrane in a controlled way. This method is commonly applied to fabricate asymmetric Polymeric Nano-composite Membranes (PNCMs). The characteristics of the fabricated membrane depends the choice of solvent, non-solvent polymer solution, coagulation bath composition and film casting conditions (Aburabie et al., 2017). The method is used to prepare photocatalyst-blended membranes. It does not have a problem of leaching of the photocatalyst, however the method leads to have a marginal increase in hydrophilicity and less reproducibility (Ngang et al., 2012; Song et al., 2012; Shaban et al., 2018). Thirdly, electrochemical anodization is the method used to prepare self-catalytic membranes. Self-catalytic membranes are an electrified membrane (EM) surface that use migration of charged

ions/colloids under the electric field (EF) and create polarization effect of organic molecules to enhance membrane separation and antifouling performance ([Sun et al., 2022](#)). The method used to prepare the membrane is different from coated or blended method in that it does not need immobilization step. Membranes prepared by this method have high hydrophilicity, large surface area, nanotubular morphology, excellent photocatalytic efficiency and high anatase crystallinity ([Li et al., 2013](#)). The membranes also have better mass transport and antifouling than the conventional membranes ([Ren et al., 2022](#); [Yu et al., 2022](#); [Mo et al., 2022](#)). However, their relatively high production cost may limit their large-scale production and industrial application ([Pan et al., 2020](#)).

3. Aims

This Ph.D. thesis is aimed to fabricate visible light driven hybrid nanocomposite ultrafiltration PVDF membrane for dairy waste water treatment. Such study can have huge contribution on development of environmentally friendly renewable energy driven membrane technology for wastewater treatment. In order to achieve the general objective, the following specific objectives have been taken in to consideration:

- Explore physic chemical characteristics of dairy wastewater.
- Selection of nano-composite material with excellent photo-catalytic activity, characterize its properties and optimize their composition for effective treatment
- Fabricate photo-catalytic membranes with synthesized nanocomposites. Characterizing and examining the optimum concentration of nano-composite loading of prepared nanocomposite membrane.
- Application of fabricated membranes for synthetic and real dairy wastewater treatment
- Examining the effect of salinity on dairy wastewater treatment
- Evaluate the efficiency of regeneration of fouled membrane with UV and visible light

4. Materials and methods

4.1 Materials

4.1.1. Chemicals and materials used

In this study commercial and fabricated PVDF membranes were used. The commercial 30 kDa PVDF membrane (JW GE Osmonics) was bought from New Logic Research Inc., USA. The other membranes were fabricated from purchased materials. These includes PVDF powder (polymer), N-methyl-2-pyrrolidone (NMP) solvent, and sodium dodecylsulfate (SDS) surfactant. The stated materials were purchased from Merck Hungary. The membrane preparation involves use of nanoparticles such as a multiwalled carbon nanotube (CNT; Kanto Chemical Co. Inc.; TNMH3 15090, Japan; Purity >98 wt. %), Aeroxide P25 type titanium dioxide (TiO₂; Merck EMD Millipore Co. Germany) and Bismuth vanadate (BiVO₄). Bismuth vanadate was synthesized from bismuth(III) nitrate pentahydrate (Bi(NO₃)₃·5H₂O; Alfa Aesar, ≥98%, ACS), nitric acid (HNO₃; Merck, 99%), sodium hydroxide (NaOH) (Sigma-Aldrich, 100%, puriss) and ammonium vanadate (NH₄VO₃; Sigma Aldrich, ≥98%). Bovine serum albumin (BSA, 69 kDa, ICN Biomedicals Inc. (USA) was used as model protein.

4.1.2. BSA model solution

Filtration performance experiments of the membranes were carried out with BSA solution, synthetic and real dairy wastewater. Since proteins are the primary fouling components in dairy wastewater, we used a bovine serum albumin (BSA) solution as a model for dairy wastewater in our study. A BSA solution with a concentration of 1g L⁻¹ was utilized as a model for dairy wastewater, as this concentration is representative of the protein content found in real dairy wastewater (Ding et al., 2019).

4.1.3. Synthetic dairy wastewater

Another model solution was synthetic dairy wastewater. This solution contains BSA and other chemical compounds (synthetic wastewater, SWW), and was prepared according to Muniz et al., 2020. The prepared synthetic dairy wastewater was labelled as SWW-BSA and is indicated in Table 3. To investigate the effect of lactose, lactose with various concentration levels (0, 0.5, 1 gL⁻¹) were considered in the synthetic dairy wastewater. SWW-BSA in the presence of lactose was labelled as SWW-BSA-L. The effect of pH on filtration performance of membranes was investigated by adjusting the pH of the synthetic dairy wastewater using sulphuric acid (1M) and Na₂HPO₄ (0.1M). Model protein solution, BSA, was used in all membranes while synthetic and real dairy wastewater were applied to pristine and best performing photocatalytic blended UF PVDF membranes.

Table 3: composition of synthetic dairy wastewater (SW-BSA)

Number	chemicals	Concentration in g/L
1	BSA	1
2	Ammonium chloride NH_4Cl	0.5833
3	Sodium dihydrogen phosphate NaH_2PO_4	0.9
4	Sodium bicarbonate	1.560
5	Magnesium sulphate heptahydrate $\text{MgSO}_4 \cdot \text{H}_2\text{O}$	0.6
6	Ferrous sulphate heptahydrate $\text{Fe}(\text{SO}_4) \cdot 7\text{H}_2\text{O}$	0.024
7	Manganese sulfate monohydrate $\text{MnSO}_4 \cdot \text{nH}_2\text{O}$	0.024
8.	Anhydrous Calcium chloride CaCl_2	0.036

4.1.3.1. Characterization of synthetic dairy wastewater

The characteristics of synthetic dairy wastewater without lactose and with lactose are presented in [Table 4](#) and [5](#) respectively. In the model dairy wastewater, the BSA concentration was measured before and after filtration using a spectrophotometric method. The method involved recording the absorbance of BSA at a wavelength of 280 nm with a UV-visible spectrophotometer (Hitachi Co., U-2000, Japan), and the concentration values were obtained from a calibration curve (Yan et al., 2021). The samples were analyzed without further treatment. To determine the chemical oxygen demand (COD) of the samples, the potassium-dichromate oxidation method was used. Specifically, 2 mL of the samples were added to test tubes (Merck) with concentrations of 0-150 or 0-1500 $\text{mg} \cdot \text{L}^{-1}$, and were digested for 2 hours at 150°C using the Lovibond ET 108 (Tintometer, Germany). The absorbances were then measured with a COD spectrophotometer (Lovibond PC-CheckIt, Tintometer, Germany). The turbidity of the samples was measured using a turbidimeter (Hach 2100AN, Germany).

Electrical conductivity (EC) and total dissolved solid (TDS) and pH were analyzed by multiparameter analyzer (Consort, Belgium). Parameters like Ca, CaCO_3 , ammonium (NH_4), ammonia (NH_3), total nitrogen- N, total Phosphorus-P and phosphate- PO_4 were analyzed by spectrophotometric analysis (Spectroquant Nova 60 Merck, Germany). Biological oxygen demand (BOD) was analyzed by BOD test using Lovibond Oxidirect (Tintometer, Germany). The values of all parameters were average of three samples.

Table 4. Characteristics of synthetic dairy wastewater (SW-BSA) with various level of salinity

Level of salinity	COD (mg·L ⁻¹)	Turbidity (NTU)	EC (mS)	Salinity (g·L ⁻¹)	TDS (g·L ⁻¹)	pH (-)
High salinity (EC > 4)	1154.33±4.22	46.67±3.05	4.14±0.01	2.2±0.00	2.17±0.01	7.5±0.00
Medium salinity (2 < EC < 4)	1148.33±6.80	21.83±1.16	2.33±0.01	1.1±0.00	1.25±0.01	7.5±0.02
Low salinity (EC < 2)	1155.67±2.89	8.16±0.01	1.59±0.01	0.8±0.00	0.85±0.01	7.5±0.00

Table 5. Characteristics of SW-BSA and SW-BSA-L

Level of lactose(g/L)	COD (mg·L ⁻¹)	Turbidity (NTU)	EC (mS)	Salinity (g·L ⁻¹)	TDS (g·L ⁻¹)	pH (-)
0	1154.33±4.22	46.67±3.05	4.14±0.01	2.2±0.00	2.17±0.01	7.5±0.00
0.5	1653.33±0.04	158.67±5.65	3.83±0.01	2.1±0.00	2.07±0.01	7.88±0.02
1	2316.66±0.04	188.33±6.50	3.80±0.00	2.1±0.00	2.23±0.01	7.81±0.00

4.1.4. Dairy wastewater

Real dairy wastewater was collected from nearby milk processing industry and kept at 0 °C. The physico-chemical characteristics of real dairy wastewater are shown in [Table 6](#).

Table 6. Physico-chemical characteristics of real influent industrial dairy wastewater

Parameter	Average of three samples	SD
pH	7.09	0.02
colour	colour-milky white	
EC (mS)	2.1	0.01
TDS (g L^{-1})	1.11	0.01
BOD (mg L^{-1})	2181	70.71
COD (mg L^{-1})	3770	20.00
Ca (mg L^{-1})	159.67	4.04
CaO (mg L^{-1})	231	1.00
CaCO ₃ (mg L^{-1})	412.33	2.52
NH ₄ (mg L^{-1})	56.87	0.31
NH ₄ N (mg L^{-1})	44.15	0.39
NH ₃ (mg L^{-1})	53.31	0.38
NO ₃ (mg L^{-1})	10.05	0.83
NO ₂ N (mg L^{-1})	2.2	0.20
TOTAL N (mg L^{-1})	74.33	1.15
PO ₄ (mg L^{-1})	1178.33	3.51
PO ⁴ -P (mg L^{-1})	40.43	2.60
P ₂ P ₅ (mg L^{-1})	89.61	1.65
TOTAL P (mg L^{-1})	39.10	1.68

4.2. Synthesis and characterizing methods for bismuth vanadate

BiVO_4 nanoparticle described as the BiVO_4 -I sample in the earlier study of [Nascimben et al, \(2020\)](#) was synthesized by hydrothermal method. It was proved, that the nanoparticles were stable, with a narrow a band gap of 2.35 eV ([Nascimben et al, 2020](#)).

The photocatalytic activity of the synthesized BiVO_4 and other used photocatalysts were examined by $1 \text{ g} \cdot \text{L}^{-1}$ BSA and methylene blue (MB) ($10^{-5} \text{ mol} \cdot \text{L}^{-1}$) degradation under visible light irradiation. The experiments were performed using 100 mL of $10^{-5} \text{ mol} \cdot \text{L}^{-1}$ methylene blue solution ([Lamdab et al., 2016](#)) with $1 \text{ g} \cdot \text{L}^{-1}$ of BiVO_4 in a thermostated (25°C) double-walled glass photoreactor, equipped with a 1 m long LED strip (5050 SMD type, ‘cool white’) ([Figure 7](#)). Before the photocatalytic experiments, nanoparticle composites were suspended in 99 mL of ultrapure water and ultrasonicated (Hielscher UP200S) for 3 minutes, then 1 mL of concentrated ($10^{-3} \text{ mol} \cdot \text{L}^{-1}$) MB solution was added, then the suspension was kept in dark for 30 minutes under stirring to reach the adsorption-desorption equilibrium and to determine the amount of adsorbed MB. Then, the suspension was irradiated with the visible light under intensive stirring with a magnetic stirrer. During the photocatalytic experiments samples were taken and centrifuged (Thermo Scientific Megafuge 16R) at 13000 rpm for 2 minutes, then the supernatants were filtered with a $0.25 \mu\text{m}$ syringe filter and the absorbance for MB and BSA were measured at $\lambda=664 \text{ nm}$ and $\lambda=280 \text{ nm}$ respectively, using a spectrophotometer (Biochrom Biowave II⁺). The same procedure was applied for TiO_2 , $\text{TiO}_2\text{-CNT}$, $\text{BiVO}_4\text{-CNT}$ and $\text{TiO}_2\text{-CNT-BiVO}_4$ samples for comparison with the following composition: 100% BiVO_4 consists of 0.1 g BiVO_4 in 100 ml MB solution; 100% TiO_2 consists of 0.1 g TiO_2 in 100 ml MB solution; $\text{TiO}_2\text{-CNT}$ consists of 98% TiO_2 and 2% CNT as 0.098 g TiO_2 and 0.002 g CNT; $\text{BiVO}_4\text{-CNT}$ consists of 98% BiVO_4 and 2% CNT as 0.098 g BiVO_4 and 0.002 g CNT.

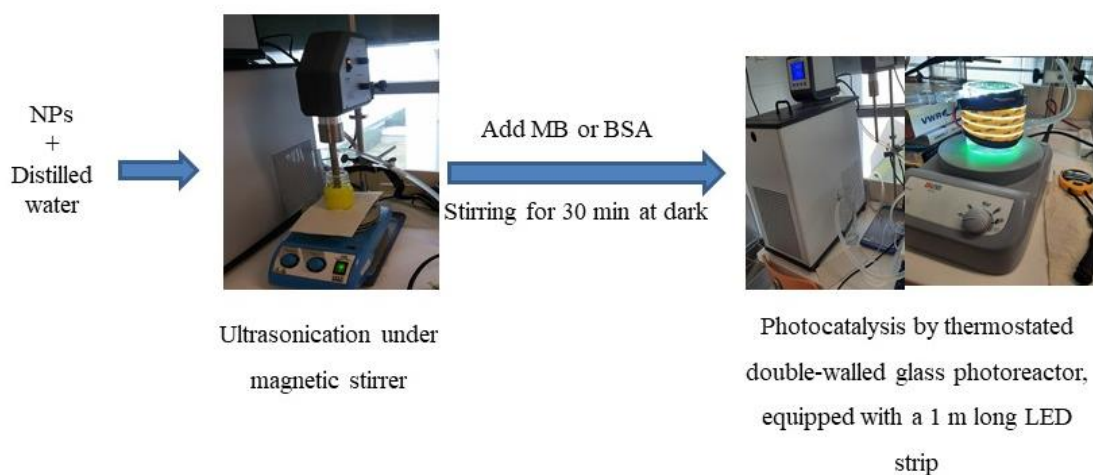


Figure 7. Visible light driven photocatalytic test

4.3. Membrane filtration experiments

Filtration experiments were carried out using a dead-end filtration cell (Millipore, XFUF04701, USA) (Fig.8). Prior to filtration experiment, for compaction, distilled water was allowed to pass at 0.1 MPa through 0.0035 m² membrane for 30 minutes. Volume reduction ratio (VRR) of each experiment was fixed to be five and obtained using volume of the feed (V_F) (m³) and permeate (V_P) (m³) the following equation:

$$VRR = \frac{V_F}{V_F - V_P} \quad \text{Eqs(1)}$$

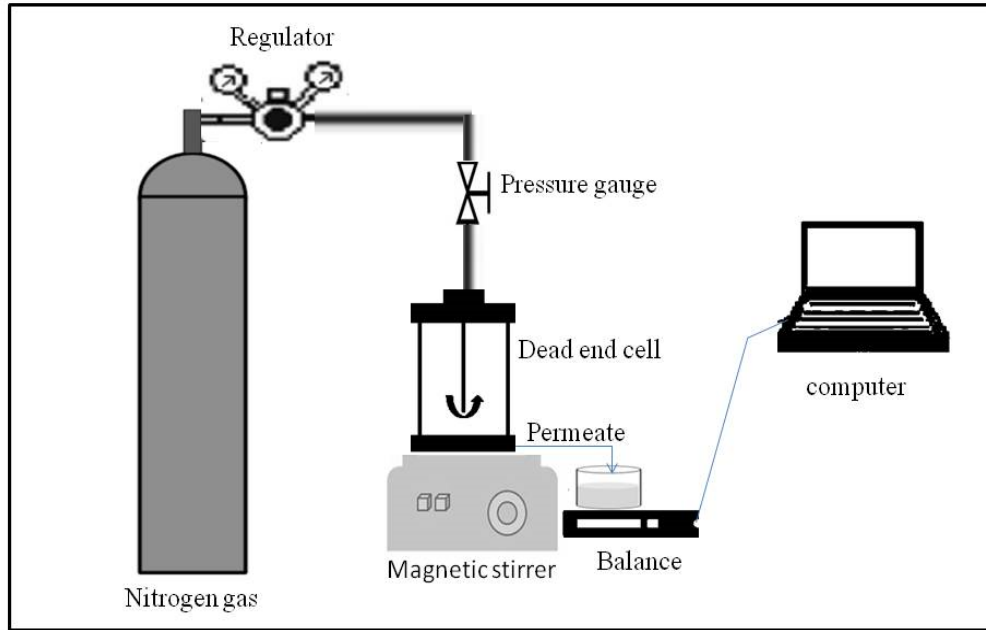


Figure 8. Graphical illustration of the dead-end filtration setup

4.4. Photocatalyst-coated membrane preparation by physical deposition

As indicated in Fig.9 showed modification of commercial PVDF membranes by physical deposition method (Kovács et al., 2018). In this method 0.04 g commercial TiO₂ Aeroxide P25 was added to 100 ml of i-propanol and ultrasonicated for 3 minutes. Then, the ultrasonicated solution was allowed to pass through a membrane in a dead-end cell at 0.3 MPa and dry for 1hr at room temperature before use. The modified membranes were used to filter 1 g·L⁻¹ bovine serum albumin (BSA) (Ding et al., 2019).

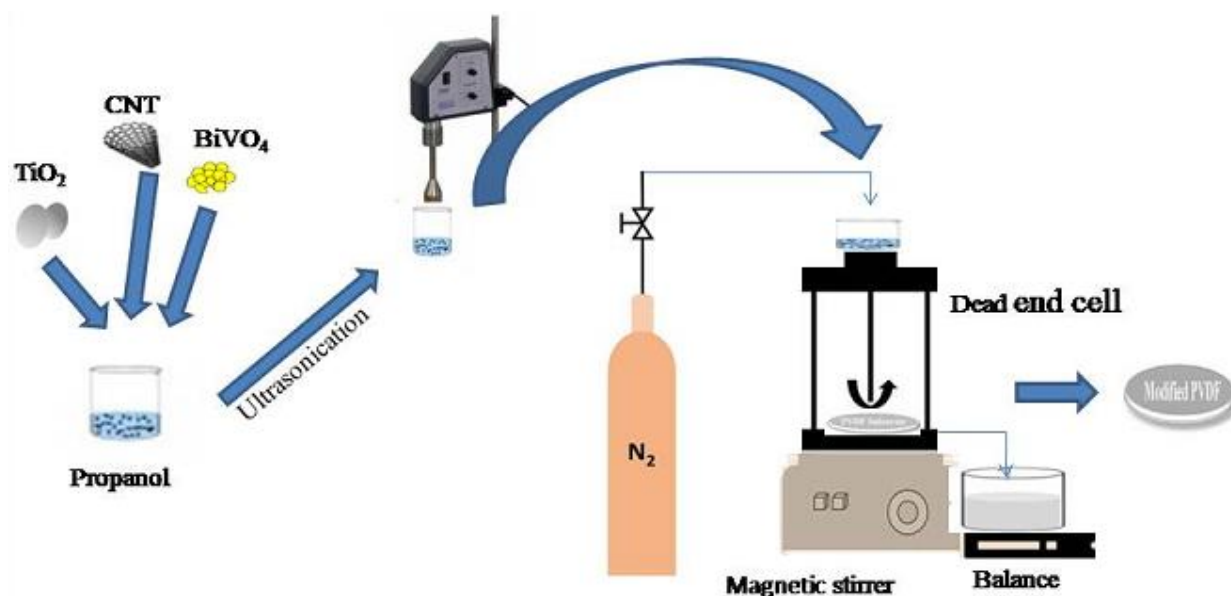


Figure 9. Graphical representation of membrane preparation by physical deposition

The labelling of the samples (Table 7.) follows the preparation method and composition of membranes as C is referring to “coated” membranes, P is the membrane material (PVDF), T is the titanium dioxide, C is the carbon nanotube and B is the bismuth vanadate. The numbers represent the ratio of the last nanoparticle in the nanoparticle mixtures. The detailed loading and ratios of TiO_2 and CNT or BiVO_4 is listed in Table 7.

Table 7. Loading and ratio of TiO_2 and CNT

Membrane	TiO_2 (g)	CNT (g)	BiVO_4 (g)	Membrane description
PVDF	-	-	-	PVDF without nanoparticles
C-PT100	0.04	-	-	Coated (C) PVDF with 100 wt% TiO_2
C-PTC2	0.0392	0.0008	-	C-PVDF with 98 wt% TiO_2 and 2 wt% CNT
C-PTC5	0.038	0.002	-	C-PVDF with 95 wt% TiO_2 and 5 wt% CNT
C-PTC10	0.036	0.004	-	C-PVDF with 90 wt% TiO_2 and 10 wt% CNT
C-PTC15	0.034	0.006	-	C-PVDF with 85 wt% TiO_2 and 15 wt% CNT
C-PTC100	-	0.04	-	C-PVDF with 100 wt% CNT
C-PTB2	0.0392	-	0.0008	C-PVDF with 98 wt% TiO_2 and 2 wt% BiVO_4
C-PTB5	0.038	-	0.002	C-PVDF with 95 wt% TiO_2 and 5 wt% BiVO_4
C-PTB10	0.036	-	0.004	C-PVDF with 90 wt% TiO_2 and 10 wt% BiVO_4
C-PTB15	0.034	-	0.006	C-PVDF with 85 wt% TiO_2 and 15 wt% BiVO_4
C-PB100	-	-	0.04	C-PVDF with 100 wt% BiVO_4

Stability of the photocatalyst-coated membranes were examined by investigating the change in flux, turbidity and mass after all coated membranes were left overnight in the stirring cell of 200 ml 300 rpm for 24 h. The mass retention ratio (MR) can be calculated by the following equation (Kovács et al., 2017).

$$MR(\%) = W_f/W_i * 100 \quad \text{Eqs (2)}$$

where W_f is the final mass of coated membrane, W_i is the initial mass of the membrane to be coated.

4.5. Photocatalyst blended membrane preparation by phase inversion method

Pristine and photocatalyst blended membranes were prepared by phase-inversion method using TQC sheen automatic film applicator (AB4120 081, Netherlands) (Fig. 10.). The preparation of the casting dope solution for membrane fabrication is shown in Table 8. The photocatalysts and PVDF powder were dried in an oven at a temperature of 80 °C for 4 h. Dried PVDF powder was added to 60 s ultrasonicated photocatalysts in 20 mL of *NMP* solution and kept at 50 °C for 12 h with stirring and 12 h without stirring in dark. The dope solution was allowed to perform 30 minutes ultrasonication aimed to remove air bubbles of the dope solution. Then, the dope solution was spread by 400 μm thick casting blood in a glass plate and subjected to 30 s for skin layer formation. The glass plate along with membrane was immersed in a bath solution containing 3 $\text{g} \cdot \text{L}^{-1}$ of sodium dodecylsulphate (SDS) surfactant at 10 °C for 3 h. In the coagulation bath the phase inversion takes place between water and *NMP* to form the pores of the membrane while the sodium dodecyl sulphate was used to prevent pore blockage and clean the pores. Finally, the membrane was cut in a desired size to explore membrane characteristics and conduct filtration experiments.

The labelling of the samples (Table 8.) follows the preparation method and composition of membranes as B is referring to “blended” membranes, P is the membrane material (PVDF), T is the titanium dioxide, C is the carbon nanotube and B is the bismuth vanadate. The numbers represent the ratio of the last nanoparticle in the nanoparticle mixtures. The detailed loading and ratios of TiO_2 and CNT or BiVO_4 is listed in Table 8.

Table 8. Loading composition and abbreviation of blended (B) hybrid membranes

Membrane	17.5wt % (16,5% PVDF + 1% nanoparticles)				82.5 wt % (Solvent)
	PVDF (g)	TiO ₂ (mg)	CNT (mg)	BiVO ₄ (mg)	NMP (mL)
PVDF	4.375	---	---	---	20
B-PT100	4.331	43.750	-	-	20
B-PTC2	4.331	42.875	0.875	-	20
B-PTC5	4.331	41.560	2.190	-	20
B-PTC10	4.331	39.375	4.375	-	20
B-PTC15	4.331	37.188	6.5625		20
B-PTB25	4.331	32.813	-	10.938	20
B-PTB50	4.331	21.875	-	21.875	20
B-PTB75	4.331	10.938	-	32.813	20
B-PB100	4.331	-	-	43.750	20
B-PTCB25	4.331	31.938	0.875	10.938	20
B-PTCB50	4.331	21.000	0.875	21.875	20
B-PTCB75	4.331	10.061	0.875	32.813	20

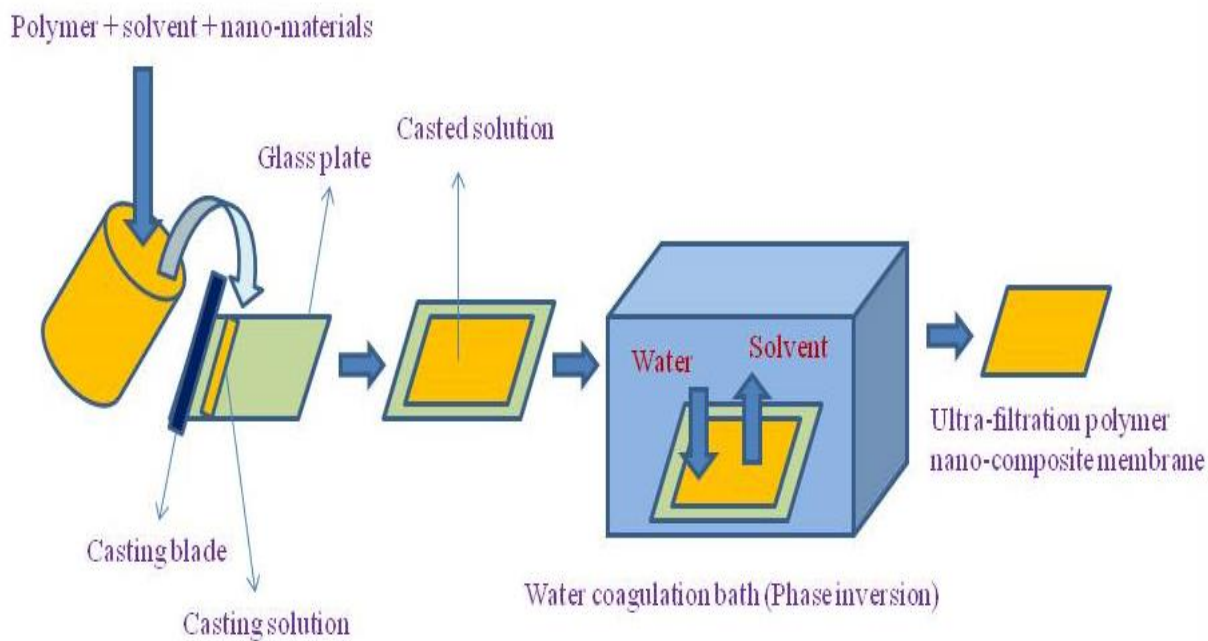


Figure 10. Graphical illustration of membrane fabrication by phase inversion method

4.6. Membrane characterization methods

4.6.1. Porosity of the prepared membranes

Porosity values of the prepared membranes were obtained using equations (3)-(4) (Srivastava et al., 2011). (As several works proved the applicability of this method (Hudaib et al, 2018; Farahani and Vatanpour, 2018; Ayyaru et al., 2019), it was applied without further stability checking.) Firstly, the water was removed from the membrane surface by wiping it out than the weight of the wet membrane was measured. Secondly the dry weigh of the membrane was measured after wet membrane was dried at 80 °C in a vacuum oven for 12 h. Finally, the porosity (ε) was calculated using

$$\varepsilon = \frac{W_1 - W_2}{\rho_w \cdot V_T} \cdot 100 \quad \text{Eqs (3)}$$

$$V_T = \frac{W_1 - W_2}{\rho_w} + \frac{W_2}{\rho_{md}}, \quad \text{Eqs (4)}$$

where W_1 (kg), W_2 (kg) and V_T are the wet, dry weight, volume of the membrane in the wet state (m^3) respectively, $\rho_w = 997 \text{ kg m}^{-3}$ is the density of water and $\rho_{md} = 1785 \text{ kg m}^{-3}$ is the density of membrane in the dry state.

Pore sizes, mean pore radius (r_m) of the membranes were obtained by filtration velocity method using Guerout–Elford–Ferry equation Eqs (5) (Ayyaru et al., 2019).

$$r_m = \sqrt{\frac{(2.9 - 1.75\varepsilon) \cdot 8\eta l Q}{\varepsilon \cdot A \cdot P}}, \quad \text{Eqs (5)}$$

where η is the dynamic viscosity of water ($8.9 \cdot 10^{-4} \text{ Pas}$ at 25°C); Q is volume flow (m^3s^{-1}), and l is thickness ($400 \mu\text{m}$), ε is porosity, A is the area (m^2); and P is pressure (Pa).

Pristine PVDF, B-PT100 and B-PB100 membranes were also characterized using Brunauer–Emmett–Teller (BET) model. Nitrogen adsorption–desorption isotherms were recorded on a Quantachrome Nova 3000e instrument at -196°C . Brunauer–Emmett–Teller (BET) model were used to calculate the total pore volumes (V) and apparent surface areas (S_{BET}). The total pore volumes (V) were determined based on the assumption that the pores are filled with liquid nitrogen and were obtained from the amount of nitrogen adsorbed at relative pressure $p/p_0 \rightarrow 1$. Barrett–Joyner–Halenda (BJH) method was applied to estimate pore size distribution from the desorption isotherms. The average pore diameter was obtained by using Equation (6).

$$d = \frac{4V}{S_{\text{BET}}} \quad \text{Eqs (6)}$$

where S_{BET} is the specific surface area (m^2) obtained using the BET model.

4.6.2. Membrane hydrophilicity

Hydrophilicity of the membranes were described by measuring contact angle using the sessile-drop method with a suitable contact angle measuring instrument (OCA15Pro, Dataphysics, Germany).

The software (ImageJ) was fixed to drop 10 μL of ultrapure water from micro-syringe onto the membrane surface. Then the image of the water droplet was recorded through a digital camera. Average of six parallel measurements were considered.

4.6.3. Membrane surface characterization

Scanning electron microscope (SEM) analysis were performed to determine membranes' surface morphology. A Hitachi S-4700 Type II scanning electron microscope (SEM) was used to conduct the analysis, applying a 10 kV accelerating voltage. To determine the elements, present in the fouled membrane, 200 mL of BSA solution (1 gL^{-1}) was filtered through the membrane and then air-dried without washing. Röntec X-Flash energy dispersive X-ray (EDX) detector was used for the analysis at a voltage of 20 keV. The BSA coverage on the membrane surface was quantified using the N/F ratio, which was calculated from the nitrogen (N) and fluorine (F) contents of the membrane (measured as both atomic percent and weight percent using the instrument).

X-ray diffraction (XRD) analyses were carried out using a Rigaku MiniFlex II diffractometer at 30 kV and 15 mA using $\text{Cu-K}\alpha$ radiation ($\lambda=0.015406 \text{ nm}$). The analysis was done to explore the crystallinity of the nanoparticles in the membranes, and the XRD patterns were performed between 20 and 40° (2θ). Scherrer equation were used to calculate the primary crystallite sizes of the nanoparticles (Holzwarth and Gibson, 2011).

Atomic force microscope (AFM; South Korea; NC-AFM) with a PSIA XE-100 was used in head mode, applying $10 \times 10 \mu\text{m}$ scan size to investigate the surface roughness.

Zeta potentials were calculated from measurements of streaming potential using Helmholtz-Smoluchowski (H-S) equation (Lawrence et al., 2006). Adjustable Gap Cell of SurPASS 3 was used to measure the streaming potential. Two samples with identical surfaces were secured onto sample holders with a cross-sectional area of $20 \text{ mm} \times 10 \text{ mm}$ using double-sided adhesive tape. The distance between the sample surfaces was adjusted by reducing the gap of the flow channel continuously until it reached $110 \pm 10 \mu\text{m}$. The surface zeta potential was determined in a potassium chloride (KCl) electrolyte solution of concentration 0.001 M in the pH range of 1-9. Zeta potential and streaming potential are explained by Helmholtz-Smoluchowski equation (7) (Lawrence et al., 2006).

$$\zeta = \frac{\Delta E}{\Delta P} \cdot \frac{\eta}{\epsilon_{\text{rel}} \cdot \epsilon_0} \cdot K_B \quad \text{Eqs (7)}$$

where ζ is the apparent zeta potential (mV), $\frac{\Delta E}{\Delta P}$ is the streaming potential developed as a result of an applied pressure gradient (V), η and ϵ_{rel} are the dynamic viscosity (Pas) and dielectric coefficient

of water (-), ϵ_0 is the permittivity of vacuum (Fm^{-1}), K_B is the electric conductivity of the aqueous solution ($\text{S}\cdot\text{m}^{-1}$).

In order to determine the reliability of the zeta potential analysis, the streaming potential was measured within a certain pressure range and the slope of the linear dependence (streaming potential vs. pressure difference) was determined and used as $\frac{\Delta E}{\Delta P}$ in calculation of surface zeta potential (Eqs (7)). Strictly linear dependence of streaming potential on the pressure gradient was observed ($R^2 > 0.99$), indicating the high reliability of the analysis.

During the measurement of zetapotential in the function of pH, the pH was scanned first at neutral pH, commenced towards the acidic range and the isoelectric point (rinsed the sample with deionized water and fresh 0.001 mol/l KCl solution and continued with a titration towards the alkaline range. The measurements showed that the zetapotential was stabilized at pH 8, thus generally the scan terminated at this pH.

4.6.4. Filtration performance of the membranes

Fluxes were obtained by Equation (8):

$$J = \frac{W}{A \cdot t}, \quad \text{Eqs (8)}$$

where J refers to the flux ($\text{kgm}^{-2}\text{h}^{-1}$), W refers to the weight of permeate (kg), A means the effective surface area of the membrane (m^2), t means time (h).

The reduction in water flux during membrane filtration is attributed to a decrease in the driving force (transmembrane pressure) and/or an increase in membrane resistance. On the basis of filtration theory, Darcy's equation can be used to model the permeate flux in the case of low feed concentrations and low transmembrane pressures, which are relevant to natural water filtration.

$$J = \frac{\Delta p}{R_T \eta_{ww}} \quad \text{Eqs (9)}$$

where J is the flux ($\text{Lm}^{-2}\text{h}^{-1}$), Δp is the transmembrane pressure (Pa), R_T is the the total resistance (m^{-1}), η is the dynamic viscosity of wastewater (Pas).

The resistances which can occur during a filtration process are membrane resistance (R_M), fouling resistances include reversible (R_{rev}) and irreversible resistances (R_{irr}), while the total resistance (R_T) can be calculated as a sum of membrane resistance, reversible and irreversible resistance, according to the resistances-in-series model, as shown in Table 9. Fluxes were measured in clean membrane, after filtration of wastewater and after rinsing the used membrane with distilled water, and were calculated by Equation (10)-(13)) (Vatanpour, et al., 2016; Nascimben et al, 2020).

Table 9. Filtration resistance formulas

Filtration resistances (m^{-1})	Formula
Membrane resistance	$RM = \frac{\Delta P}{J_0 \cdot \eta_w}$ Eqs (10)
Irreversible resistance	$R_{irrev} = \frac{\Delta P}{J_w \cdot \eta_w} - RM$ Eqs (11)
Reversible resistance	$R_{rev} = \frac{\Delta P}{J_w \cdot \eta_{ww}} - RF - RM$ Eqs (12)
Total resistance	$RT = RM + R_{irr} + R_{rev}$ Eqs (13)

where, Δp is the change of pressure (Pa), J_0 is water flux of clean membrane, J_w is the water flux of the fouled membrane, J_w is the water flux after the fouled membrane is rinsed ($\text{L}\cdot\text{m}^{-2}\text{h}^{-1}$), η_w is the dynamic viscosity of water (Pas), and η_{ww} is the dynamic viscosity of wastewater (Pas).

The examination of antifouling performances of the membranes prepared was carried out using the flux recovery ratio (FRR), which was calculated using equation (14).

$$\text{FRR} = \frac{J_c}{J_0} \cdot 100\% \quad \text{Eqs (14)}$$

where J_0 is the water flux of clean membrane ($\text{L}\cdot\text{m}^{-2}\text{h}^{-1}$) and J_c is the water flux of used membrane after cleaning ($\text{L}\cdot\text{m}^{-2}\text{h}^{-1}$) in the same experiment.

The efficiency of membrane regeneration was evaluated by conducting flux recovery experiments in the photocatalytic membrane reactors. In this experiment, the water fluxes were measured after the membrane was flushed with distilled water following BSA filtration. The fluxes were remeasured after 3 h and 21 h UV (360 nm, in case of TiO_2 and/or CNT containing composites) or visible light (“cool white”, in case of BiVO_4 -containing composites) irradiation to describe the efficiency of photocatalytic flux recovery.

The protein rejection was calculated by:

$$\text{Rejection}(\%) = \frac{c_1 - c_2}{c_1} \cdot 100\% \quad \text{Eqs (15)}$$

where c_1 is the concentration of feed, and c_2 is concentration of permeate.

4.6.5. Data analysis

One-way analysis of variance (ANOVA) was performed using Stata17 statistical software program Besides, Microsoft Excel program was used for performing calculation of standard deviations. In all cases at least three parallel measurements were performed.

5. Results and discussion

5.1. Photocatalytic activities of bismuth vanadate and nanoparticle mixtures

The photocatalytic activity of the synthesized BiVO_4 , the pure TiO_2 and TiO_2 -CNT, BiVO_4 -CNT and TiO_2 -CNT- BiVO_4 mixtures of photocatalysts were assessed by examining methylene blue (MB) degradation using visible light for the excitation of the photocatalysts (Fig. 11a). In this figure, the first 30 minutes represents the adsorption of MB in dark by the nanoparticles, which followed this order: TiO_2 - BiVO_4 -CNT > BiVO_4 -CNT > BiVO_4 > TiO_2 -CNT > TiO_2 , which show, that the BiVO_4 composites has higher adsorption capacity than TiO_2 composites. Comparing the degradation rate after the dark adsorption (Fig. 11b) the results show that BiVO_4 -composites show higher degradation rate than TiO_2 -composites; this is due to large visible light absorbance potential of BiVO_4 (Sadeghzadeh-Attar, 2020). This result revealed that the synthesized BiVO_4 has excellent photocatalytic activity under visible light. Negligible degradation of MB in absence of any catalyst also proved that MB is stable in visible-light irradiation. The presence of CNT in the mixture resulted in higher degradation rate of MB; probably enhanced electron-hole separation by CNT (Barakat et al., 2020), which may increase the overall quantum yield of the photocatalytic reactions. And the mixture containing all of nanoparticles (TiO_2 - BiVO_4 -CNT) was the most effective in MB degradation.

Similar result was obtained in the next series of experiments, where photocatalytic activity of BiVO_4 and TiO_2 - BiVO_4 -CNT composite were compared in presence of BSA (Fig 11 cd); better BSA degradation was observed by TiO_2 - BiVO_4 -CNT composite as compared to BiVO_4 .

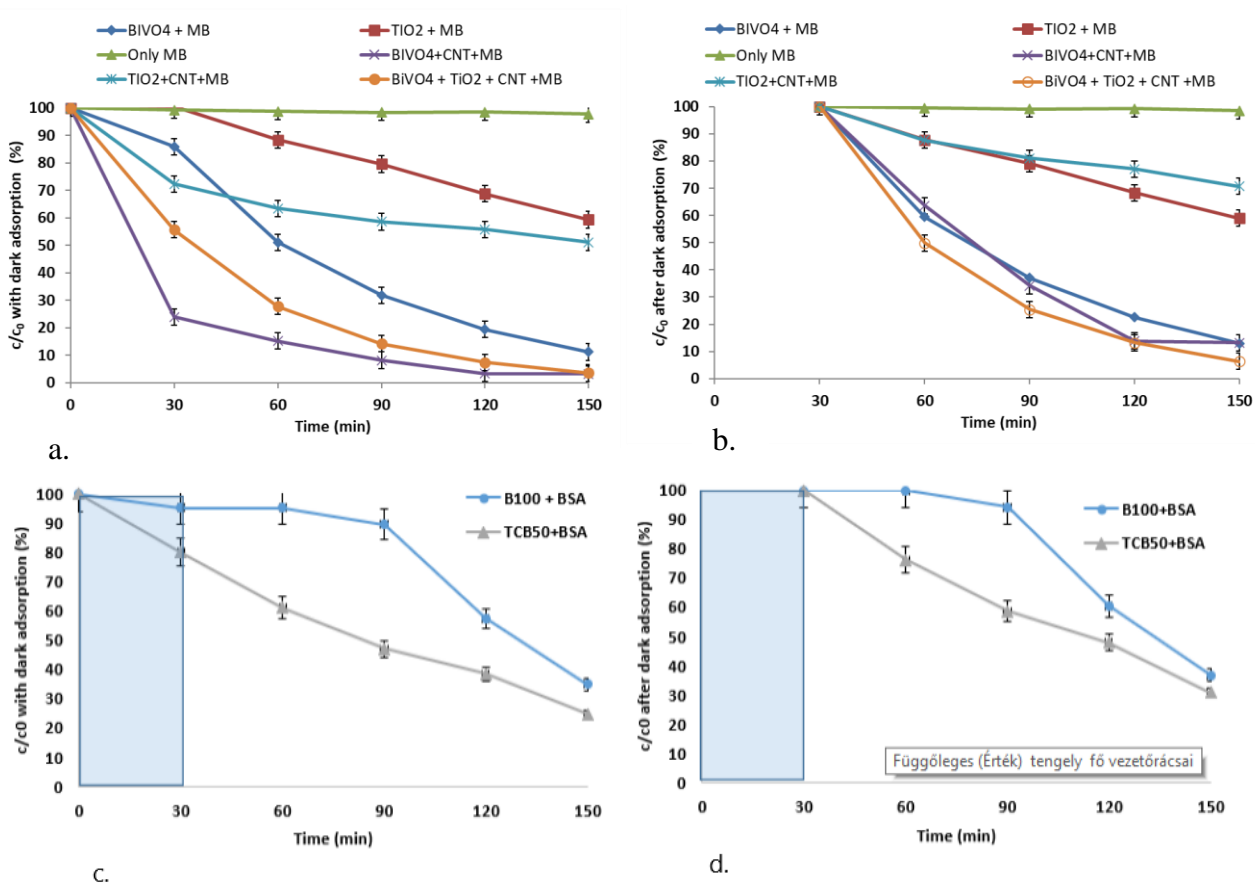


Figure 11. Photocatalytic activity of nanoparticles, described by the absorbance reduction of methylene blue or BSA during 30 min dark adsorption, followed by 120 min VIS irradiation. a. MB concentration decrease in the solution by adsorption and photodegradation. b. MB concentration decrease in the solution by photodegradation after adsorption, c. BSA concentration decrease in the solution by adsorption and photodegradation. b. BSA concentration decrease in the solution by photodegradation after adsorption.

5.2. Performance of physically coated membranes

The aim of the experiment was to investigate and compare the performance of the physically coated photocatalytic UF PVDF membrane and pristine PVDF membrane. In this experiment physically coated photocatalytic membranes were prepared, by covering PVDF membranes with TiO_2 or TiO_2 -CNT mixtures containing different ratio of CNT or TiO_2 - BiVO_4 mixtures containing different amount of BiVO_4 (see Table 7.) Comparison were performed between the filtration and regeneration performance of the photocatalytic membranes and pristine PVDF membrane, and among the photocatalytic membranes.

5.2.1. Investigation of stability of nanoparticle-coated membranes

TiO_2 -coated PVDF membranes were prepared by physical deposition and were investigated for stability of the membrane using mass retention ratio (MR), flux retention ratio (FR) and turbidity parameters. MR and FR were 98.13 %, and 99.14 % respectively. Besides, the turbidity of 40 mg TiO_2 coated membrane which were left overnight in the string cell of 200 ml at 300 rpm for 24 h is compared with turbidity of 5mg, 10 mg, 20 mg of TiO_2 in 200 ml (Table 10). As we can see from Table 10 the turbidity of the coated membrane is insignificant as compared with turbidities of 5 mg, 10 mg and 20 mg TiO_2 solution. Thus, the results revealed that there is slight leaching of TiO_2 coated membrane.

Table 10. Turbidity of distilled water containing TiO_2 coated membrane and various concentration of TiO_2

No	Items in 200 ml distilled water	Turbidity (NTU)
	Distilled water only	0.075± 0.00
1	40 mg TiO_2 coated membrane	1.55± 0.07
2	5 mg of TiO_2	90.63± 0.27
3	10 mg of TiO_2	190± 1
4	20 mg of TiO_2	450.33± 2.89

5.2.2. Characterization of nanoparticle-coated membranes

5.2.2.1. Water contact angle measurements

Hydrophilicity of the prepared membranes was examined by measuring water contact angle and were presented by mean \pm standard deviation (STDEV) of six sample points. The values are indicated in Table 11. The contact angle of the pristine PVDF membrane was 75.1 ± 3.63 , which means slightly hydrophilic nature. Contact angle values below 90° mean, that the water droplet spreads out on the membrane surface, showing that it is hydrophilic. It was found that the addition of TiO_2 made the PVDF membrane very hydrophilic (0° contact angle means, that the droplet is diminishing, completely spreading on the surface), which is positively affect the water permeability of the membranes. Addition of CNT also decreased the contact angle, the membrane covered by CNT without TiO_2 (C-PC100) also has high hydrophilicity. The possible explanation of the effect of CNT could be related to formation of hydrophobic-to-hydrophobic bond between the open ends of CNT and PVDF that lead fluoride ions of PVDF to make hydrophilic membranes and increased surface negative charge density (Dhand et al., 2019). However, better result was obtained by adding TiO_2 -CNT mixture with 2% CNT content. Further increasing of CNT ratio resulted in decreasing hydrophilicity, probably due to its hydrophobic nature compared to TiO_2 . A similar study by Farahani and Vatanpour (2018) indicated hydrophilicity improvement of pristine PVDF membrane by nanoparticles. Addition of BiVO_4 was also exhibited a decreasing trend of CA, this is due to the hydrophilic nature of BiVO_4 .

Table 11. Contact angle of TiO_2 -CNT and TiO_2 - BiVO_4 coated membranes.

no	Membrane	Contact angle ($^\circ$)
1	PVDF	75.1 ± 3.63
2	C-PT100	0
3	C-PTC2	0
4	C-PTC5	13.17 ± 1.54
5	C-PTC10	30.73 ± 4.21
6	C-PTC15	25.3 ± 1.93
7	C-PC100	23.92 ± 0.8
8	C-PTB2	69.05 ± 1.99
9	C-PTB5	72.22 ± 2.21
10	C-PTB10	71.43 ± 3.34
11	C-PTB15	71.45 ± 1.99
12	C-PB100	72.22 ± 2.37

5.2.2.2. Zeta potential of nanoparticle-coated PVDF membranes

As indicated in Fig. 12, zeta potential is decreasing as pH is increasing. The isoelectric points (IEP) for pristine and TiO_2 -PVDF coated (C-PT) membrane was observed at the at pH 4 and 3.6 respectively. The zeta potential of both membranes was negative at neutral pH and had zeta potential of -50 mV and -19 mV respectively. The zeta potential result indicated that the electrical property of pristine membrane is changed by TiO_2 . The zeta potential result indicated that the electrical property of pristine membrane is changed by TiO_2 . PVDF- BiVO_4 membranes show similar changes, their zeta potential change parallel with PT-coated membrane. On the other hand, addition of carbon nanotubes had no effect on zeta potential below pH 5, while at higher pHs the zeta potential increased with CNT concentration, at neutral pH it was only -7.5 and -16 mV in case of 10% and 5% CNT containing membranes.

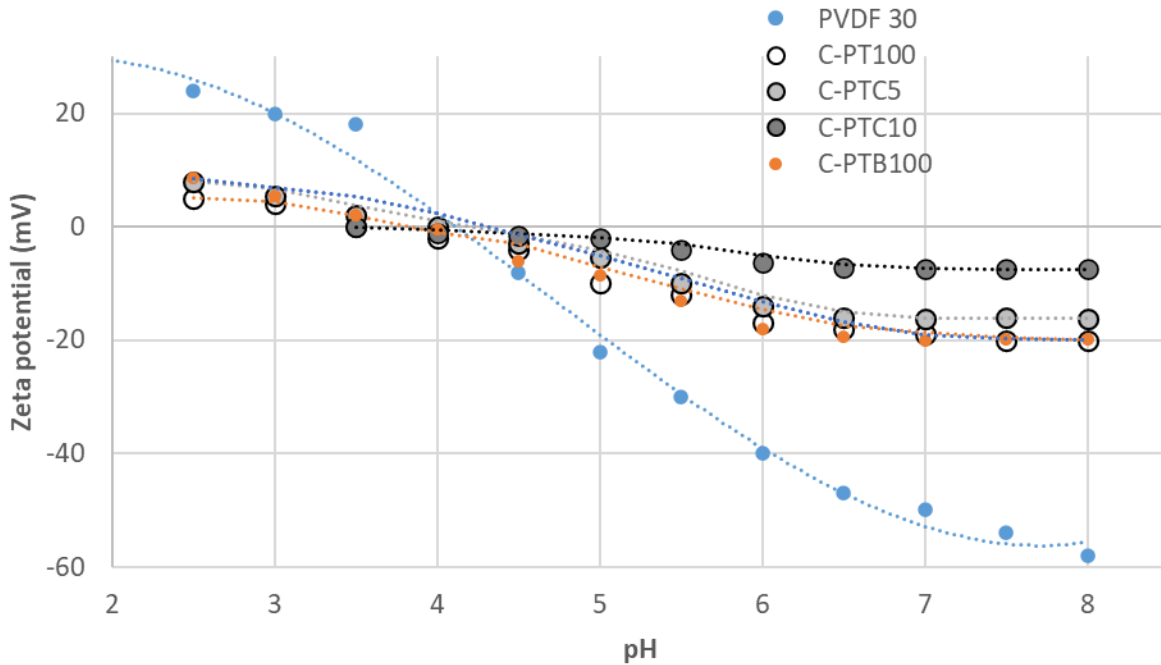


Figure 12. pH dependence of Zeta potential for pristine and TiO_2 coating PVDF membrane

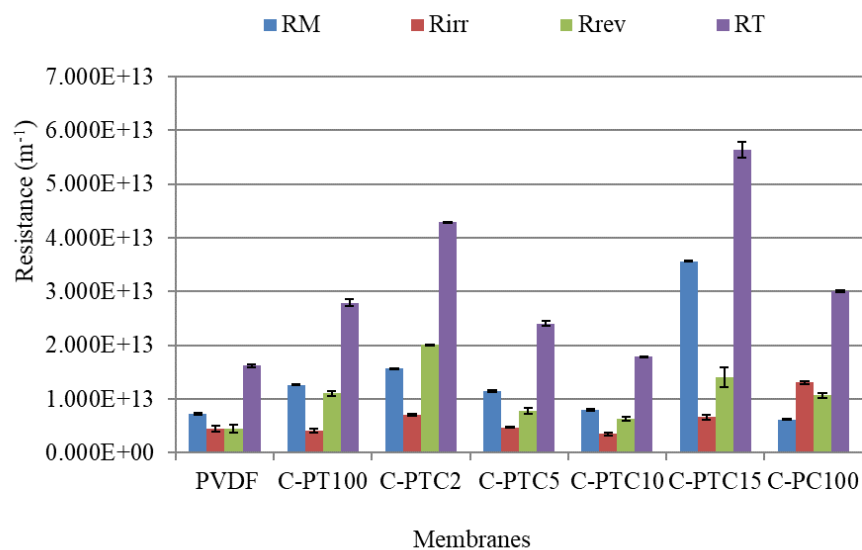
5.2.3. Filtration performance of pristine and physically coated PVDF membranes

The aim of this experiment was to investigate and compare the effects of coating nanoparticles on filtration performance of PVDF membrane. In this experiment physically coated C-PVDF- TiO_2 , C-PVDF- TiO_2 -CNT and C-PVDF- TiO_2 - BiVO_4 membranes were prepared. Comparisons were

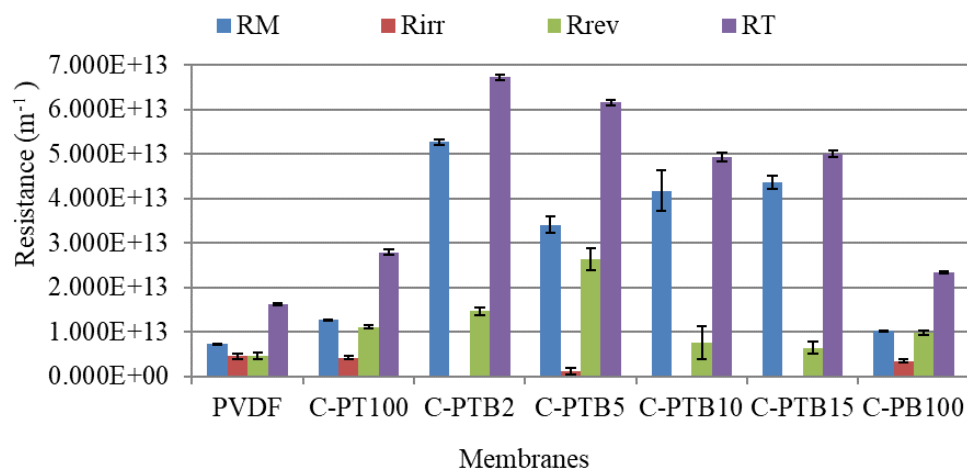
performed between the filtration and regeneration performance of the coated PVDF membranes and pristine PVDF membrane, and among the coated PVDF membranes.

5.2.3.1. Effects of nanoparticle coating on flux and filtration resistances during filtration of model wastewaters

In order to reveal the effect of nanoparticles on filtration performance, filtration resistances were calculated from fluxes of BSA containing model wastewater filtration by means of resistances-in-series method. Membrane resistance (RM), irreversible resistances (R_{irr}), reversible resistances (R_{rev}) and total resistances (RT) which were calculated by means of Eqs. (10)–(13). The lowest filtration resistance was observed by pristine membrane (Fig.13 a.). It was found that modification with TiO_2 and CNT significantly increased the total filtration resistances which may be associated to pore blockage or additional coating layer formed by the nanoparticle. It is proved by the increased reversible resistances, which can be easily removed from the surface of the membrane by rinsing. Our results are in accordance with the earlier observations (Ismail et al., 2013; Ding et al., 2019), who were found that adding more nanoparticles such as TiO_2 on the membrane surface leads to blockage of pores and reduced water flux. To get more sophisticated analysis of the results ANOVA was performed for these data and regression results show that there is no significant difference among the replication but there was significant difference between the pristine PVDF membrane (control) and treatment (modified membrane) for total and irreversible resistances (Appendix 1, 2, 3 and 4).



(a)



(b)

Figure 13. Filtration resistances of TiO₂-CNT coated PVDF membranes (a) and TiO₂-BiVO₄ coated PVDF membranes (b)

5.2.3.2. Effects of nanoparticle coating on rejection of BSA

In the next series of experiments BSA and COD rejections for TiO_2 -CNT coated PVDF membranes (a) and TiO_2 - BiVO_4 coated PVDF membranes (b) were investigated and compared (Fig. 14). It was found that TiO_2 -CNT coated PVDF membranes exhibited a gradual decreasing trend of BSA and COD rejection performance as CNT content increased. Pristine PVDF membrane performed better BSA (86%) and COD (83%) rejection as compared to C-PT100 or C-PC100 or all TiO_2 -CNT coated PVDF membranes. This is a very surprising result as the modification increased filtration resistances, thus it was expected, that the enhanced irreversible and reversible resistance would lead to increased protein rejection. However, this result is similar to the result obtained by Farahani and Vatanpour (2018). One possible explanation may be related to the effect of the nanoparticles' surface on the protein structure, resulted in changed the structure, behaviour, and function of proteins. These changes may allow the protein to easily pass the membrane and reduce rejection. Another possible reason could be the tendency of nanoparticles' agglomeration that might lead to the formation of larger pores (Farahani and Vatanpour, 2018).

TiO_2 - BiVO_4 coated PVDF (C-PTB) membranes (Fig. 14b) exhibited comparable BSA and COD rejection performance with pristine PVDF membrane. This could be due to lower effect of BiVO_4 on contact angle reduction, which is directly related to the hydrophilicity of the membrane.

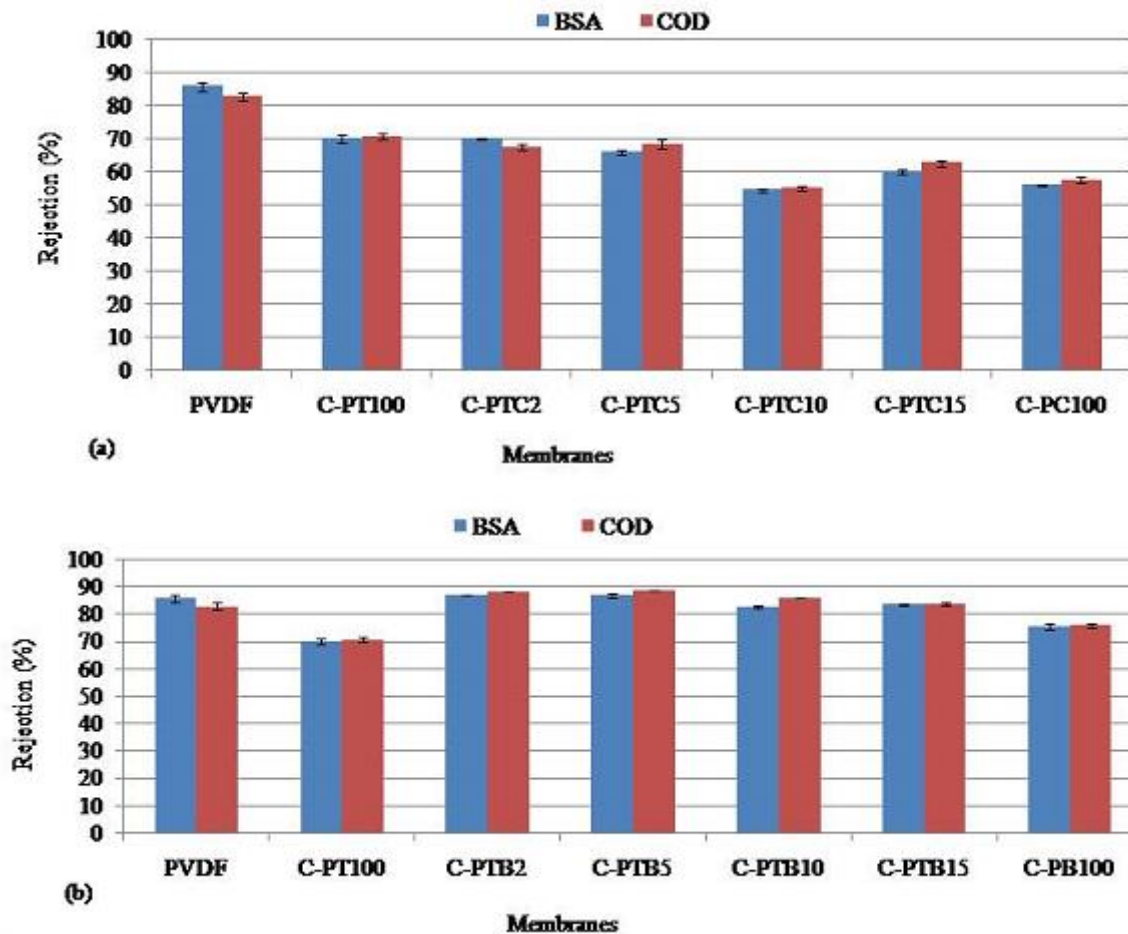


Figure 14. BSA and COD rejection performance of TiO₂-CNT coated PVDF membranes (a) and TiO₂-BiVO₄ coated PVDF membranes (b)

5.2.3.3. Regeneration of physically modified fouled membranes

Fouled membrane regeneration experiments were performed by cleaning of fouled membranes by UV ($\lambda_{\text{max}}=360$ nm) light (TiO₂ and TiO₂-CNT containing (C-PT and C-PTC) membranes) or visible light (BiVO₄ containing membranes (C-PB)). Coated PT or all coated PTC membranes performed more than 97% regeneration by UV light, while the pristine PVDF showed only 60 %. At 3h UV light exposure, coated C-PTC5 (99.13 %) and PTC10 (99.70 %) showed slightly higher regeneration as compared to C-PT100 (98.80 %). The reasons for this phenomenon could be due to the reduction in recombination of electrons/holes and enhancement of photocatalytic activity of TiO₂ by CNT as it sinks electrons/holes (Selvaraj et al., 2020). At 2h UV light exposure, the best regeneration was obtained by C-PTC2. The lowest regeneration was observed by coated PC100 membrane and this is due to the low photocatalytic activity nature of CNT. All TiO₂- BiVO₄ coated PVDF membranes or C-PB membranes exhibited better regeneration by visible light than pristine PVDF or C-PT. For TiO₂-BiVO₄ coated PVDF membranes visible light-based regeneration was

observed only by coated PTB2 and PB100 membranes. The FRR of coated C-PTB2 and C-PB100 for 2 h visible light exposure was about 84.7% and 84.90% respectively. The other $\text{TiO}_2\text{-BiVO}_4$ coated PVDF membranes did not show regeneration due to no or little irreversible foulant left after washing the membrane by water. These imply that antifouling property of membrane can be improved by adding BiVO_4 , which was also proved by lower N/F ratio (see Fig.20b). For Figure 15, the regression results between the pristine PVDF membrane (control) and treatment (modified membrane) for flux recovery ratio (FRR) were significant according to ANOVA calculations (Appendix 5 and 6). This imply that the photocatalytic property of modified membranes was improved significantly.

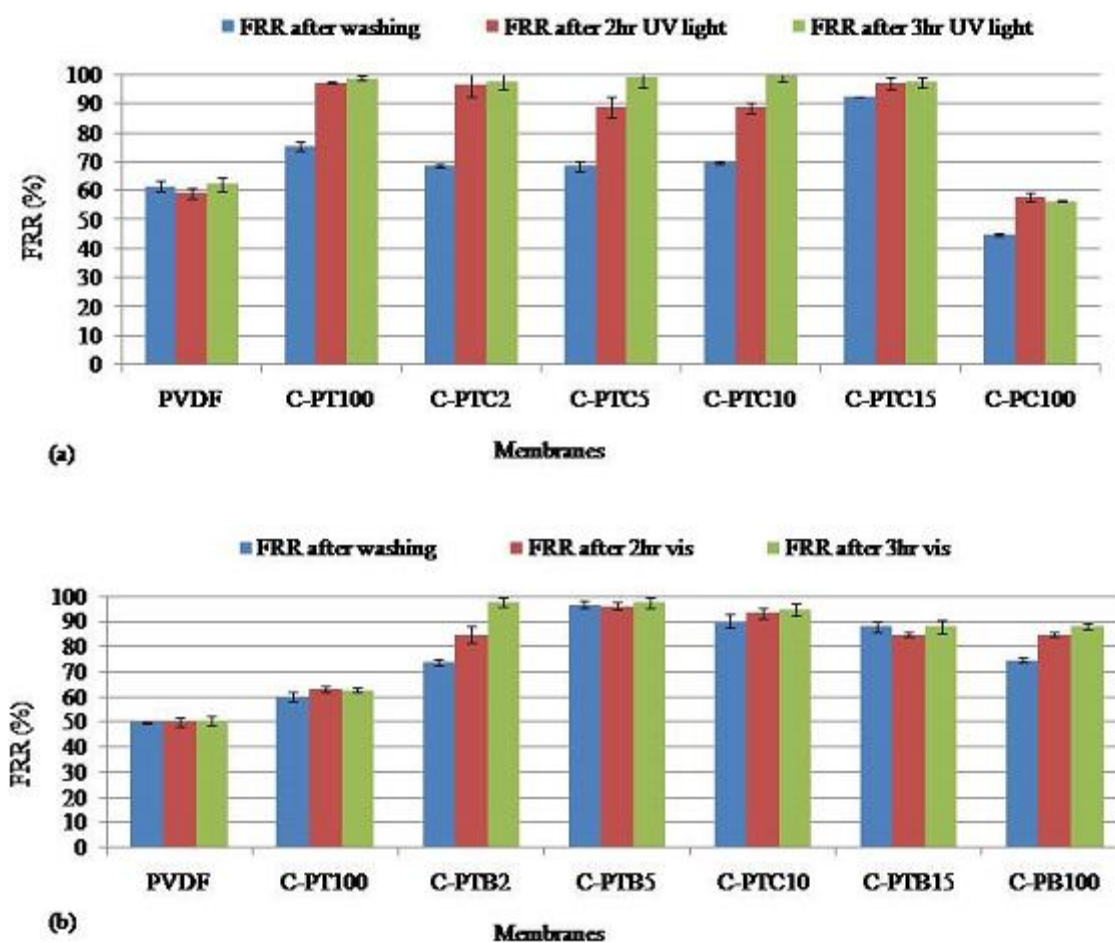


Figure 15. Regeneration of BSA fouled $\text{TiO}_2\text{-CNT}$ coated PVDF membranes (a) and $\text{TiO}_2\text{-BiVO}_4$ coated PVDF membranes (b)

5.3. Photo-catalytic blended ultrafiltration membranes

Next part of my experimental work deal to incorporate the investigated nanoparticles into the membrane material to fabricate photocatalytic composite membranes. The aim of these experiments was to investigate the filtration and photocatalytic performance of the blended UF PVDF membrane during BSA solution or synthetic dairy wastewater or real dairy wastewater. Photocatalytic blended UF PVDF membranes were prepared by phase inversion method, then comparison was performed between the filtration and regeneration performance of the blended membranes and pristine PVDF membrane.

5.3.1. Effects of TiO_2 concentration on the performance of PVDF- TiO_2 photocatalytic blended ultrafiltration membranes

The experiment was aimed to investigate the effects of TiO_2 concentration on filtration and regeneration performance of PVDF membrane during BSA solution filtration. In this experiment blended PVDF- TiO_2 photocatalytic ultrafiltration membranes (labelled as B-PT membranes) with various concentrations were prepared. Comparisons were performed between the filtration and regeneration performance of the pristine PVDF membrane and PVDF- TiO_2 photocatalytic blended membranes and among the PVDF- TiO_2 photo-catalytic membranes.

5.3.1.1. Contact angle, water flux and rejection performance

Membrane surface hydrophilicity was examined by measuring the contact angles of distilled water between membrane surface and air interface. Contact angle (CA), water flux and BSA rejection characteristics of B-PT ultrafiltration membranes across various concentrations of TiO_2 is shown in [Table 12](#). The contact angles and water flux of B-PT membranes exhibit a decreasing and increasing trend respectively as the concentration of TiO_2 increased from 0 to 2.5 %. Results imply that the increased concentration of TiO_2 enhance the hydrophilicity of pristine PVDF, similarly to coated membranes ([Section 5.2](#)), although the presence of PVDF membrane material on the surface (unlike in case of coated membranes) doesn't allow developing super hydrophilic (with a contact angle of 0°) membrane surfaces. Our results are in accordance with the results obtained by ([Farahani and Vatanpour, \(2018\)](#) in that TiO_2 loading (0.2 to 4 w %) exhibited a decreasing trend of CA. BSA rejection for fabricated pristine PVDF membrane was 98.88 % and a comparable rejection performance was observed by B-PT1 and B-PT1.5 membranes ([Table 12](#)). ([Sisay et al., 2022](#))

Table 12. Characteristics of TiO₂/PVDF photo-catalytic blended ultrafiltration membranes (Sisay et al., 2022)

Membrane types	Water contact angle (°)	Water Flux (Lm ⁻² h ⁻¹)	Rejection (%)	
			BSA	COD
PVDF	78.1±4.59	67.22±0.7	98.88 ± 0.09	99.83 ± 0.08
B-PT1	73.45±4.33	82.94±1.56	97.59 ± 0.57	99.74 ± 0.09
B-PT1.5	72.26 ±4.0.6	90.78±1.33	99.06 ± 0.87	98.47 ± 0.09
B-PT2	70.48±2.82	110.04±1.30	97.74 ± 0.84	96.27 ± 0.04
B-PT2.5	66.72±3.44	157.88±1.41	95.8 ± 0.85	98.27 ± 0.26

5.3.1.2. Filtration resistances for blended PVDF-TiO₂ photocatalytic UF membranes

In order to investigate the effectiveness of the modified membranes in reducing fouling, protein (BSA) solutions were filtered, and the filtration resistances were determined using equations (10) through (13). The resulting membrane resistance (RM), irreversible resistance (R_{irr}), reversible resistance (R_{rev}), and total resistance (RT) values are shown in Figure 16. The unmodified PVDF membrane shows the highest filtration resistances with considerably high irreversible fouling. It was found that the modification significantly decreases the filtration resistances. The resistances also decrease as the concentration of TiO₂ increased (Figure 16).

Unlike the neat membrane, in case of 1-1.5-2 % TiO₂ containing membranes reversible fouling resistances were higher than irreversible fouling. This can be explained by enhanced hydrophilicity (proved by decreased contact angles) as compared with the pristine membrane, which prevent the strong (unwashable) bonding BSA to the membrane surface. These results are in accordance with the earlier results (Liu et al., 2018; Ding et al., 2019). In case of higher TiO₂ content it reversed, this is due to the pore blockage by nanoparticulates or agglomerated nanoparticulates at higher concentration. Thus, this phenomenon can reduce the favorable effect of hydrophilicity and morphology on water permeation (Farahani and Vatanpour, 2018).

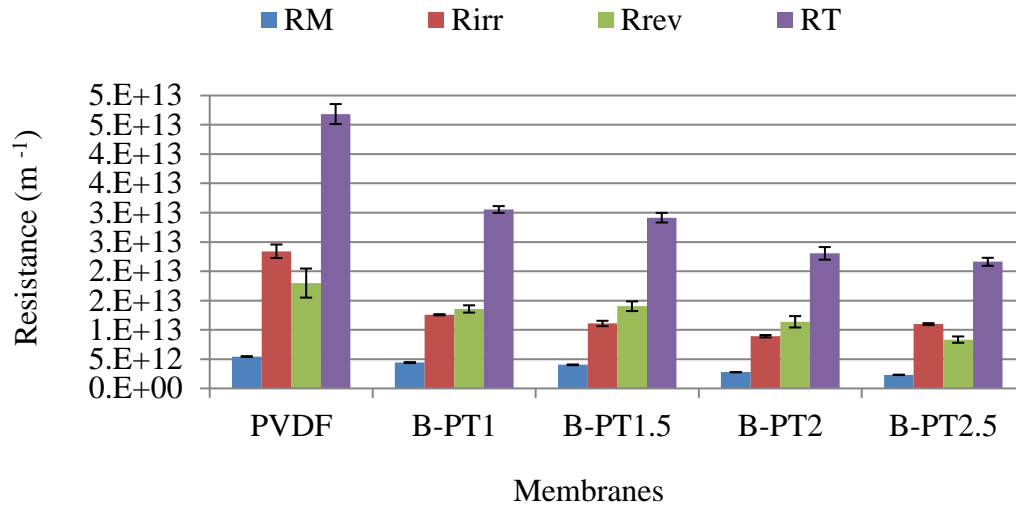


Figure 16. Filtration resistances of B-PT photocatalytic UF membranes with different TiO₂ concentrations

5.3.1.3. Regeneration of BSA fouled blended PVDF-TiO₂ photocatalytic UF membranes

The aim of regeneration experiment was to investigate the effect of TiO₂ concentration on regeneration performance of BSA fouled B-PT membranes under UV light. The experiment was performed mainly to examine the photocatalytic degradation of irreversible foulants attached to membrane during filtration of BSA solution at its own pH, 6.5 ± 0.08 .

Regeneration of BSA fouled B-PT photocatalytic UF membranes are presented in Fig.17. The cleaning of a various BSA fouled pristine PVDF and B-PT photo-catalytic membranes were conducted by distilled water and UV radiation ($\lambda_{\text{max}} = 360 \text{ nm}$) light for 2 and 3 h. It was found that flux was improved after cleaning the B-PT membranes by UV radiation but the extent of flux restoration of all photocatalytic membranes were small. The highest and the lowest regeneration performance (expressed by FRR, 37.47 % and 26.02 %, respectively) were observed after 3h UV light exposure in case of B-PT1.5 and B-PT2.5 blended membranes respectively. The study by Farahani and Vatanpour (2018) revealed that larger pores can be formed at higher TiO₂ concentration. So, the lower regeneration at higher concentration of TiO₂ could be due to higher tendency of irreversible foulant formation in larger pores as observed in B-PT2 and B-PT2.5.

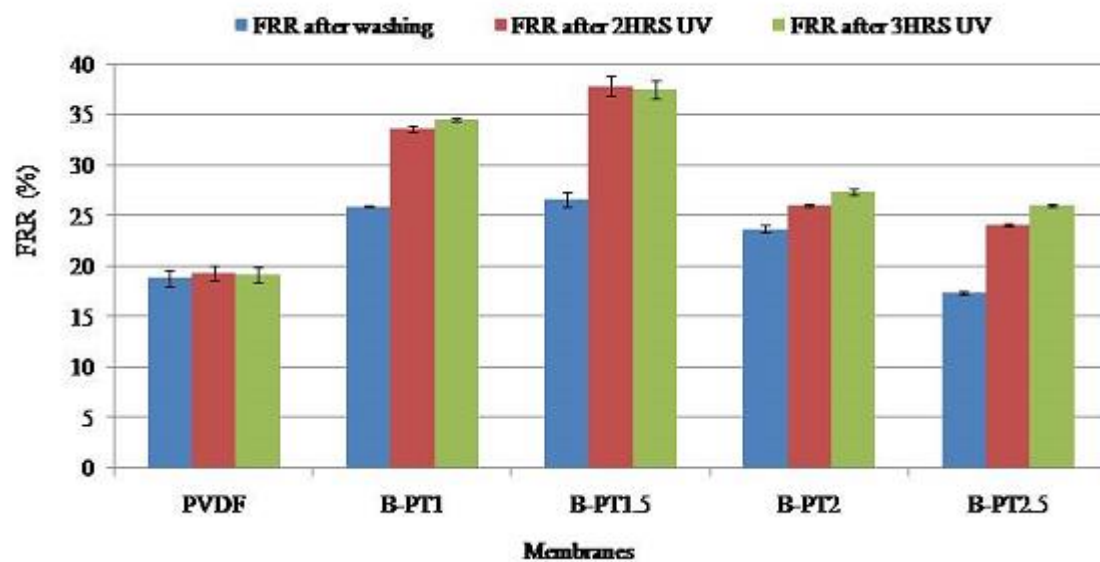


Figure 17. Regeneration of BSA fouled PVDF and B-PT UF membranes with various TiO_2 concentrations.

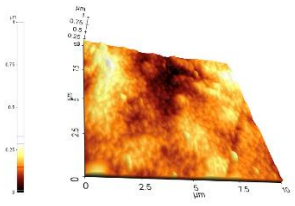
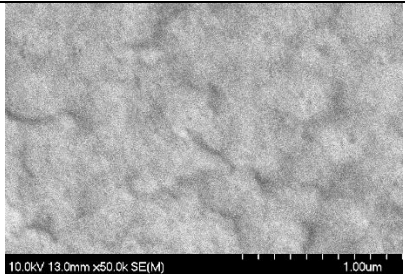
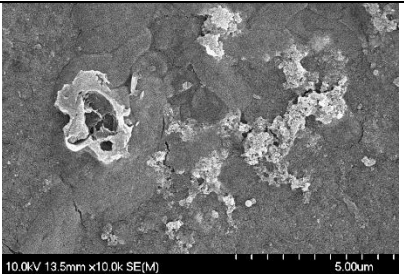
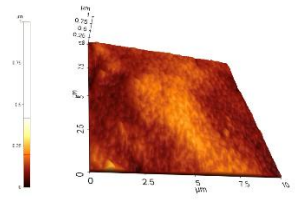
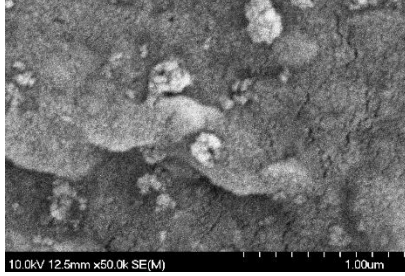
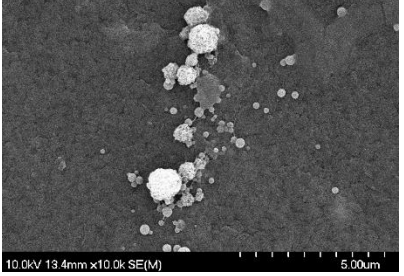
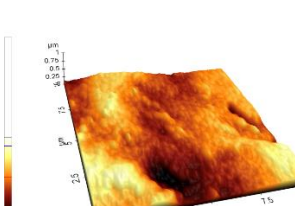
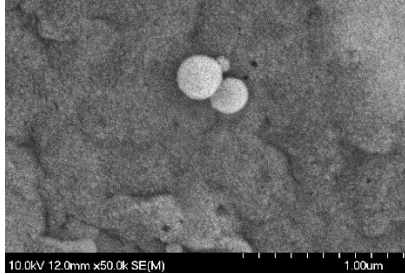
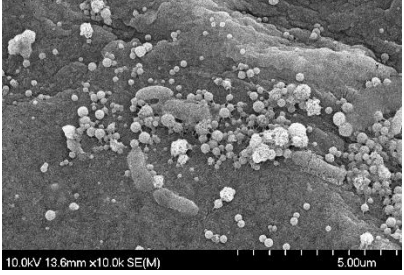
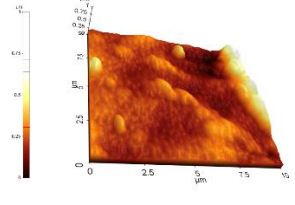
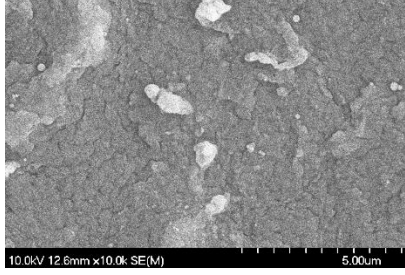
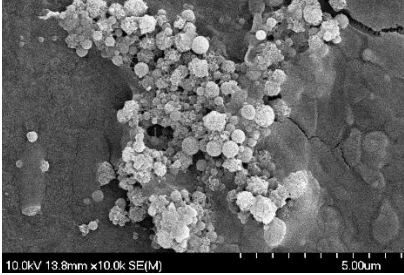
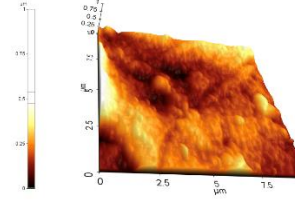
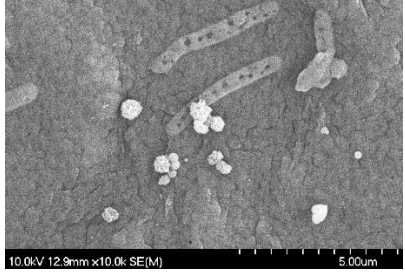

5.3.2. Characterization of blended PVDF-TiO₂-CNT-BiVO₄ photocatalytic membranes

The next series of experiments has dealt to characterize and compare the pristine, and TiO₂, CNT and BiVO₄ blended membranes (labelled as B-PTC of TiO₂ and CNT containing, B-PTB of TiO₂ and BiVO₄ containing and B-PTCB of TiO₂ CNT and BiVO₄ containing membranes as it was summarized in [Table 8](#)). Besides, the experiment was aimed to investigate their filtration and regeneration performance after BSA model solution filtration at its own pH. Comparison of filtration and regeneration performance between pristine PVDF and blended membranes, and among the blended membranes were performed using ANOVA. Based on the obtained results, best performer B-PTB50 and B-PTCB50 membranes along with the controls (pristine PVDF, B-PT and B-PB) were considered for further membrane characterization. The membranes were characterized by porosity and pore size (BET), crystal and surface structure (XRD and SEM, respectively), roughness (AFM), zeta potential, contact angle, and N/F ratio (EDX) of fouled membranes.

5.3.2.1. Crystalline and morphological structure of blended membranes (XRD, SEM and AFM)

XRD measurements for blended hybrid membranes were performed to investigate crystal structure and patterns characteristic of TiO₂, BiVO₄, and CNTs. Weaker signals at 25.28, 26.98, 31.62, and 36.02, and a major diffraction peak below 22° were observed for base PVDF membrane. The CNT crystallographic plane (002) was observed at 25.8° (JCPDS card. No. 96-101-1061), but due to overlapping with other compounds, no relevant information could be obtained for CNT. Monoclinic BiVO₄ (JCPDS No. 14-0688) diffraction peaks with a primary crystallite size of 16.4 nm were detected in B-PTBC50, B-PTB50, and B-PB100 membranes. The (101) plane of anatase TiO₂ (JCPDS No. 21-1272) was easily identified with the major diffraction peak at 25.38°, indicating the presence of TiO₂. The primary crystallite size of anatase TiO₂ was calculated as 20.4 nm, which is consistent with that of Evonik Aeroxide P25. Although the signals of TiO₂ in B-PTB50 and B-PTBC50 were weak, they were still visible through the signal at 25.38°. Morphology of the fabricated blended membranes (PVDF, B-PT100, B-PB100, B-PTB50 and B-PTBC50) was studied and shown in [Table 15](#). According to the AFM measurements shown in [Figure 20](#), the surfaces of the nanocomposite blended membranes were slightly rougher compared to the neat PVDF membrane. This could be due to the presence of nanoparticles (200-300 nm) that were aggregated on the surface. Despite the XRD results showing primary crystallite sizes in the range of 10-25 nm, SEM pictures indicated that the TiO₂ and BiVO₄ nanoparticles were present in the membrane material as aggregates, as shown in [Table 13](#). ([Sisay et al, 2022](#)).

Table 13. AFM and SEM pictures of the membrane surface

Mem-brane	AFM micrographs	SEM pictures of the top of the membranes	SEM pictures of BSA-fouled membranes
PVDF			
B-PT100			
B-PB100			
B-PTB50			
B-PTBC50			

5.3.2.2. Porosity and pore size estimation

Porosity was measured by Eqs. (3) and (4). And the average pore size was obtained by two methods, flux measurements based Guerout–Elford–Ferry equation (Eqs (5)) and Brunauer–Emmett–Teller (BET) method. However, the first method has its own drawback in that the calculations were based on flux measurements, which are dependent not only on the pore size, but on the wettability of the membrane too. Table 14 shows the pore size, porosity, water flux, contact angle and BSA rejection of the fabricated UF membranes. The porosity and pore size of modified photocatalytic blended membranes were larger than the pristine B-PVDF membrane. This could be due to the presences of hydrophilic nanoparticle in the dope solution that result in the high exchange rate between solvent and non-solvent, leading the development of larger pores and porosity improvement.

The largest porosity was 89.50 % for B-PTCB50 and the largest pore size was 47.33 nm for B-PB100 as compared to 84 % and 30.04 nm of pristine B-PVDF membrane respectively. Our porosity and pore size results consistent with the result obtained by [Hudaib, et al., 2018](#), [Farahani and Vatanpour., 2018](#), and [Ayyaru et al., 2019](#)) in that the pore size and porosity of the modified membranes were larger than the pristine membrane.

Table 14. Characteristics of fabricated PVDF and photocatalytic blended UF membranes ([Sisay et al., 2022](#))

Membrane type	Porosity (%)	Mean pore size (nm)	Contact angle (°)	Water flux ($\text{L}\cdot\text{m}^{-2}\cdot\text{h}^{-1}$)	Rejection (%)	
					BSA	COD
PVDF	84.00±0.00	30.04±0.04	78.10±5.99	67.22±0.7	99.79±0.09	99.75±0.08
B-PT100	85.30±0.02	33.43±0.58	73.45±4.30	85.63±0.66	98.87±0.60	99.74±0.09
B-PTC2	85.43±0.06	33.52±0.21	71±5.3	82.23±0.09	98.89±0.10	99.34±0.12
B-PTC5	85.73±0.03	32.81±0.19	67.45±3.50	81.07±0.05	97.45±0.34	97.05±0.34
B-PTC10	84.93±0.01	36.31±0.24	66.05±7.00	92.26±0.08	98.55±0.25	98.13±0.6
B-PTC15	86.82±0.07	40.78±0.17	65.67±5.00	110.78±0.07	98.79±0.28	96.98±0.2
B-PTB25	86.54±0.00	40.85±2.97	69.68±3.24	131.79±2.07	97.09±0.16	96.88±0.09
B-PTB50	85.59±0.00	44.61±8.00	62.3±4.24	153.56±1	97.75±0.03	97.48±0.15
B-PTB75	84.80±0.00	34.87±0.00	71.35±2.73	92.06±1.2	98.01±0.09	94.96±0.02
B-PB100	83.38±0.00	47.33±0.11	76.53±2.42	163.87±3.23	98.01±0.0	96.68±0.75
B-PTCB25	85.35±0.00	43.00±0.03	72.74±2.58	141.78±2.51	98.88±1.0	98.31±0.25
B-PTCB50	89.50±0.00	34.50±0.00	69.875±5.01	150.52±2.04	97.10±0.77	95.51±0.15
B-PTCB75	84.71±0.00	26.12±0.00	69.53±2.39	86.27±1.09	97.75±0.09	96.72±0.11

Brunauer-Emmett-Teller (BET) measurements were performed to support the flux measurement-based **pore size estimation**. In this method specific surface area and pore size were obtained from BET adsorption–desorption isotherms. [Table 15](#) and [Fig.18](#) shows the specific surface area and pore size distribution respectively for the neat PVDF, B-PT100 and B-PB100 membranes.

[Table 15](#). Specific surface area of neat PVDF, B-PT100 and B-PB100 membranes by method (Sisay et al., 2022)

Membranes	Surface area (m ² /g)	Pore volume (cc/g)	Average pore diameter (nm)
PVDF	4.43	0.00849	7.67
B-PT100	4.548	0.0099	8.72
B-PB100	4.021	0.00658	6.55

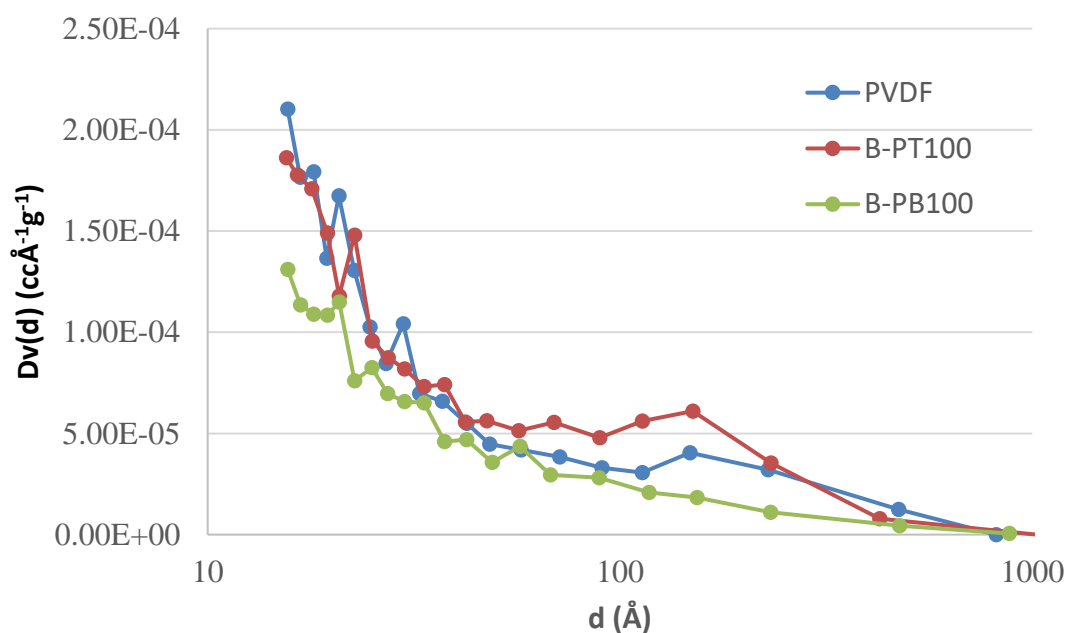


Figure 18. Pore size distributions of neat PVDF, B-PT100 and B-PB100 membranes by the BJH approach

The above pore size distribution curve showed many small pores rather than the large pores. These small pores probably did not have any role in membrane filtration. However, considering them in a pore size calculation resulted in a lower average pore size in BET approach than that obtained

from flux-based pore size estimation. These pore size distribution results show that the presence of nanoparticles in PVDF had only a limited effect on the pore size distribution.

5.3.2.3. Wettability

Wettability of the membrane was characterized by **contact angle measurements** (Table 14.) The contact angle of pristine PVDF membrane was $78.10 \pm 5.99^\circ$, which means only slightly hydrophilic surface. The contact angle of all blended UF PVDF membranes was smaller than this value; all of modification increased the hydrophilicity of the membrane, similarly to the results of coated membranes (Section 5.2). This resulted in superior water flux too. There also was a decreasing trend of contact angle with the increasing concentration of CNTs in TiO₂-CNT, which resulted in increased water permeability. Our result is in accordance with earlier results, where the increased flux was explained by the increased pore size and porosity (Wang et al., 2015) or the increased hydrophilicity (Dhand et al., 2019). The formation of strong bonds between hydrophobic open ends of PVDF and CNTs, leads the PVDF surface to have more fluoride ions resulting in better hydrophilic membranes (Dhand et al., 2019). A similar decreasing trend of contact angle was observed for B-PB membranes. This is due to the superior hydrophilic nature of pure BiVO₄ (Pi et al., 2021).

Water fluxes of the fabricated pristine PVDF and blended PVDF membranes are also presented in Table 14. All blended membranes exhibited higher flux than that of the pristine PVDF membrane; the best water flux results were obtained by BiVO₄-containing membranes. Generally, the water flux increased as the concentration of CNT or BiVO₄ increased.

5.3.2.4. Zeta potential of fabricated PVDF and blended photocatalytic PVDF membranes

The zeta potentials were calculated using Eq. (7). Fig. 19. illustrates the zeta potentials of unused membranes as a function of pH. The membrane zeta potential curves of all modified membranes are quite different from the pristine PVDF curve due to presence of TiO₂, CNT and BiVO₄ particles, which may govern the electrical properties of the surface, and the different composition of particles lead to the different zeta potential pattern of the surface.

The zeta potentials of all membranes are negative at neutral pH, although isoelectric point of all modified membranes (Fig. 19.b-e) was lower than pristine membrane. This finding is particularly important considering the various pHs of dairy wastewater (Table 2), which is approximately between 4.1-8.8. At the acidic operating pHs, positively charged PVDF membranes would be fouled by the negative feed constituents (e.g. isoelectric point of BSA is around 4.5), while the modified membranes will repel the negatively charged proteins even in lower pHs. This has a substantial contribution on reducing fouling of the membranes.

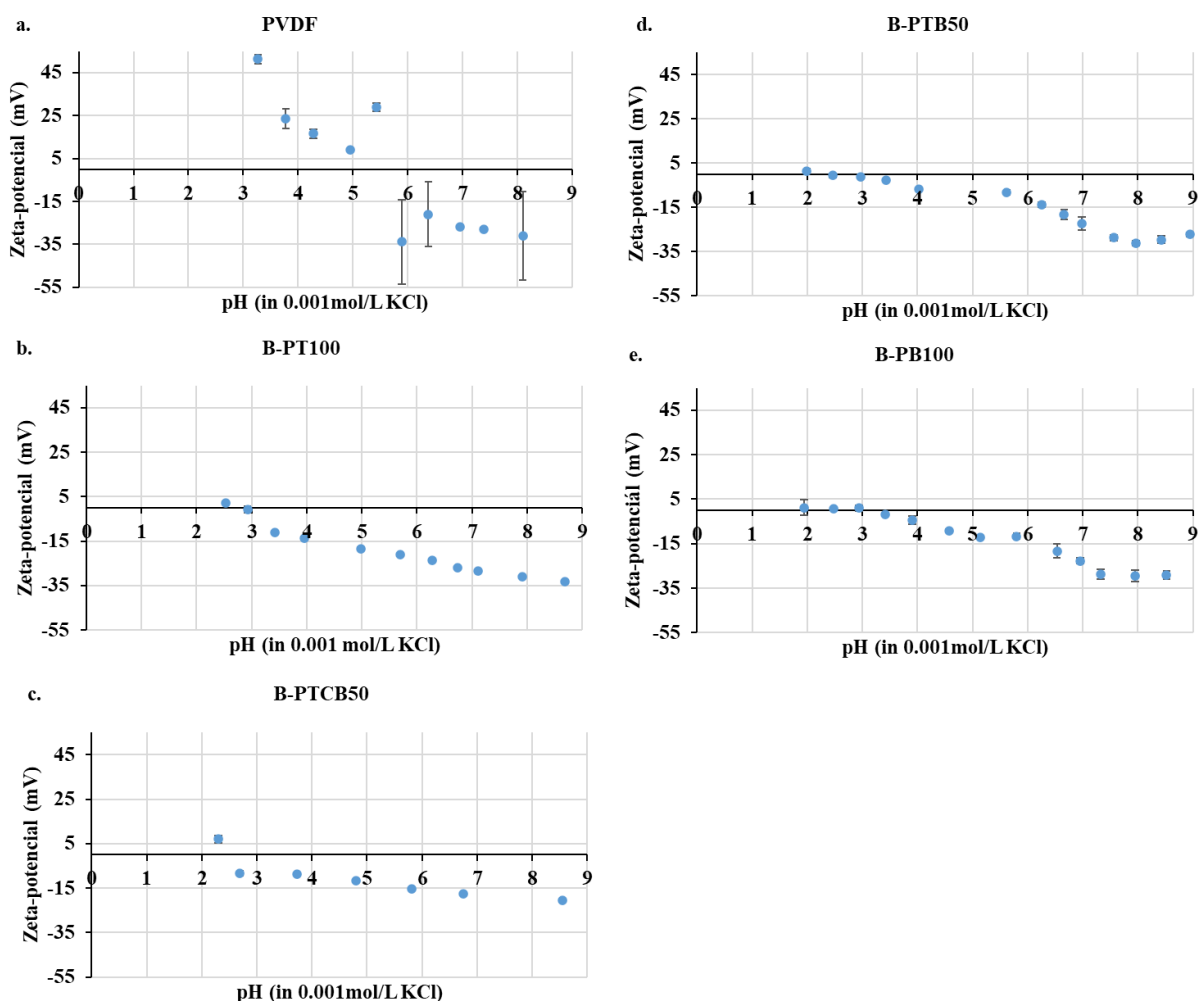


Figure 19. Zeta potential of unused PVDF, B-PT100, B-PB100, B-PTB50 and B-PTCB50 blended membranes as a function of pH at 10^{-3} M KCl.

5.3.2.5. Rejection and extent of fouling

The modified membranes had slightly lower rejection rates (Table 14). than the unaltered PVDF membrane (with BSA rejection ($99.79 \pm 0.09\%$) and COD rejection ($99.75 \pm 0.08\%$)), but they were still above 97% for BSA and 96% for COD. The decrease in rejection rates of modified membranes could be attributed to changes in the BSA appearance on the surface (Fig 21 and Table 13). The BSA molecules covered a relatively large area of the unaltered PVDF membrane, which resulted in a relatively high N/F ratio (Fig 21) as measured by energy-dispersive X-ray spectroscopy (EDX). As a "protein layer" developed on the membrane surface, it acted as an additional filter, "trapping" most of the BSA molecules. In nanoparticle-containing membranes, BSA cannot covered the surface, it formed small and more compact particles, which left larger areas of uncovered, neat

PVDF surface (Table 13), according to the decrease in N/F ratio. Without the "protein layer," more protein molecules could pass through the membrane, leading to lower rejection rates. Although there was an inverse relationship between surface roughness and BSA coverage, the addition of nanoparticles may alter the surface charge, which affected BSA binding to the surface at a BSA solution pH of 6.5, rather than the surface morphology. (Sisay et al, 2022)

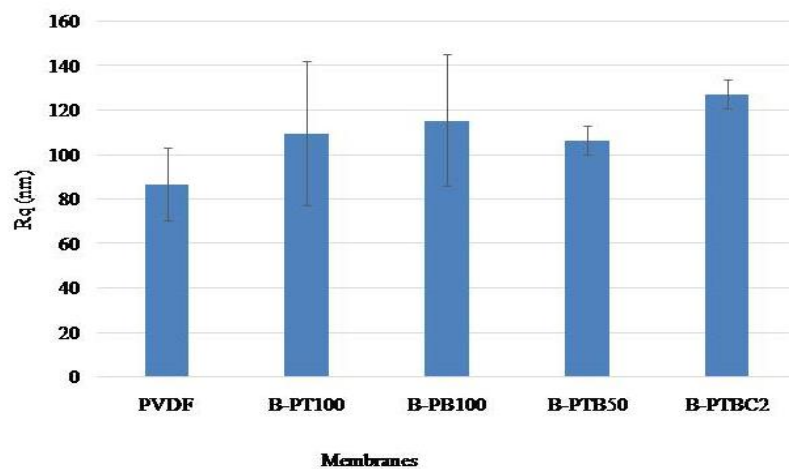


Figure 20. Surface roughness of unused blended membranes

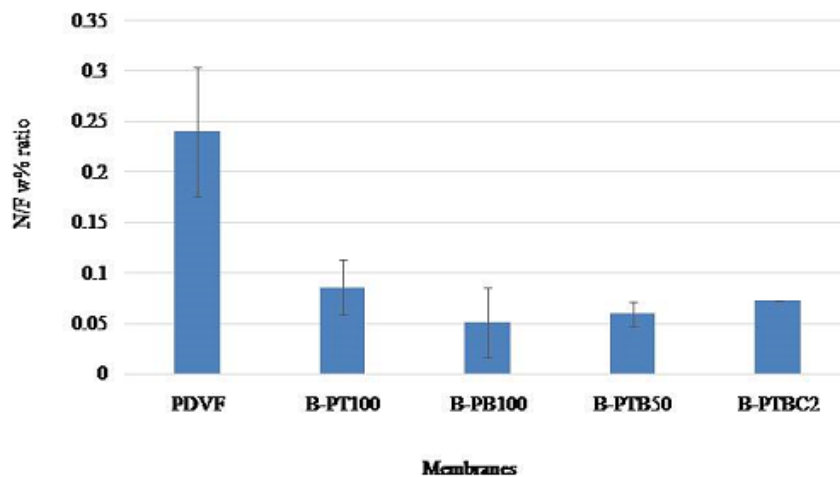


Figure 21. N/F ratio of fouled blended membranes

5.3.3. Fouling mitigation and photocatalytic regeneration of nanocomposite membranes

The study examined the filtration resistances of membranes caused by the filtration of BSA solutions. The total resistances (RT), membrane resistances (RM), irreversible resistances (Rirr),

and reversible resistances (R_{rev}) were calculated to describe the filtration resistances of the membranes. The results indicated that all modified membranes were more beneficial than the pristine PVDF membrane in terms of irreversible fouling. This may be due to the lower surface charge of the modified membranes, which prevents protein fouling. The water flux also exhibited an increasing trend with increasing CNT concentration, which can be explained by the increased hydrophilicity confirmed by contact angle measurements. The lowest total resistance was achieved for the B-PTC2 composite membrane, indicating that 2% CNT concentration resulted in the best fluxes and the lowest irreversible fouling during the filtration of BSA. Increasing CNT loading enhanced the fouling, which may be due to the hydrophobic nature of CNTs that makes possible the adsorption of hydrophobic parts of protein molecules onto the surface.

The effect of BiVO_4 addition on fouling mitigation was also examined. The addition of BiVO_4 nanoparticles considerably reduced filtration resistance and had a slightly more beneficial effect than TiO_2 addition. The filtration performance of blended PTCB composites with different BiVO_4 and 2% CNT content was also investigated. In line with the previous experiments, it was found that the best performance was achieved by adding 2% CNTs. The addition of BiVO_4 reduced the total filtration resistance while filtering BSA, but the irreversible resistances showed a slight increase in the presence of BiVO_4 . ANOVA was performed, and the regression results between the pristine PVDF membrane and the modified membranes for total and irreversible resistances were significant. This implies that the antifouling property of modified membranes was significantly enhanced ([Appendix 7, 8, 9 and 10.](#)).

The cleanability of nanocomposite membranes was evaluated by calculating their flux recovery ratio (FRR) values, which were found to be informative. The FRR results for TiO_2 -CNT composites were presented in [Figs. 23a–c](#). UV light was used for the regeneration of TiO_2 -CNT composites as TiO_2 is efficiently excited by UV light. Water flux increased with increasing CNT concentration, but the fouling pattern was different, as the irreversible fouling was more extended. The cleanability of the membranes was also affected by their CNT content. Membranes with higher CNT content were less cleanable by UV radiation, and B-PTC2 provided the highest FRR (64%) ([Fig. 23a](#)).

[Fig. 23b](#) demonstrates that visible-light-induced photocatalytic purification was used to regenerate the surfaces of BiVO_4 -containing membranes fouled with BSA. The restoration of flux was found to be more efficient for all BiVO_4 -based membranes than for the neat PVDF membrane, even before photocatalytic cleaning of membranes. The PTB composites were found to have better performance in photocatalytic regeneration than PB. The regeneration performance was found to increase with increasing BiVO_4 concentration due to its photocatalytic activity under visible light, but the presence of TiO_2 was necessary to achieve superior performance.

The regeneration of BSA-fouled PTCB membrane surfaces using photocatalytic purification with visible light is presented in Fig. 23c. The flux recovery for membranes containing CNT was better than that for PTB membranes without CNT before photocatalysis. However, the efficiency of photocatalytic regeneration decreased with the presence of CNTs, probably due to their light absorption. (Sisay et al., 2022) ANOVA was performed for Figure 20, and regression results between the control (pristine PVDF membrane) and the modified membrane treatments for flux recovery ratio (FRR) were significant (Appendix 11, 12, and 13).

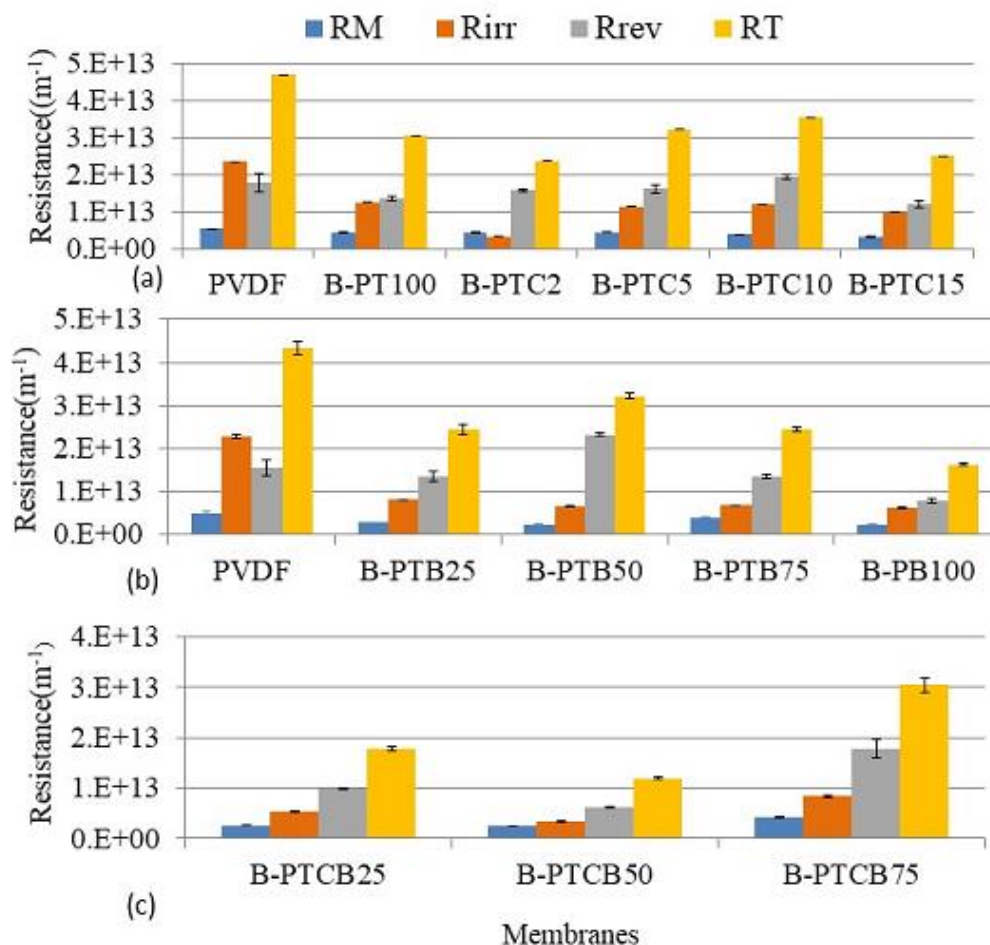


Figure 22. Filtration resistances of (a) PVDF, B-PT and B-PTC membranes, (b) PVDF, B-PTB and B-PB membranes, and (c) different B-PTCB membranes with 2% CNT content.

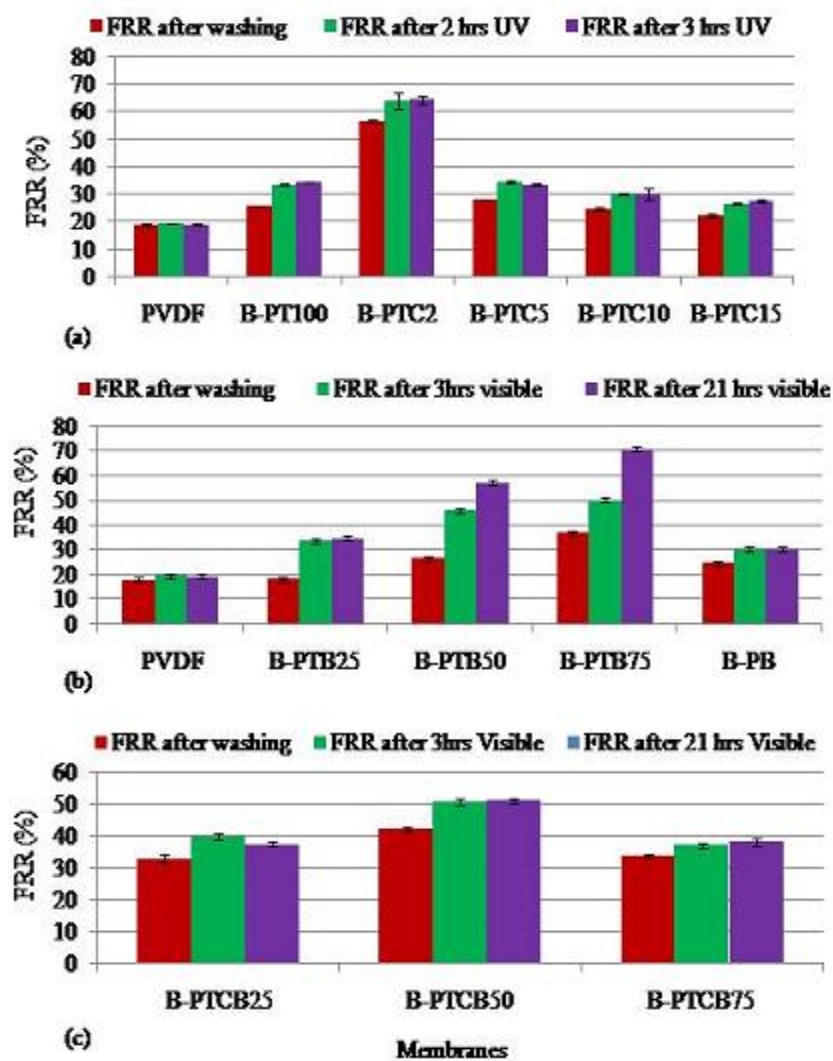


Figure 23. FRRs of BSA-fouled (a) PVDF, B-PT and B-PTC membranes, (b) PVDF, B-PTB and B-PB membranes, and (c) different B-PTCB membranes with 2% CNT content.

5.4. Application of best performing fabricated photocatalytic blended UF PVDF membranes for synthetic and real dairy wastewater treatment

This part of the work aimed to evaluate the applicability of photocatalytic blended UF PVDF membranes to treat real dairy wastewater. Pristine PVDF and best performing photocatalytic blended (B-PTB50 and B-PTCB50) membranes were considered in this series of experiments.

5.4.1. Synthetic dairy wastewater treatment

The aim of this set of experiments was to investigate the effect of pH, and the dairy wastewater components as salinity, and lactose on filtration performance of selected blended membranes during synthetic dairy wastewater filtration (SW-BSA).

5.4.1.1. Effects of salinity on membrane performance

Figure 24 illustrates the impact of salinity on membrane fouling and rejection. The modified membranes (B-PTB50 and B-PTCB50) exhibited lower irreversible and total resistances at all salinity levels compared to the pristine PVDF membrane (Figure 24a), which is significant for mitigating fouling. All investigated membranes showed COD and turbidity rejections above 91% for all salinity levels (Figure 24b). However, at the highest salinity level (EC > 4), slightly lower COD rejection was observed, compared to the medium and lowest salinity levels, possibly due to the shielding effect of saline ions. Turbidity rejection was above 98% for all membranes (Sisay et al, 2023).

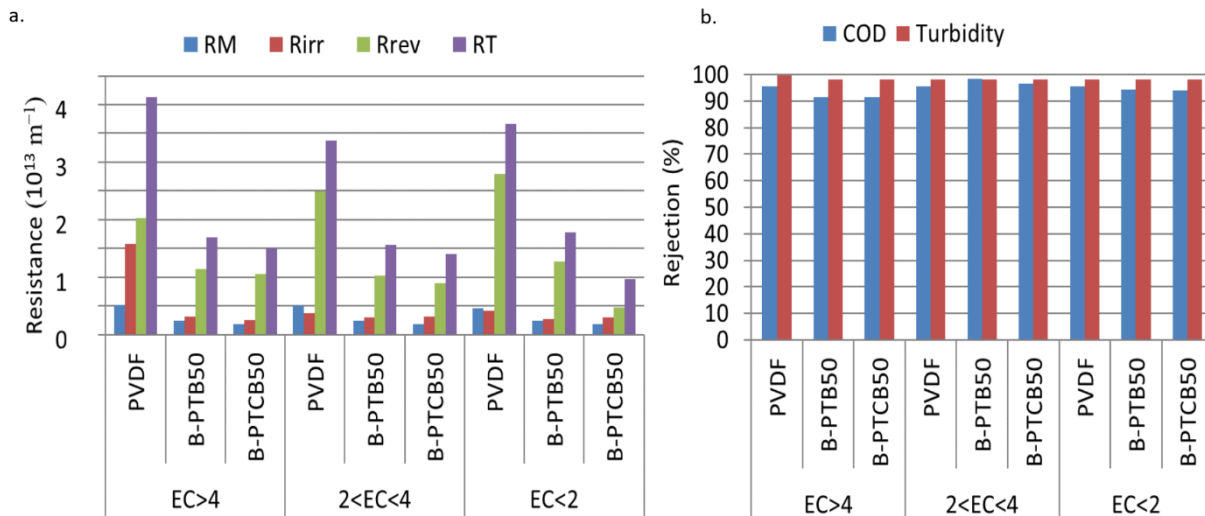


Figure 24. Effect of salinity during synthetic dairy wastewater membrane filtration on membrane fouling (a) or COD and turbidity rejection (b)

5.4.1.2. Effects of lactose on membrane performance

In the next set of experiments the impact of lactose concentration on membrane performance was studied. It was found, that at 0.5 gL^{-1} , lactose concentration of the irreversible and total resistances of all membranes increased, while at higher, 1 gL^{-1} concentration the total resistance decreased (Figure 25a). As expected, in case of higher amount of lactose (1 gL^{-1} lactose) containing synthetic dairy wastewater, the COD rejection of all membranes was decreased to approximately 50% (Figure 25b). This was due to the ease with which lactose could pass through the membranes during filtration. Furthermore, composite membranes performed better in all cases, with decreasing reversible and irreversible fouling, which mainly manifested in reduced irreversible resistances. This indicates that the produced membranes possessed significant antifouling properties, even in the presence of lactose.

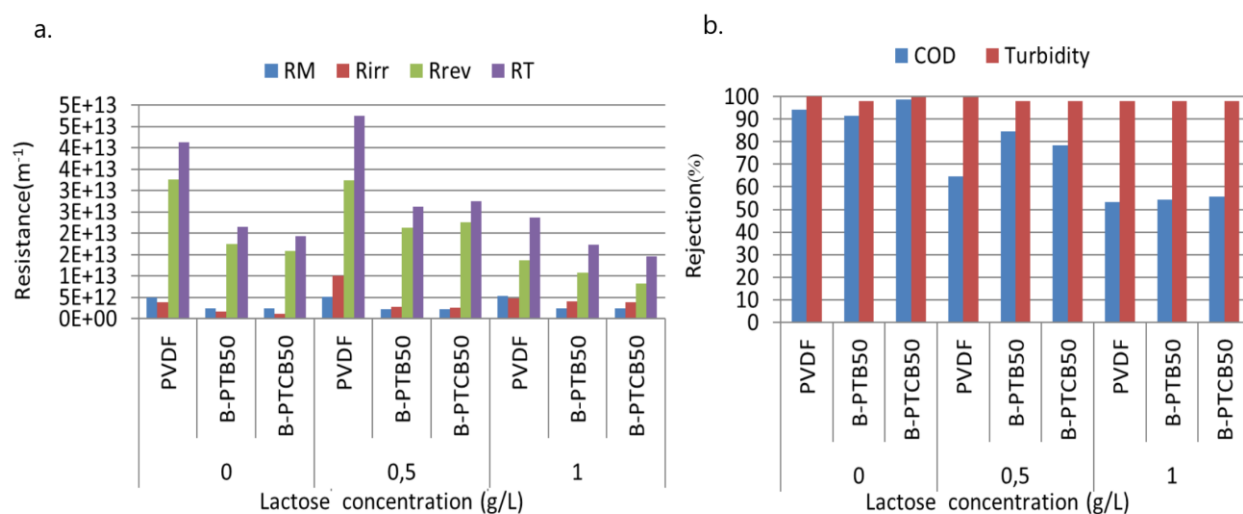


Figure 25. Effect of lactose during synthetic dairy wastewater (SW-BSA-L) membrane filtration on membrane fouling (a) or COD and turbidity rejection (b)

5.4.1.3. Effects of pH on membrane performance

In the next set of experiments, three different pH values (4, 7.5, and 9.5) were chosen to investigate their effect on membrane fouling and COD and turbidity rejection (Figure 26). B-PTB50 and B-PTCB50 showed lower resistances at pH 7.5 and pH 9.5, respectively, compared to the pristine PVDF membrane (Figure 26a). It can be explained by the strong repulsion forces between the negatively charged surface and the negatively charged protein as BSA has an isoelectric point around pH 4.5. In acidic medium (pH 4), higher fouling was experienced due to the van der Waals forces between the nearly isoelectric membranes (see Fig 19) and BSA. It is important to note that the membrane modification most effectively reduced the irreversible resistances, resulting in more negatively charged membrane surfaces. Figure 26b demonstrates that changes of pH only slightly

affected COD rejection, and had no effect on turbidity rejection. The turbidity rejection was above 98%, while the COD rejection was above 90% in all cases. (Sisay et al., 2023)

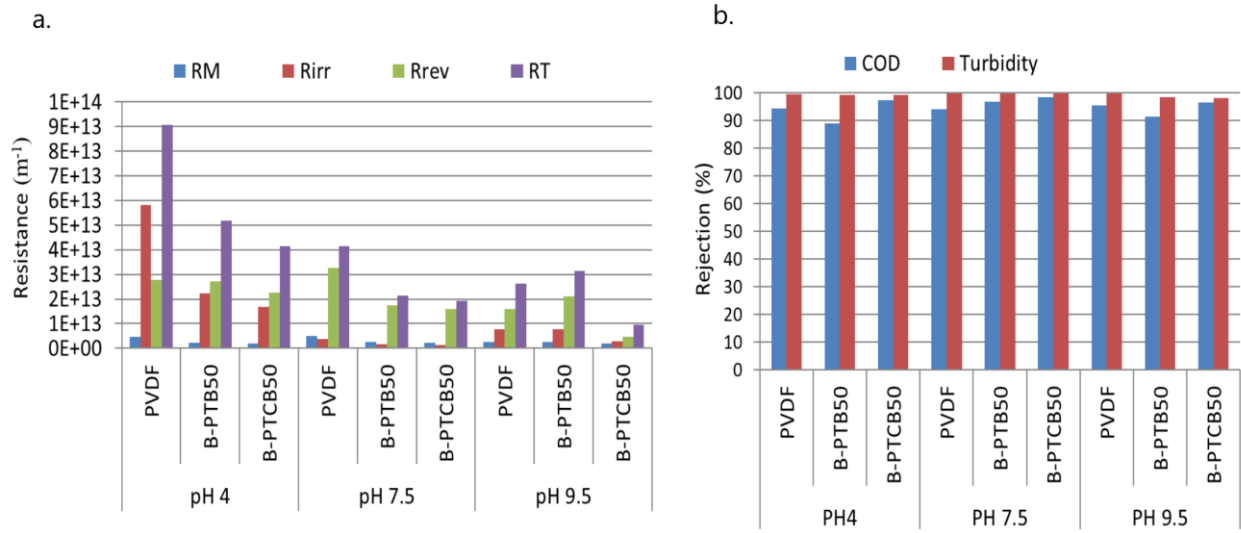


Figure 26. Effect of pH during synthetic dairy wastewater (SW-BSA) membrane filtration on membrane fouling (a) or COD and turbidity rejection (b)

5.4.2. Real dairy wastewater treatment

The objective of this study was to assess the suitability of PVDF, PTB50, and PTCB50 composite membranes for the treatment of actual dairy wastewater. The filtration and regeneration efficacy of the composite membranes, namely PVDF, B-PTB50, and B-PTCB50, were examined at a pH of 7.09.

5.4.2.1. Filtration resistances during filtration of real dairy wastewaters

Figure 27 illustrates the filtration resistances of selected membranes during filtration of real dairy wastewater. As it was expected, the raw wastewater (Figure 27a) displayed higher resistances compared to the pre-filtered wastewater (Figure 27b), indicating the requirement for pre-filtration in membrane-based dairy wastewater treatment processes. Nonetheless, the total and irreversible resistance of neat membrane was higher than those of the composite (B-PTB50 and B-PTCB50) membranes in both scenarios.

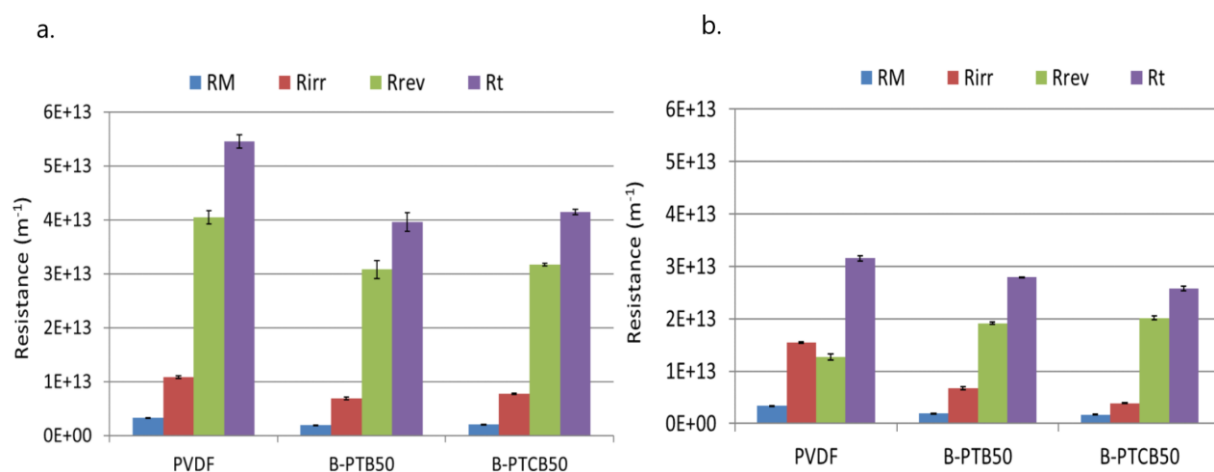


Figure 27. Filtration resistances of PVDF, B-PTB50 and B-PTCB50 membranes for real dairy wastewater, unfiltered (a) or pre-filtered (0.2 μm filter paper) (b)

5.4.2.2. COD and turbidity rejection

Figure 28 illustrates the rejection efficiency of selected membranes during real dairy wastewater filtration. The results indicate that B-PTCB50 and neat PVDF showed the highest and lowest COD rejections of 60% and 25%, respectively, during UF of raw and pre-filtered real dairy wastewater (Figure 28a). All membranes showed almost 100% turbidity rejection for raw real dairy wastewater (Figure 28a). However, due to small molecule size of lactose, which enable it to pass through the membranes, lower COD rejection rates were observed (Figure 28b) than in case of synthetic wastewaters containing only BSA, highlighting the need for further treatment.

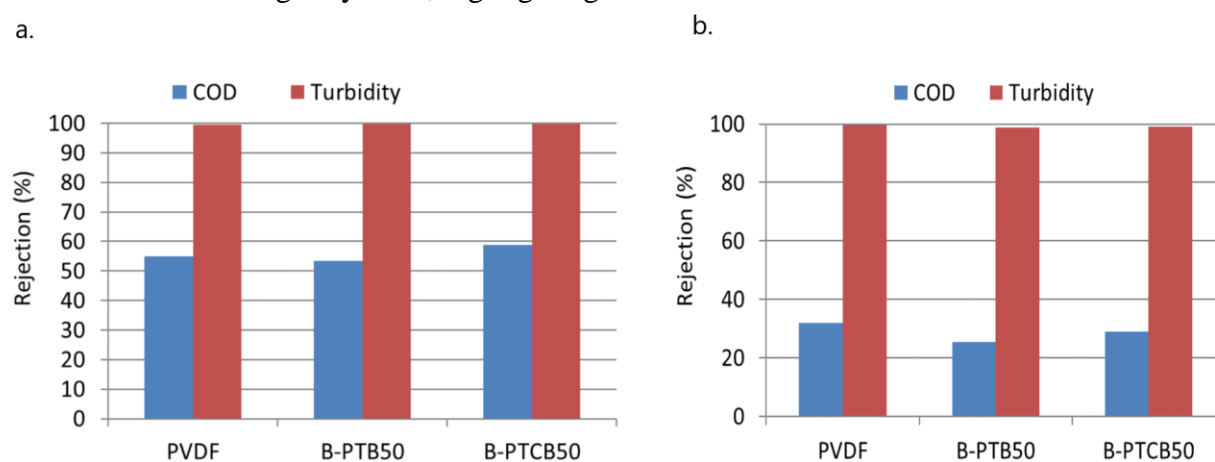


Figure 28. Rejection performance of pristine PVDF, B-PTB50 and B-PTCB50 membranes during real dairy wastewater filtration, raw (a) or pre-filtered (0.2 μm filter paper) (b)

5.4.2.3. Visible-light regeneration of fouled membranes

Figure 29 displays the outcomes of the regeneration process applied to membranes fouled by real dairy wastewater components. As depicted in the figure, the modified membranes were able to be regenerated to a greater extent visible light photocatalysis after pre-filtered real dairy wastewater filtration (Figure 29b), compared to raw real dairy wastewater filtration (Figure 29a). Notably, the PTCB membranes showed better flux restoration after water flushing than PTB membranes (Figure 29b). Additionally, the inclusion of 2% CNTs in the membranes led to slightly better regeneration performance, possibly due to their ability to prevent electron recombination (Figure 29b).

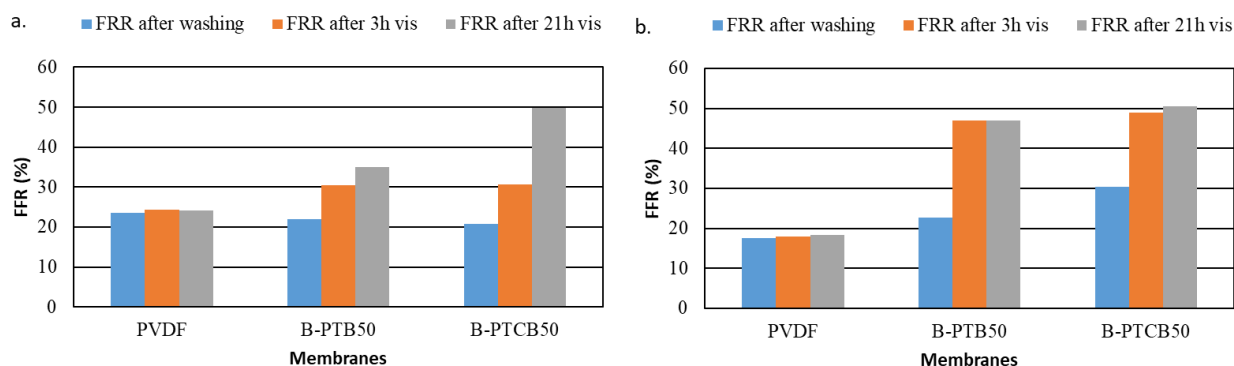


Figure 29. Regeneration performance of fouled PVDF, B-PTB50 and B-PTCB50 membranes of real dairy wastewater, raw (a) or pre-filtered (0.2µm filter paper) (b)

6. Conclusions

Industrial dairy wastewater treatment by means of hybrid nanocomposite PVDF membranes hold great potential for addressing various environmental issues, particularly those related to water scarcity and pollution. They also present a valuable chance to utilize visible light for cleaning the membranes, thereby decreasing reliance on costly and ecologically harmful chemicals or energy-intensive UV light.

This PhD work dealt to fabricate nanocomposite PVDF membranes by adding of TiO_2 , and/or CNT, and/or BiVO_4 , and to examine their antifouling performance during the filtration of BSA solution, synthetic and real dairy wastewater. Another target was to investigate the possibility of cleaning of the fouled membranes by means of UV or visible light photocatalysis. Two fabrication methods were applied, physical coating and blending.

In case of coated membranes commercial PVDF, PVDF- TiO_2 (C-PT) and PVDF- TiO_2 -CNT (C-PTC) membranes were investigated. It was concluded that C-PT or all C-PTC membranes performed more than 97% regeneration by UV light, moreover all TiO_2 - BiVO_4 modified PVDF membranes or PB membranes exhibited better regeneration by visible light than pristine PVDF or PT. After ultrafiltration of BSA model solution the best regeneration flux recovery ratio, (FRR=96.8 %) can be obtained by C-PTC membrane after 2h UV light irradiation, while FRR of 84 % and 97.7 %, can be obtained by C-PTB membranes after 3h and 21 h visible light irradiation respectively.

Pristine PVDF and blended PVDF- TiO_2 (B-PT), PVDF- BiVO_4 (B-PB), PVDF- TiO_2 - BiVO_4 (B-PTB) and PVDF- TiO_2 -CNT- BiVO_4 (B-PTCB) membranes were fabricated by phase inversion method. XRD and SEM measurements for B-PT, B-PB, B-PTB and B-PTCB blended membranes showed that 200–300 nm-sized, aggregated nanoparticles were present in the membrane surface, which enhanced the roughness of composite blended membranes (AFM results). During BSA solution ultrafiltration, excellent antifouling properties of blended membranes were observed, higher flux, decreased fouling and lower N/F ratio on the surface (EDX), than those of the pristine membrane. The neat PVDF membrane showed a good BSA rejection. Composite membranes exhibited comparable, but slightly lower BSA and COD rejections than those of the neat membrane. Extent of fouling in membrane surface can easily be studied by Energy-dispersive X-ray spectroscopy (EDX).

The aim of adding TiO_2 into PVDF was to enhance hydrophilicity and antifouling property of the membrane. The study revealed that incorporating TiO_2 into the membrane improved its performance compared to the membrane without TiO_2 . Moreover, the addition of CNTs further enhanced the hydrophilicity and filtration performance of the membrane. However, it was found that the optimal concentration of CNTs was 2%, as higher concentrations led to irreversible fouling.

Therefore, this concentration was utilized for all CNT-based membrane preparations. Additionally, composite membranes containing both BiVO₄ and TiO₂ exhibited better performance than those containing only one of these nanoparticles. The B-PTCB composites demonstrated the best antifouling properties. The most effective composite was the one with a ratio of 2 wt% CNT and 50-50 wt% TiO₂ and BiVO₄. Although the B-PTB composites had the best regeneration performance under visible light, the restoration of flux for CNT-BiVO₄-containing membranes was superior to that of BiVO₄-containing membranes without photocatalysis. Nevertheless, the presence of CNTs decreased the efficiency of photocatalytic regeneration, likely due to the absorption of light by CNTs.

Blended membranes used for ultrafiltration of synthetic dairy wastewater are significantly impacted by salinity (EC level), pH, and lactose concentration. These factors influence the filtration resistance and rejection performance of the membranes. When the EC level was higher (>4), there was a higher total and irreversible resistance, and a slightly lower COD rejection. The presence of lactose resulted in an increase in irreversible resistance and a significant reduction in COD rejection. Specifically, in the presence of 1gL⁻¹ lactose during UF filtration of synthetic dairy wastewater, COD rejection was reduced to approximately 50-60% for all investigated membranes. Decreased fouling and slightly enhanced COD rejection were observed at pH 7.5 and pH 9.5 compared to pH 4, owing to the strong repulsion force between the negative charge on the membrane surface and the negative charge of the protein (BSA). During ultrafiltration of unfiltered or prefiltered real dairy waste water, both the total and irreversible resistances of B-PTB50 and B-PTCB50 hybrid blended membranes were lower than pristine membranes. The highest and the lowest COD rejection were 60% for B-PTCB50 and 25% for pristine PVDF respectively. The lower rejection performances of the membranes were due to ability of lactose to pass through the membranes which requires further treatment.

7. Summary

In this PhD dissertation, I have fabricated hybrid nanocomposite PVDF membranes by adding of TiO_2 , and/or CNT, and/or BiVO_4 , and investigated their antifouling performance during the filtration of BSA solution, synthetic dairy wastewater and real dairy waste water. I have also studied the regeneration performance of the fouled membranes under UV or visible light.

In the Literature review section, I have provided an overview on the application of membrane filtration in dairy industry processes. Besides I presented the characteristics of industrial dairy wastewater. I highlighted membrane filtration application for industrial dairy wastewater treatment and, discussed the problem of membrane fouling and their mechanisms in membrane filtration of dairy wastewater. I have presented and discussed factors affecting membrane fouling, that may include membrane properties (hydrophilicity, roughness, functional groups and surface charge), composition of the wastewater: foulant type (concentration, pH, ionic strength) and hydrodynamic operating condition: (trans-membrane pressure (TMP), flow velocity, temperature). I have presented and discussed the most important membrane fouling control and mitigation strategies. These strategies include pre-treatment of feed solution, physical membrane cleaning, chemical membrane cleaning, physicochemical membrane cleaning and membrane modification. A focus was given to membrane modification by semiconductor heterogeneous photo-catalysts. I have discussed this topic in detail. I have also presented classification of catalytic membrane reactors and methods of preparation.

In my result and discussion section, I have presented the photocatalytic activity of composite nanoparticles containing TiO_2 , BiVO_4 and CNT. I fabricated coated and blended nanocomposite membranes by physical deposition and phase inversion method respectively. I have presented and discussed the characteristics of the fabricated membranes. Hydrophilicity of the membranes were described by measuring contact angle using the sessile-drop method with a suitable contact angle measuring instrument. I have also presented the porosity and pore size of the membranes which were performed by Guerout–Elford–Ferry equation and Brunauer-Emmett-Teller (BET) measurements. I have presented the surface zeta potentials of the membrane which were calculated from measurements of streaming potential (measured from SurPASS 3) using Helmholtz-Smoluchowski (H-S) equation. I have presented the crystalline and morphological structure of blended membranes.

X-ray diffraction (XRD) and Scanning electron microscope (SEM) measurements for B-PT, B-PB, B-PTB and B-PTCB hybrid blended membranes revealed that the nanoparticles were present as 200–300 nm-sized aggregates in the membrane, which increased the roughness of composite blended membranes (AFM results). I have also presented the extent of fouling explained by N/F ratio obtained from energy-dispersive X-ray spectroscopy (EDX) measurements. Among the characterized fabricated membranes,

During ultrafiltration of BSA solution, The PVDF hybrid blended membranes demonstrated superior antifouling properties, higher flux, and lower filtration resistance than the pristine PVDF membrane. The pristine membrane exhibited a rejection rate of over 99% for both BSA and BSA expressed in COD, while the composite membranes had comparable but slightly lower BSA and COD rejections than the pristine membrane. The blended PTCB composite membranes exhibited the best antifouling performance, with the optimal nanoparticle ratio being 2 wt% CNT and 50-50 wt% TiO₂ and BiVO₄. However, the blended PTB composite membranes demonstrated the best regeneration performance under visible light. B-PTB and B-PTCB blended membranes showed encouraging results, therefore they were selected for investigation their applicability in synthetic and real dairy wastewater treatment. I performed filtration experiments of PVDF, B-PTB and B-PTCB blended membranes using synthetic and real dairy wastewater. I presented the effects of pH, salinity (EC) and lactose on filtration resistances (calculated by resistances-in-series model) and rejection performance of synthetic dairy wastewater UF. I have also presented the filtration resistance and rejection of PVDF, B-PTB and B-PTCB blended nanocomposite membranes during real dairy wastewater filtration. Finally, I have presented the regeneration of fouled membrane using visible light.

Application of B-PTB and B-PTCB blended nanocomposite membranes for real dairy wastewater treatment offers several benefits at large scale. First, these membranes can recover water and reduce water shortage problem. Second, these membranes reduce contaminants and prevent water pollution.

Third, these membranes offer opportunity to eliminate membrane fouling using visible light; that reduce use of chemicals which are costly and environmentally unfriendly. All objectives of this PhD research thesis are achieved; however, I propose some researches in future. These include:

- Investigating nanoparticles that can degrade all components of real dairy wastewater and enhance regeneration performance of UF membranes
- Investigating lactose rejection performance of a combination of UF and NF membranes during real dairy wastewater treatment.

8. Összefoglalás

Doktori munkám során TiO_2 és/vagy CNT és/vagy BiVO_4 nanorészecskékkel módosított PVDF hibrid nanokompozit membránokat állítottam elő, és vizsgáltam eltömődést gátló teljesítményüket BSA oldat, szintetikus tejipari szennyvíz és valódi tejipari szennyvíz szűrése során. Vizsgáltam továbbá a szennyezett membránok regenerálhatóságát UV vagy látható fény hatására.

Az Irodalmi részben áttekintést adtam a membránszűrés tejipari alkalmazásáról, emellett bemutattam a tejipari szennyvíz jellemzőit. Kiemeltem a membránszűrés alkalmazhatóságát a tejipari szennyvíz kezelésében, és tárgyaltam a membránok eltömődésének problémáját és mechanizmusait. Bemutattam a membránok eltömődését befolyásoló tényezőket, így a membrán tulajdonságait (hidrofilítás, érdesség, funkcionális csoportok és felületi töltés), a szennyvíz összetételét (a szennyezőanyag típusa, koncentráció, pH, ionerősség) és a hidrodinamikai működési feltételeket (transzmembrán nyomás (TMP), áramlási sebesség, hőmérséklet). Bemutattam a legfontosabb membráneltömődést csökkentő stratégiákat. Ezen stratégiák közé tartozik a betáplált szennyvíz előkezelése, a fizikai és kémiai membrántisztítás, a fizikai-kémiai membrántisztítás és a membrán módosítása. Kiemelten foglalkoztam a félvezető heterogén fotokatalizátorokkal történő membránmódosítással. Bemutattam a katalitikus membránreaktorok osztályozását és az előállítási módszereket is.

Az Eredmények és értékelésük fejezetben bemutattam a TiO_2 -ot BiVO_4 -ot és szén nanocsöveket tartalmazó keverékek fotokatalitikus aktivitását. A bevont és anyagában módosított nanokompozit membránokat fizikai leválasztással, illetve fázis inverziós módszerrel állítottam elő. Bemutattam az előállított membránok jellemzőit. A membránok hidrofilítását a kontaktszög mérésével jellemeztem. Bemutattam továbbá a membránok porozitását és pórusméretét, amelyeket Guerout-Elford-Ferry egyenlet alkalmazásával és Brunauer-Emmett-Teller (BET) mérések során kaptam. Bemutattam a membránok felületi zéta-potenciálját, amelyet az áramlási potenciál mérésekből a Helmholtz-Smoluchowski (H-S) egyenlet segítségével számítottam. Vizsgáltam az anyagában módosított membránok szerkezetét.

A B-PT, B-PB, B-PTB és B-PTCB hibrid kevert membránok röntgendiffrakciós (XRD) és pásztázó elektronmikroszkópos (SEM) mérései azt mutatták, hogy a nanorészecskék 200-300 nm méretű aggregátumokként voltak jelen a membránban, ami növelte a kompozit membránok felületi érdességét (AFM eredmények). Bemutattam továbbá, hogy a szennyezők kisebb mértékben rakódnak le a módosított membránok felületén, amelyet bizonyított az energiadisziperzív röntgenspektroszkópiás (EDX) mérésekből kapott felületi N/F-arány is.

A BSA oldat ultraszűrése során a hibrid membránok kiváló eltömődést gátló tulajdonságokat, nagyobb fluxust és alacsonyabb szűrési ellenállást mutattak, mint a tiszta PVDF membrán. A tiszta PVDF-membrán nagyon jó elválasztási hatékonysággal rendelkezik, a visszatartás több, mint 99%-

os volt a BSA esetében. A kompozit membránok hasonló, de kissé alacsonyabb BSA- és COD-visszaautasítást mutattak, mint a tiszta PVDF membrán.

A legjobb eltömődést gátló teljesítményt az anyagában módosított PVDF-TiO₂-CNT-BiVO₄ kompozit membránok esetében tapasztaltam; a leghatékonyabbnak a 2% CNT és 50-50% TiO₂, illetve BiVO₄ tartalmú membrán bizonyult. A látható fénnel történő regeneráció szempontjából a legjobb teljesítményt a PVDF-TiO₂-BiVO₄ kompozit membránok nyújtották. A B-PTB és B-PTCB membránok biztató eredményeket mutattak, ezért ezeket választottam ki a szintetikus és valós tejipari szennyvizek szűrésére való alkalmazhatóságuk vizsgálatára. Szűrési kísérleteket végeztem PVDF, B-PTB és B-PTCB kevert membránokkal szintetikus és valós tejipari szennyvíz felhasználásával. Bemutattam a pH, a sótartalom (EC) és a laktóz hatását a szűrési ellenállásra (a sorba kapcsolt ellenállások modelljével számolva) és a visszatartásra szintetikus tejipari szennyvíz ultraszűrése esetében. Bemutattam továbbá a PVDF, B-PTB és B-PTCB nanokompozit membránok szűrési ellenállását és visszatartását valós tejipari szennyvíz szűrése során. Végül vizsgáltam az eltömődött membrán látható fénnel való regenerálhatóságát.

A B-PTB és B-PTCB nanokompozit membránok alkalmazása valós tejipari szennyvizek kezelésére számos előnyt kínálhat. Először is, ezen membránok alkalmazása lehetővé teszi a víz visszaforgatását a technológiai folyamatba, és csökkentheti a vízhiány problémáját. Másodszor, ezek a membránok jó szennyezőanyag-visszatarással rendelkeznek, ezáltal megakadályozzák a vízszennyezést.

Harmadszor, a membránok könnyen tisztíthatók látható fénnel történő besugárzással, ami lehetővé teszi a költséges és környezetszennyező vegyszerek használatának mellőzését. A doktori értekezés minden célkitűzése megvalósult; azonban a jövőbeli vizsgálatokhoz a következő javaslataim vannak:

- További kutatások szükségesek olyan nanorészecskék kifejlesztéséhez, amelyek képesek lebontani a valódi tejipari szennyvíz minden összetevőjét, és növelik az UF-membránok regenerációs teljesítményét.
- A laktóz hatékony elválasztása érdekében szükség van az ultraszűrés és a nanoszűrés kombinációjára, amennyiben a valós tejipari szennyvíz kezelése során szükséges a szerves szennyezők mennyiségének további csökkentése.

9. New scientific results

1. New TiO₂ and CNT containing PVDF based photocatalytic composite UF membranes were produced. It was proved that despite its hydrophobic nature, addition of CNT enhanced the hydrophilicity of the membrane. I have determined the optimal CNT ratio in the membrane, and it was 2%.
 - a. The enhanced hydrophilicity of the membrane was proved by reduced contact angle (from 75° pristine commercial PVDF to 0° of C-PTC2 and from 78° of fabricated pristine PVDF to 71° B-PTC2,)
 - b. It was proven that these membranes can be successfully regenerated by UV-irradiation. Best regeneration with 96.89 % flux recovery ratio (FRR) was achieved in case of coated membrane (C-PTC2, containing 11.37 gm⁻² TiO₂ and 0.057 gm⁻² CNT), while FRR=64.07% can be obtained by blended PVDF-TiO₂-CNT (B-PTC2, containing 0.98 % TiO₂ and 0.02 % CNT in the PVDF) after 2h UV light exposure.
2. BiVO₄ blended photocatalytic PVDF membranes were fabricated. It was proven, that BiVO₄ was successfully built to PVDF-base membranes resulting in new, visible light-active photocatalytic composite membranes.
 - Membrane performance can be further enhanced by addition of TiO₂ or CNT.
 - The highest and improved water flux (150.52 L m⁻² h⁻¹) was obtained by PVDF-TiO₂-CNT- BiVO₄ blended hybrid UF membrane.
 - High (more than 97%) BSA rejection was obtained by PVDF-TiO₂-CNT-BiVO₄ blended hybrid UF membrane
 - Lower irreversible and total resistances were gained by PVDF-TiO₂/BiVO₄ and PVDF-TiO₂/CNT/ BiVO₄ blended hybrid UF membranes than pristine PVDF.
 - The lowest irreversible and total resistance were presented by PVDF-TiO₂/CNT/ BiVO₄ blended hybrid UF membrane
 - The best antifouling propriety which was proved by lowest irreversible and total resistance was exhibited by PVDF-TiO₂-CNT/-BiVO₄ blended hybrid UF membrane
 - Energy-dispersive X-ray spectroscopy (EDX) measurements revealed that the nitrogen to fluorine ratio (N/F) of BSA fouled PVDF membrane was 3-4 times higher than fouled PVDF-TiO₂-BiVO₄ and PVDF-TiO₂-CNT--BiVO₄ blended hybrid UF membranes, which imply that the antifouling propriety of the hybrid membranes is better than the pristine PVDF membrane.

- PVDF-TiO₂/BiVO₄ blended hybrid membrane showed best photocatalytic regeneration performance under visible light, provided the best, (70%) flux recovery ratio during BSA solution filtration.
3. The effect of salt content, pH and concentration of lactose on filtration performance were investigated in order to establish the application of composite membranes for treatment of dairy wastewaters.
- It was proved that the salinity affects the membrane performance as higher irreversible and total resistance, and slightly lower COD rejection was observed at higher EC level (>4) than lower EC level.
 - The presences of lactose increased the irreversible resistance and severely reduce COD rejection. In the presence of 1gL⁻¹ of lactose during synthetic dairy waste water UF filtration, the COD rejection of pristine PVDF, B-PTB50 and B-PTCB50 membranes were reduced to about 50-60 %.
 - Lower resistances and slightly better COD rejection were observed at pH 7.5 and pH 9.5 as compared to pH 4. The lower resistance at higher pH was due to strong repulsion force between negative charge surface of the membranes and the negative charge of the protein (BSA).
4. It was proved PVDF-TiO₂-BiVO₄ and PVDF-TiO₂-CNT-BiVO₄ blended hybrid membranes performed better antifouling, flux, regeneration and COD rejection during real dairy waste water treatment as compared to pristine PVDF.
- During real dairy waste water UF, both the total and irreversible resistances of B-PTB50 (containing 0.5 wt % TiO₂ and 0.5 wt % BiVO₄ in PVDF) and B-PTCB50 (containing 0.48 wt % TiO₂, 0.02 wt % CNT and 0.5 wt % BiVO₄) hybrid blended membranes were lower than pristine membranes.
 - The highest COD rejection performance for unfiltered and prefiltered real dairy wastewater were 60 % by B-PTCB50 and 30 % by pristine PVDF membrane respectively
 - During real dairy waste water UF B-PTCB50 blended hybrid UF membrane performed the best regeneration, about 50% FRR under visible light.

10. Publications

1. Sisay, Elias Jigar, Szabolcs Kertész, Ákos Fazekas, Zoltán Jákói, Endre Zsolt Kedves, Tamás Gyulavári, Áron Ágoston, Gábor Veréb, and Zsuzsanna László, (2023) Application of BiVO₄/TiO₂/CNT Composite Photocatalysts for Membrane Fouling Control and Photocatalytic Membrane Regeneration during Dairy Wastewater Treatment" Catalysts 13, no. 2: 315. <https://doi.org/10.3390/catal13020315> (Q2, IF 4.5)
2. Sisay, Elias Jigar; Veréb, Gábor; Pap, Zsolt; Gyulavári Tamas; Ágoston, Áron; Kopniczky, Judit; Hodúr, Cecília; Arthanareeswaran, Gangasalam; Krishnan, Gokula; Arumugam, Sivasundari; Laszló, Zsuzsanna: (2022) Visible-light-driven photocatalytic PVDF-TiO₂/CNT/BiVO₄ hybrid nanocomposite ultrafiltration membrane for dairy wastewater treatment. CHEMOSPHERE 307:1. 135589, <https://doi.org/10.1016%2Fj.chemosphere.2022.135589> (Q1, IF: 8.943)
3. Elias Jigar and László, Zsuzsanna (2021) Trend and Novel Possibilities of Dairy Wastewater Treatment by Membrane Filtration. Journal of engineering Science and Technology Review. 14(1):46-55. <http://dx.doi.org/10.25103/jestr.141.04> (Q3)
4. Elias Jigar; Bagi, Krisztina; Fazekas, Ákos; Kertész, Szabolcs; Veréb, Gábor; László, Zsuzsanna (2020) Filtration of BSA through TiO₂ Photocatalyst Modified PVDFmembranes. Desalination and Water Treatment 192 pp. 392-399., 8 p. <https://doi.org/10.5004%2Fdwt.2020.25464> (Q3, IF: 1.254)
5. Elias Jigar, Sisay; Ákos, Fazekas; Gábor Veréb, Zsuzsanna, László: Investigation of inorganic nanoparticles containing photocatalytic PVDF membranes for model dairy wastewater treatment (In progress)

MTMT identification number: 10066623

Conference presentations

1. **Elias Jigar, Sisay;** Ákos, Fazekas ; Zsuzsanna, László: Effects of TiO₂ concentrations on ultrafiltration PVDF/TiO₂ membrane for dairy wastewater treatment. ICOSTEE conference book of abstracts, Szeged, Hungary (2022)
2. **Elias Jigar, Sisay;** Ákos, Fazekas; Zsuzsanna, László: Fabrication and Characterization of PVDF/TiO₂/BiVO₄ Nano composite Polymeric Ultrafiltration Membranes for Wastewater

Treatment. Membrane Materials - Modification and Separation (M3-S) Conference) Programme Booklet Toruń, Poland (2021). p34

3. **Elias, Jigar Sisay**; Ákos, Fazekas; Zsuzsanna, László: Poly(vinylidene fluoride) / TiO₂-CNT nanocomposite ultrafiltration membranes for wastewater treatment in: Alapi, Tünde; Berkecz, Róbert; Ilisz, István (ed.) Proceedings of the 26th International Symposium on Analytical and Environmental Problems Szeged, Hungary: University of Szeged (2020) 405 p. pp. 49-53., 5 p
4. **Elias Jigar, Sisay**; László, Zsuzsanna; Fazekas, Ákos Ferenc: Membrane separation process for dairy wastewater treatment in: Alapi, Tünde; Ilisz, István(szerk). Proceedings of the 25th International Symposium on Analytical and Environmental Problems Szeged, Magyarország: University of Szeged, (2019) pp. 84-84., 1 p.
5. **Elias Jigar, Sisay**; Krisztina, Bagi; Ákos, Fazekas; Szabolcs, Kertész; Gábor, Veréb; Zsuzsanna, László: Dairy wastewater treatment using photocatalytic polymer nanocomposite membrane in: Gábor, Rákhely; Cecilia, Hodúr (szerk.) II. Sustainable Raw Materials Conference Book - International Project Week and Scientific Conference Szeged, Magyarország: University of Szeged, (2019) pp. 258-266., 9 p.
6. **Elias Jigar Sisay**; Krisztina, Bagi; Ákos, Fazekas; Szabolcs, Kertész; Gábor, Veréb; Zsuzsanna, László: Filtration of proteins through TiO₂ photocatalyst modified PVDF membranes in: Hungarian, Chemical Society (szerk.) PERMEA 2019 - Membrane Conference of Visegrád Countries - Program and Book of Abstracts Budapest, Magyarország: Hungarian Chemical Society, (2019) p. 81

Conference presentations as co-author

1. Fazekas, Ákos Ferenc; **Elias, Jigar Sisay**; Erika, Nascimben Santos; Beszédes, Sándor; Kertész, Szabolcs; Veréb, Gábor; Hodúr, Cecília; László, Zsuzsanna: Nanoparticle Modified Membranes in Wastewater Treatment: Hungarian Water and Wastewater Technology Association Dr. DulsőDulovics Junior Symposium -Abstract booklet (2021) pp. 17-18., 2 p.
2. Fazekas, Ákos Ferenc; David, Major; **Elias, Jigar Sisay**; Gábor, Veréb; Zsuzsanna, László: Possibilities of Applying Modified Polymer Membranes for Wastewater Treatment in: Bozena, Muszynska 3rd - International Conference on Pharmaceutical and Medical Sciences Krakow, Poland: ZOZ Osrodek UMEA Shinoda-Kuracejo (2020) pp. 201-202.,
3. Fazekas, Ákos Ferenc; Bagi, Krisztina; **Elias, Jigar Sisay**; Veréb, Gábor; Kertész, Szabolcs; Beszédes, Sándor; Hodúr, Cecília; László, Zsuzsanna: Use of Titanium Dioxide Modified PVDF Membranes to remove Dairy Contaminants in: Majdik, Kornélia (ed.) 25th

- International Conference on Chemistry. Cluj-Napoca, Romania: Hungarian Technical Scientific Society of Transylvania (EMT) (2019) 140 p. p. 87
4. Zsuzsanna, László; Mihály, Zakar; Ákos, Fazekas; **Elias Jigar, Sisay**; Gábor, Veréb: Effect of Advanced Oxidation Pretreatments on Membrane Filtration of Proteins Containing Waste Waters. In: Hussain, Al-Ekabi, Tünde Alapi: Proceedings of 5th International conference on new photocatalytic materials for environment, energy, and sustainability(NPM-5) & The 6th international conference on photocatalytic and advanced oxidation technologies for the treatment of water, air, soil and surfaces(PAOT-6). Szeged, Hungary, University of Szeged (2021). pp. 79-79.,1 p. Scientific.
 5. Fazekas Ákos Ferenc; Bagi Krisztina; Elias Jigar Sisay; Veréb Gábor; Kertész Szabolcs; Beszédes Sándor; Hodúr Cecília; László Zsuzsanna: Titán-dioxiddal módosított PVDF membránok alkalmazása tejipari szennyezők eltávolítására. In: Majdik Kornélia (eds.)25th International Conference on Chemistry Kolozsvár, Cluj-Napoca, Romania 2019.10.24. - 2019.10.26. (Hungarian Technical Scientific Society from Transilvania) Cluj-Napoca: Hungarian Technical Scientific Society from Transilvania, p. 87. (2019) (Nemzetközi Vegyészkonferencia 1843-6293).
 6. Fazekas Ákos Ferenc; **Elias Jigar Sisay**; Erika Nascimben Santos; Beszédes Sándor; Kertész Szabolcs; Veréb Gábor; Hodúr Cecília; László Zsuzsanna: Nanorészecskékkel módosított membránok a szennyvízkezelésben. in: Magyar Víz- és Szennyvíztechnikai Szövetség Dr. Dulovics Dezső Junior Szimpózium – Absztraktfüzet 2021.03.03. - 2021.03.04. pp 17-18 (2021)

ACKNOWLEDGEMENTS

I would like to express my sincere gratitude to my supervisor Prof. Dr. László Zsuzsanna for her scientific advice and knowledge. I would like to thank for her helpful and excellent guidance, constructive ideas and feedbacks, and continuous encouragement throughout my Ph.D. studies. I really appreciate that she motivated and guided me towards my academic life. I am glad that I could pursue my doctoral studies under her supervision.

My special thanks also go to Prof. Dr. Gangasalam Arthanareeswaran, Prof. Dr. Cecilia Hodùr, Dr. Gábor Veréb and Dr. Szabolcs Kertész who actively took part and significantly contributed to my study. They help me in many technical and professional issues and offered many meaningful suggestions.

I extend my gratitude to all my lab members Erika Nascimben Santos, Ákos Fazekas, Hadid Sukmana and Liceth Pantoja for their help, support, and a pleasant environment during the long hours in the lab.

My grateful acknowledgement also goes to the Department of Applied and Environmental Chemistry, Doctoral School of Environmental Sciences, for offering me the chance to pursue my doctoral studies at University of Szeged. I extend my gratitude to all colleagues in the Department of Biosystems Engineering for their valuable help in my research and for giving me the opportunity of being part of their research team.

I would also like to take this opportunity to acknowledge Indo-Hungarian project (Hungarian Science and Research Foundation, 2017-2.3.7-TÉT-IN-2017-00016 and Ministry of Science and Technology of the Government of India, DST/INT/HUN/P17/2017), and Tempus Public Foundation (Stipendium Hungaricum Scholarship) for providing financial support to conduct the research work of my doctoral study smoothly.

Finally, many thanks to my family, my parents and my friends for the immense support they offered to me in all these years, without their support, I would not have stayed strong to finish my study.

References

- Abazari, R., Mahjoub, A. R., Shariati, J., & Noruzi, S. (2019). Photocatalytic wastewater purification under visible light irradiation using bismuth molybdate hollow microspheres with high surface area. *Journal of cleaner production*, 221, 582-586.
- Abdelkader S., Gross F., Winter D., Went J., Koschikowski J, Geissen S. U. Bousselmi L. (2019). Application of direct contact membrane distillation for saline dairy effluent treatment: performance and fouling analysis. *Environmental Science and Pollution Research*. 26, 18979–18992.
- Aburabie J., Villalobos L.F. & Peinemann K.V. (2017). Composite Membrane Formation by Combination of Reaction-Induced and Non Solvent-Induced Phase Separation. *Macromolecular Materials and Engineering*, 302(9). 1700131
- Ahmad, T., Aadil, R. M., Ahmed, H., ur Rahman, U., Soares, B. C., Souza, S. L., ... & Cruz, A. G. (2019). Treatment and utilization of dairy industrial waste: A review. *Trends in Food Science & Technology*, 88, 361-372.
- Ahmad, A. L., Che Lah, N. F., Ismail, S., & Ooi, B. S. (2012). Membrane antifouling methods and alternatives: Ultrasound approach. *Separation & Purification Reviews*, 41(4), 318-346.
- Akamatsu, K., Kagami, Y., & Nakao, S. I. (2020). Effect of BSA and sodium alginate adsorption on decline of filtrate flux through polyethylene microfiltration membranes. *Journal of Membrane Science*, 594, 117469.
- Akhavan, O. (2009). Lasting antibacterial activities of Ag–TiO₂/Ag/a-TiO₂ nanocomposite thin film photocatalysts under solar light irradiation. *Journal of colloid and interface science*, 336(1), 117-124.
- Aktij, S. A., Taghipour, A., Rahimpour, A., Mollahosseini, A., & Tiraferri, A. (2020). A critical review on ultrasonic-assisted fouling control and cleaning of fouled membranes. *Ultrasonics*, 108, 106228.
- Al Aani, S., Mustafa, T. N., & Hilal, N. (2020). Ultrafiltration membranes for wastewater and water process engineering: A comprehensive statistical review over the past decade. *Journal of Water Process Engineering*, 35, 101241.
- Al-Gharabli, S., El-Rub, Z. A., Hamad, E. M., Kujawski, W., Flanc, Z., Pianka, K. & Kujawa, J. (2022). Toward anti-fouling properties and enhanced performance in separation process-carbon nanotubes-PVDF hybrids. *Applied Surface Science*, 602, 154341.
- Altaee, A., Al-Rawajfeh, A. E., & Baek, Y. J. (2009). Application of vibratory system to improve the critical flux in submerged hollow fiber MF process. *Separation science and technology*, 45(1), 28-34.

- Andrade, L. H., Mendes, F. D. S., Espindola, J. C., & Amaral, M. C. S. (2014). Nanofiltration as tertiary treatment for the reuse of dairy wastewater treated by membrane bioreactor. *Separation and Purification Technology*, 126, 21-29.
- Angelo, D. D., Filice, S., Scarangella, A., Iannazzo, D., Compagnini, G., & Scalese, S. (2019). Bi2O3/Nexar® polymer nanocomposite membranes for azo dyes removal by UV-vis or visible light irradiation. *Catalysis Today*, 321, 158-163.
- Anis, S. F., Lalia, B. S., Hashaikh, R., & Hilal, N. (2022). Titanium coating on ultrafiltration inorganic membranes for fouling control. *Separation and Purification Technology*, 282, 119997.
- Atra, R., Vatai, G., Bekassy-Molnar, E., & Balint, A. (2005). Investigation of ultra-and nanofiltration for utilization of whey protein and lactose. *Journal of food engineering*, 67(3), 325-332.
- Ayyaru, S., & Ahn, Y. H. (2017). Application of sulfonic acid group functionalized graphene oxide to improve hydrophilicity, permeability, and antifouling of PVDF nanocomposite ultrafiltration membranes. *Journal of Membrane Science*, 525, 210-219.
- Ayyaru, S., Pandiyan, R., & Ahn, Y. H. (2019). Fabrication and characterization of anti-fouling and non-toxic polyvinylidene fluoride-Sulphonated carbon nanotube ultrafiltration membranes for membrane bioreactors applications. *Chemical Engineering Research and Design*, 142, 176-188.
- Bacchin P., Aimar P., Field R., Aimar R.F. (2006). Critical and sustainable fluxes: theory, experiments and applications, *Journal of Membrane Science*, 281, 42-69.
- Barakat, M. A., Anjum, M., Kumar, R., Alafif, Z. O., Oves, M., & Ansari, M. O. (2020). Design of ternary Ni (OH) 2/graphene oxide/TiO2 nanocomposite for enhanced photocatalytic degradation of organic, microbial contaminants, and aerobic digestion of dairy wastewater. *Journal of Cleaner Production*, 258, 120588.
- Bellardita M., Camera R.G., Loddo V., Parrino F., & Palmisano L. (2018). Coupling of the membrane and photocatalytic technologies for selective formation of high added-value chemicals. *Catalysis Today*, 340. 128–144.
- Bixio, Davide, C. Thoeve, J. De Koning, Darko Joksimovic, Dragan Savic, T. Wintgens, and Thomas Melin. (2006) "Wastewater reuse in Europe." *Desalination* 187, no. 1-3: 89-101.
- Bortoluzzi A.C., Faitão J.A., Di Luccio M., Dallago R.M., Steffens J., Zabot G.L., Tres M.V. (2017). Dairy wastewater treatment using integrated membrane systems. *Journal of Environmental Chemical Engineering*, 5(5), 4819–4827.
- Bottino, A., Capannelli, G., & Comite, A. (2002). Preparation and characterization of novel porous PVDF-ZrO2 composite membranes. *Desalination*, 146(1-3), 35-40.

- Bustillo-Lecompte, C. F., & Mehrvar, M. (2015). Slaughterhouse wastewater characteristics, treatment, and management in the meat processing industry: A review on trends and advances. *Journal of environmental management*, 161, 287-302.
- Cai, W., Gao, Z., Yu, S., Lv, M., Shi, Y., & Wang, J. (2021). New insights into membrane fouling formation during ultrafiltration of organic wastewater with high salinity. *Journal of Membrane Science*, 635, 119446.
- Cai, W., Zhang, J., Li, Y., Chen, Q., Xie, W., & Wang, J. (2022). Characterizing membrane fouling formation during ultrafiltration of high-salinity organic wastewater. *Chemosphere*, 287, 132057
- Camara, H. W., Doan, H., & Lohi, A. (2020). In-situ ultrasound-assisted control of polymeric membrane fouling. *Ultrasonics*, 108, 106206.
- Cao, Q., Yu, Q., Connell, D. W., & Yu, G. (2013). Titania/carbon nanotube composite (TiO₂/CNT) and its application for removal of organic pollutants. *Clean Technologies and Environmental Policy*, 15, 871-880.
- Carroll, T., King, S., Gray, S. R., Bolto, B. A., & Booker, N. A. (2000). The fouling of microfiltration membranes by NOM after coagulation treatment. *Water Research*, 34(11), 2861-2868.
- Catenacci, A., Bellucci, M., Yuan, T., & Malpei, F. (2020). Dairy wastewater treatment using composite membranes. *Current Trends and Future Developments on (Bio-) Membranes*, 261-288.
- Chang, X., Wang, Z., Quan, S., Xu, Y., Jiang, Z., & Shao, L. (2014). Exploring the synergetic effects of graphene oxide (GO) and polyvinylpyrrolidone (PVP) on poly(vinylidene fluoride)(PVDF) ultrafiltration membrane performance. *Applied Surface Science*, 316, 537-548.
- Chang, Y. R., Lee, Y. J., & Lee, D. J. (2019). Membrane fouling during water or wastewater treatments: Current research updated. *Journal of the Taiwan Institute of Chemical Engineers*, 94, 88-96.
- Chang, X., Lin, T., Chen, W., Xu, H., Tao, H., Wu, Y., & Yao, S. (2020). A new perspective of membrane fouling control by ultraviolet synergic ferrous iron catalytic persulfate (UV/Fe (II)/PS) as pretreatment prior to ultrafiltration. *Science of the Total Environment*, 737, 139711.
- Chew, N. G. P., Zhao, S., Malde, C., & Wang, R. (2017). Superoleophobic surface modification for robust membrane distillation performance. *Journal of Membrane Science*, 541, 162-173.
- Chen, G. Q., Leong, T. S. H., Kentish, S. E., Ashokkumar, M., & Martin, G. J. O. (2019). Membrane Separations in the Dairy Industry. *Separation of Functional Molecules in Food by Membrane Technology*.

- Chen, G. Q., Talebi, S., Gras, S. L., Weeks, M., & Kentish, S. E. (2018). A review of salty waste stream management in the Australian dairy industry. *Journal of environmental management*, 224, 406-413.
- Das, T., Rocquefelte, X., Laskowski, R., Lajaunie, L., Jobic, S., Blaha, P., & Schwarz, K. (2017). Investigation of the optical and excitonic properties of the visible light-driven photocatalytic BiVO₄ material. *Chemistry of Materials*, 29(8), 3380-3386.
- Das, B., Sarkar, S., Sarkar, A., Bhattacharjee, S., & Bhattacharjee, C. (2016). Recovery of whey proteins and lactose from dairy waste: A step towards green waste management. *Process Safety and Environmental Protection*, 101, 27-33.
- Deshannavar, U. B., Basavaraj, R. K., & Naik, N. M. (2012). High rate digestion of dairy industry effluent by upflow anaerobic fixed-bed reactor. *Journal of Chemical and Pharmaceutical Research*, 4(6), 2895-2899.
- Deshpande, D. P., Patil, P. J., & Anekar, S. V. (2012). Biomethanation of Dairy Waste. *Research Journal of Chemical Sciences*, 2(4), 35-39.
- Dhand, V., Hong, S. K., Li, L., Kim, J. M., Kim, S. H., Rhee, K. Y., & Lee, H. W. (2019). Fabrication of robust, ultrathin and light weight, hydrophilic, PVDF-CNT membrane composite for salt rejection. *Composites Part B: Engineering*, 160, 632-643.
- Ding, Y., Ma, B., Liu, H., & Qu, J. (2019). Effects of protein properties on ultrafiltration membrane fouling performance in water treatment. *Journal of Environmental Sciences*, 77, 273-281.
- Di Mauro, A., Cantarella, M., Nicotra, G., Pellegrino, G., Gulino, A., Brundo, M. V., ... & Impellizzeri, G. (2017). Novel synthesis of ZnO/PMMA nanocomposites for photocatalytic applications. *Scientific reports*, 7(1), 1-12.
- Du, J., Li, N., Tian, Y., Zhang, J., & Zuo, W. (2020a). Preparation of PVDF membrane blended with graphene oxide-zinc sulfide (GO-ZnS) nanocomposite for improving the anti-fouling property. *Journal of Photochemistry and Photobiology A: Chemistry*, 400, 112694.
- Du, J. R., Zhang, X., Feng, X., Wu, Y., Cheng, F., & Ali, M. E. (2020b). Desalination of high salinity brackish water by an NF-RO hybrid system. *Desalination*, 491, 114445.
- Du, C., Wang, Z., Liu, G., Wang, W., & Yu, D. (2021). One-step electrospinning PVDF/PVP-TiO₂ hydrophilic nanofiber membrane with strong oil-water separation and anti-fouling property. *Colloids and Surfaces A: Physicochemical and Engineering Aspects*, 624, 126790.
- Dutta, A. K., Maji, S. K., & Adhikary, B. (2014). γ -Fe₂O₃ nanoparticles: an easily recoverable effective photo-catalyst for the degradation of rose bengal and methylene blue dyes in the waste-water treatment plant. *Materials Research Bulletin*, 49, 28-34.
- Elimelech, M., & Phillip, W. A. (2011). The future of seawater desalination: energy, technology, and the environment. *science*, 333(6043), 712-717.

- Farahani, M. H. D. A., & Vatanpour, V. (2018). A comprehensive study on the performance and antifouling enhancement of the PVDF mixed matrix membranes by embedding different nanoparticulates: clay, functionalized carbon nanotube, SiO₂ and TiO₂. *Separation and Purification Technology*, 197, 372-381.
- Farrell Jr, H. M., Jimenez-Flores, R., Bleck, G. T., Brown, E. M., Butler, J. E., Creamer, L. K., ... & Swaisgood, H. E. (2004). Nomenclature of the proteins of cows' milk sixth revision. *Journal of dairy science*, 87(6), 1641-1674.
- Fujishima, A., Zhang, X., & Tryk, D. A. (2008). TiO₂ photocatalysis and related surface phenomena. *Surface science reports*, 63(12), 515-582.
- Gao, Y., Hu, M., & Mi, B. (2014). Membrane surface modification with TiO₂-graphene oxide for enhanced photocatalytic performance. *Journal of Membrane Science*, 455, 349-356.
- Galvão, D. F. (2018). Membrane Technology and Water Reuse in a Dairy Industry. *Technological Approaches for Novel Applications in Dairy Processing*. doi:10.5772/intechopen.76464
- Geise, G. M., Lee, H. S., Miller, D. J., Freeman, B. D., McGrath, J. E., & Paul, D. R. (2010). Water purification by membranes: the role of polymer science. *Journal of Polymer Science Part B: Polymer Physics*, 48(15), 1685-1718.
- Gong, Y. W., Zhang, H. X., & Cheng, X. N. (2012). Treatment of dairy wastewater by two-stage membrane operation with ultrafiltration and nanofiltration. *Water Science and Technology*, 65(5), 915-919.
- Gong, Y., Ma, X., Dang, R., Liu, J., & Cao, J. (2017). Synthesis of highly dispersed and versatile anatase TiO₂ nanocrystals on graphene sheets with enhanced photocatalytic performance for dye degradation. *Journal of Materials Science: Materials in Electronics*, 28, 18883-18890.
- Goodyer, C. E., & Bunge, A. L. (2012). Mass transfer through membranes with surface roughness. *Journal of membrane science*, 409, 127-136.
- Guerra-Rodríguez, S., Oulego, P., Rodríguez, E., Singh, D. N., & Rodríguez-Chueca, J. (2020). Towards the implementation of circular economy in the wastewater sector: Challenges and opportunities. *Water*, 12(5), 1431.
- Guan, D., Dai, J., Siddiqui, M. A., & Chen, G. (2018). Comparison of different chemical cleaning reagents on fouling recovery in a Self-Forming dynamic membrane bioreactor (SFDMBR). *Separation and Purification Technology*, 206, 158-165.
- Guan, Y. F., Boo, C., Lu, X., Zhou, X., Yu, H. Q., & Elimelech, M. (2020). Surface functionalization of reverse osmosis membranes with sulfonic groups for simultaneous mitigation of silica scaling and organic fouling. *Water Research*, 185, 116203.
- Guo, M., Xiang, H., Tang, S., Guo, X., Yang, Y., & Zhang, X. (2022). Effect of pyrolysis temperature on structure and photocatalytic properties of biochar-coupled BiVO₄. *Journal of Environmental Chemical Engineering*, 10(2), 107255.

- Gupta, N., Gupta, S. M., & Sharma, S. K. (2019). Carbon nanotubes: Synthesis, properties and engineering applications. *Carbon Letters*, 29, 419-447.
- Han, J. L., Xia, X., Haider, M. R., Jiang, W. L., Tao, Y., Liu, M. J., ... & Wang, A. J. (2018). Functional graphene oxide membrane preparation for organics/inorganic salts mixture separation aiming at advanced treatment of refractory wastewater. *Science of the Total Environment*, 628, 261-270.
- Hausmann A., Sanciolo P., Vasiljevic T., Weeks M., Schroën K., Gray S., Duke M. (2013). Fouling of dairy components on hydrophobic polytetrafluoroethylene (PTFE) membranes for membrane distillation. *Journal of Membrane Science*, 442, 149–159.
- He, Y., Huang, X., Li, T., Lv, X., Tang, N., Feng, C., & Shi, B. (2022). Ultrafiltration membrane fouling control by two-stage coagulant dosing with moderate pH adjustment. *Desalination*, 537, 115893.
- He, Y., Li, L., Fan, W., Zhang, C., & Leung, M. K. (2018). A novel and facile solvothermal-and-hydrothermal method for synthesis of uniform BiVO₄ film with high photoelectrochemical performance. *Journal of Alloys and Compounds*, 732, 593-602.
- Hemmatpour, P., Nezamzadeh-Ejhieh, A., & Ershadi, A. (2022). A brief study on the Eriochrome Black T photodegradation kinetic by CdS/BiVO₄ coupled catalyst. *Materials Research Bulletin*, 151, 111830.
- Holzwarth, U., & Gibson, N. (2011). The Scherrer equation versus the 'Debye-Scherrer equation'. *Nature nanotechnology*, 6(9), 534-534.
- Hou, J., Jiao, S., Zhu, H., & Kumar, R. V. (2011). Facile synthesis and visible-light photocatalytic activity of bismuth titanate nanorods. *Journal of Nanoparticle Research*, 13, 5557-5564.
- Hou T., Dong G., Ye Y. & Chen V. (2014). Enzymatic degradation of bisphenol-A with immobilized laccase on TiO₂ sol-gel coated PVDF membrane. *Journal of Membrane Science*, 469. 19–30.
- Huang, Y., Li, R., Chen, D., Hu, X., Chen, P., Chen, Z., & Li, D. (2018). Synthesis and characterization of CNT/TiO₂/ZnO composites with high photocatalytic performance. *Catalysts*, 8(4), 151.
- Huang, J., Ma, Y., Chen, Q., Zhu, J., Jiang, H., Li, H., & Hong, M. (2022). Effect of water-oil ratio on the photocatalytic performance of visible light-active BiVO₄ nanoparticles prepared by inverse microemulsion-calcination method. *Chemosphere*, 299, 134454.
- Hudaib, B., Gomes, V., Shi, J., Zhou, C., & Liu, Z. (2018). Poly (vinylidene fluoride)/polyaniline/MWCNT nanocomposite ultrafiltration membrane for natural organic matter removal. *Separation and Purification Technology*, 190, 143-155.
- Huisman I.H., Prádanos P., Hernández A. (2000). The effect of protein – protein and protein – membrane interactions on membrane fouling in ultrafiltration, 179, 79–90.

- Hung, Y.-T., Britz, T., & van Schalkwyk, C. (2005). Treatment of Dairy Processing Wastewaters. *Waste Treatment in the Food Processing Industry*, 1–28.
- Isari, A. A., Mehregan, M., Mehregan, S., Hayati, F., Kalantary, R. R., & Kakavandi, B. (2020). Sono-photocatalytic degradation of tetracycline and pharmaceutical wastewater using WO₃/CNT heterojunction nanocomposite under US and visible light irradiations: a novel hybrid system. *Journal of hazardous materials*, 390, 122050.
- Ismail N., Lau W.J., Ismail A.F. , & Goh P. (2013). Preparation and Characterization of Polysulfone/Polyphenylsulfone/Titanium Dioxide Composite Ultrafiltration Membranes for Palm Oil Mill Effluent Treatment. *JurnalTeknologi*, 65(4).
- Jang, D., Hwang, Y., Shin, H., & Lee, W. (2013). Effects of salinity on the characteristics of biomass and membrane fouling in membrane bioreactors. *Bioresource Technology*, 141, 50–56.
- Ji, J., Liu, F., Hashim, N. A., Abed, M. M., & Li, K. (2015). Poly (vinylidene fluoride) (PVDF) membranes for fluid separation. *Reactive and Functional Polymers*, 86, 134–153.
- Jiang S., Li Y., Ladewig B.P. (2017). A review of reverse osmosis membrane fouling and control strategies. *Science of The Total Environment*, 595, 567–583.
- Jiang S, Zhang Y., Zhao F., Yu Z., Zhou X. & Chu H. (2018). Impact of transmembrane pressure (TMP) on membrane fouling in microalgae harvesting with a uniform shearing vibration membrane system. *Algal Research*, 35, 613–623.
- Kazemimoghadam, M., & Mohammadi, T. (2007). Chemical cleaning of ultrafiltration membranes in the milk industry. *Desalination*, 204(1-3), 213–218.
- Khan, S. A., Arshad, Z., Shahid, S., Arshad, I., Rizwan, K., Sher, M., & Fatima, U. (2019). Synthesis of TiO₂/Graphene oxide nanocomposites for their enhanced photocatalytic activity against methylene blue dye and ciprofloxacin. *Composites Part B: Engineering*, 175, 107120.
- Kokko M., Bayerköhler F., Erben J., Zengerle R., Kurz P., & Kerzenmacher S. (2017). Molybdenum sulphides on carbon support as electrocatalysts for hydrogen evolution in acidic industrial wastewater. *Applied Energy*, 190. 1221–1233.
- Kola A., Ye Y., Le-Clech P., Chen V. (2014). Transverse vibration as novel membrane fouling mitigation strategy in anaerobic membrane bioreactor applications, *Journal of Membrane Science*, 455, 320–329
- Kovács, I., Kertész, S., Veréb, G., Papp, I. Z., & Kukovecz, Á. (2017). Membrane fouling control by means of TiO₂ coating during model dairy wastewater filtration. *Desalination and Water Treatment*, 73, 415–421.
- Kovács, I., Veréb, G., Kertész, S., Hodúr, C., & László, Z. (2018). Fouling mitigation and cleanability of TiO₂ photocatalyst-modified PVDF membranes during ultrafiltration of model

- oily wastewater with different salt contents. *Environmental Science and Pollution Research*, 25, 34912-34921.
- Krishan, A., & Srivastava, A. (2015). Recovery of Nutrients from Dairy Wastewater by Struvite Crystallization, 3(5), 591–597.
- Kumar, P., Sharma, N., Ranjan, R., Kumar, S., Bhat, Z. F., & Jeong, D. K. (2013). Perspective of membrane technology in dairy industry: A review. *Asian-Australasian Journal of Animal Sciences*, 26(9), 1347.
- Kumar J., Bansal A. (2013). Photocatalysis by Nanoparticles of Titanium Dioxide for Drinking Water Purification: A Conceptual and State-of-Art Review. *Materials Science Forum*, 764, 130–150.
- Kunduz, S., & Soylu, G. S. P. (2015). Highly active BiVO₄ nanoparticles: the enhanced photocatalytic properties under natural sunlight for removal of phenol from wastewater. *Separation and Purification Technology*, 141, 221-228.
- Kurian M., Nair D.S. (2015). Heterogeneous Fenton behaviour of nano nickel-zinc ferrite catalysts in the degradation of 4-chlorophenol from water under neutral conditions. *Journal of Water Process Engineering*, 8, e37–e49.
- Lakra, R., Choudhury, S., & Basu, S. (2021). Recovery of protein and carbohydrate from dairy wastewater using ultrafiltration and forward osmosis processes. *Materials Today: Proceedings*, 47, 1400-1403.
- Lamdab, U., Wetchakun, K., Phanichphant, S., Kangwansupamonkon, W., & Wetchakun, N. (2016). In VO₄–BiVO₄ composite films with enhanced visible light performance for photodegradation of methylene blue. *Catalysis Today*, 278, 291-302.
- Lavand A.B., Malghe Y.S. (2018). Synthesis, characterisation and visible light photocatalytic activity of carbon and iron modified ZnO. *Journal of King Saud University - Science*, 30(1), 65–74.
- Lawrence, N. D., Perera, J. M., Iyer, M., Hickey, M. W., & Stevens, G. W. (2006). The use of streaming potential measurements to study the fouling and cleaning of ultrafiltration membranes. *Separation and Purification Technology*, 48(2), 106-112.
- Lee, J., Jeong, S., Ye, Y., Chen, V., Vigneswaran, S., Leiknes, T., & Liu, Z. (2017). Protein fouling in carbon nanotubes enhanced ultrafiltration membrane: fouling mechanism as a function of pH and ionic strength. *Separation and Purification Technology*, 176, 323-334.
- Leong, S., Razmjou, A., Wang, K., Hapgood, K., Zhang, X., & Wang, H. (2014). TiO₂ based photocatalytic membranes: A review. *Journal of Membrane Science*, 472, 167-184.
- Li, G., Bai, Y., & Zhang, W. F. (2012). Difference in valence band top of BiVO₄ with different crystal structure. *Materials Chemistry and Physics*, 136(2-3), 930-934.

- Li T., Law A.W.K., Cetin M., Fane A.G. (2013). Fouling control of submerged hollow fibre membranes by vibrations. *Journal of Membrane Science*, 427, 230-239.
- Li.Y, Bilad M.R., Vankelecom I.F.G. (2014). Application of a magnetically induced membrane vibration (MMV) system for lignocelluloses hydrolysate filtration. *Journal of Membrane Science*, 452, 165–170.
- Li M., Wen Q., Chen Z., Tang Y., Yang B. (2019). Comparison of ozonation and UV based oxidation as pre-treatment process for ultrafiltration in wastewater reuse: Simultaneous water risks reduction and membrane fouling mitigation. *Chemosphere*, 125449.
- Li P., Cheng X., Zhou W., Luo C., Tan F., Ren Z., Wu D. (2020). Application of sodium percarbonate activated with Fe(II) for mitigating ultrafiltration membrane fouling by natural organic matter in drinking water treatment. *Journal of Cleaner Production*, 122228.
- Li, X., Shen, S., Xu, Y., Guo, T., Dai, H., & Lu, X. (2021). Application of membrane separation processes in phosphorus recovery: A review. *Science of the Total Environment*, 767, 144346.
- Li Menglin., Huang G., Qiao Y., Wang J., Liu Z., Liu X., Mei Y. (2013). Biocompatible and freestanding anatase TiO₂ nanomembrane with enhanced photocatalytic performance. *Nanotechnology*, 24. 305706.
- Lin, J. C. T., Lee, D. J., & Huang, C. (2010). Membrane fouling mitigation: Membrane cleaning. *Separation Science and Technology*, 45(7), 858-872.
- Lin, X., Lv, P., Guan, Q., Li, H., Zhai, H., & Liu, C. (2012). Bismuth titanate microspheres: directed synthesis and their visible light photocatalytic activity. *Applied Surface Science*, 258(18), 7146-7153.
- Lin, Y. C., Tseng, H. H., & Wang, D. K. (2021). Uncovering the effects of PEG porogen molecular weight and concentration on ultrafiltration membrane properties and protein purification performance. *Journal of Membrane Science*, 618, 118729.
- Lin, Y. L., Zheng, N. Y., Hsu, Y. J., Dong, C. D., Chen, C. W., & Wu, C. H. (2022). In-situ radical graft modification of NF270 to improve membrane separation: Effects of water salinity and fouling types. *Environmental Technology & Innovation*, 27, 102758.
- Liu, F., Hashim, N. A., Liu, Y., Abed, M. M., & Li, K. (2011). Progress in the production and modification of PVDF membranes. *Journal of membrane science*, 375(1-2), 1-27.
- Liu, C., Wu, L., Zhang, C., Chen, W., & Luo, S. (2018). Surface hydrophilic modification of PVDF membranes by trace amounts of tannin and polyethyleneimine. *Applied Surface Science*, 457, 695-704.
- Louie J.S, Pinnau I, CiobanuI, Ishida K.P., Ng A., Reinhard M. (2006). Effects of polyether-polyamide block copolymer coating on performance and fouling of reverse osmosis membranes. *Journal of Membrane Science*, 280(1–2), 762–770.

- Luján-Facundo, M. J., Mendoza-Roca, J. A., Cuartas-Urbe, B., & Álvarez-Blanco, S. (2017). Membrane fouling in whey processing and subsequent cleaning with ultrasounds for a more sustainable process. *Journal of Cleaner Production*, 143, 804-813.
- Ma, Y., Jiang, H., Zhang, X., Xing, J., & Guan, Y. (2014). Synthesis of hierarchical m-BiVO₄ particles via hydro-solvothermal method and their photocatalytic properties. *Ceramics International*, 40(10), 16485-16493.
- Madaeni, S. S., & Mansourpanah, Y. (2004). Chemical cleaning of reverse osmosis membranes fouled by whey, *Desalination*, 161, 13–24.
- Madaeni S.S., Mansourpanah Y. (2006). Screening membranes for COD removal from dilute wastewater. *Desalination*, 197(1–3), 23–32.
- Malathi, A., Arunachalam, P., Kirankumar, V. S., Madhavan, J., & Al-Mayouf, A. M. (2018). An efficient visible light driven bismuth ferrite incorporated bismuth oxyiodide (BiFeO₃/BiOI) composite photocatalytic material for degradation of pollutants. *Optical Materials*, 84, 227-235.
- Malato, S., Fernández-Ibáñez, P., Maldonado, M. I., Blanco, J., & Gernjak, W. (2009). Decontamination and disinfection of water by solar photocatalysis: recent overview and trends. *Catalysis today*, 147(1), 1-59.
- Man, H. C., Abba, M. U., Abdulsalam, M., Azis, R. A. S., Idris, A. I., & Hamzah, M. H. (2020). Utilization of Nano-TiO₂ as an influential additive for Complementing Separation Performance of a Hybrid PVDF-PVP Hollow Fiber: Boron removal from leachate. *Polymers*, 12(11), 2511.
- Mancosu, N., Snyder, R. L., Kyriakakis, G., & Spano, D. (2015). Water scarcity and future challenges for food production. *Water*, 7(3), 975-992.
- Maskooki, A., Mortazavi, S. A., & Maskooki, A. (2010). Cleaning of spiralwound ultrafiltration membranes using ultrasound and alkaline solution of EDTA. *Desalination*, 264(1-2), 63-69.
- McCartney, T. R., Gharaibeh, S., & Shank, R. (2017). Improved methods for removal of silicate deposits. *Heat Exchanger Fouling and Cleaning XII* ISBN, 978-0.
- McMahon, D. J., & Oommen, B. S. (2008). Supramolecular structure of the casein micelle. *Journal of dairy science*, 91(5), 1709-1721.
- Mehta V., Chavan A. (2009). Physico-chemical treatment of tar-containing wastewater generated from biomass gasification plants. *World Academy of Science, Engineering and Technology*, 57(9), 161–168 (2009).
- Mehta C.M., Khunjar W.O., Nguyen V., Tait S., Batstone D.J. (2015). Technologies to recover Nutrients from Waste Streams: A Critical Review. *Crit. Rev. Environ. Sci. Technol.* 45, 385-427(2015).

- Miao R., Wang L., Mi N., Gao Z., Liu T., Lv Y., Yang Y. (2015). Enhancement and Mitigation Mechanisms of Protein Fouling of Ultra Filtration Membranes under Different Ionic Strengths, 49, 6574–6580. (2015).
- Mishra, J. R., Samal, S. K., Mohanty, S., & Nayak, S. K. (2021). Polyvinylidene fluoride (PVDF)/Ag@ TiO₂ nanocomposite membrane with enhanced fouling resistance and antibacterial performance. *Materials Chemistry and Physics*, 268, 124723.
- Mo, Y., Zhang, L., Zhao, X., Li, J., & Wang, L. (2022). A critical review on classifications, characteristics, and applications of electrically conductive membranes for toxic pollutant removal from water: Comparison between composite and inorganic electrically conductive membranes. *Journal of Hazardous Materials*, 129162.
- Moslehyani, A., Ismail, A. F., Othman, M. H. D., & Matsuura, T. (2015). Design and performance study of hybrid photocatalytic reactor-PVDF/MWCNT nanocomposite membrane system for treatment of petroleum refinery wastewater. *Desalination*, 363, 99-111.
- Muniz, G. L., Borges, A. C., & da Silva, T. C. F. (2020). Performance of natural coagulants obtained from agro-industrial wastes in dairy wastewater treatment using dissolved air flotation. *Journal of Water Process Engineering*, 37, 101453.
- Muthukumaran.S., Yang K., Seuren A., Kentish S., Ashokkumar M., Stevens G., Grieser F. (2004). The use of ultrasonic cleaning for ultrafiltration membranes in the dairy industry. *Separation and Purification Technology*, 39(1-2), 99–107. (2004)
- Muthukumaran, S., Kentish, S. E., Ashokkumar, M., & Stevens, G. W. (2005). Mechanisms for the ultrasonic enhancement of dairy whey ultrafiltration. *Journal of membrane science*, 258 (1-2), 106-114.
- Muthukumaran, S., Kentish, S. E., Stevens, G. W., Ashokkumar, M., & Mawson, R. (2007). The application of ultrasound to dairy ultrafiltration: the influence of operating conditions. *Journal of Food Engineering*, 81(2), 364-373.
- Nadimi, M., Saravani, A. Z., Aroon, M. A., & Pirbazari, A. E. (2019). Photodegradation of methylene blue by a ternary magnetic TiO₂/Fe₃O₄/graphene oxide nanocomposite under visible light. *Materials Chemistry and Physics*, 225, 464-474.
- Nady N., Franssen M.C.R., Zuilhof H., Mohy M.S., Boom R. & Schroën K. (2011). Modification methods for poly (arylsulfone) membranes : A mini-review focusing on surface modification, 275. 1–9.
- Nascimben Santos, E., Agoston, A., Kertész, S., Hodúr, C., László, Z., Pap, Z., ... & Veréb, G. (2020). Investigation of the applicability of TiO₂, BiVO₄, and WO₃ nanomaterials for advanced photocatalytic membranes used for oil-in-water emulsion separation. *Asia-Pacific Journal of Chemical Engineering*, 15(5), e2549.

- Natarajan S., Lakshmi D.S., Thiagarajan V., Mrudula P., Chandrasekaran N., Mukherjee A. (2018) Antifouling and anti-algal effects of chitosan nanocomposite (TiO₂/Ag) and pristine (TiO₂ and Ag) films on marine microalgae *Dunaliella salina*. *Journal of Environmental Chemical Engineering*, 6(6), 6870–6880.
- Navarro-Lisboa R., Herrera C., N. Zú R., Enrione J., Guzmán F., Matiacevich S., Astudillo-Castro C. (2016). Food and Bioproducts Processing Quinoa proteins (*Chenopodium quinoa* Willd) fractionated by ultrafiltration using ceramic membranes: The role of pH on physicochemical and conformational properties, 2, 20–30. (2016).
- Nezar S., Cherif Y.i, Barras A., Added A., Dogheche E., Saoula N., Laoufi N.A., Roussel P., Szurenits S., Boukherroub R. (2019). Efficient reduction of Cr(VI) under visible light irradiation using CuS nanostructures. *Arabian Journal of Chemistry* 12(2), 215-224.
- Ng L.Y., Abdul W.M., Choe P.L., Nidal H. (2013). Polymeric Membranes Incorporated with Metal/Metal Oxide Nanoparticles: A Comprehensive Review, *Desalination* 308, 15–33. (2013).
- Ng, K. S., Haribabu, M., Harvie, D. J., Dunstan, D. E., & Martin, G. J. (2017). Mechanisms of flux decline in skim milk ultrafiltration: A review. *Journal of Membrane Science*, 523, 144-162.
- Ngang H.P., Ooi B.S., Ahmad A.L & Lai S.O. (2012). Preparation of PVDF–TiO₂ mixed-matrix membrane and its evaluation on dye adsorption and UV-cleaning properties. *Chemical Engineering Journal*, 197(2012) 359–367.
- Nguyen, B. T. (2012). Faculty of Bioscience Engineering Influence of membrane fouling on the removal of pharmaceutical.
- Orimolade, B. O., & Arotiba, O. A. (2020). Bismuth vanadate in photoelectrocatalytic water treatment systems for the degradation of organics: A review on recent trends. *Journal of Electroanalytical Chemistry*, 878, 114724.
- Pal, P. (2020). Membrane technology to convert dairy waste into value-added products. *Membrane-Based Technologies for Environmental Pollution Control*, 649–701.
- Pan, Z., Yu, F., Li, L., Liu, M., Song, C., Yang, J., ... & Wang, T. (2020). Low-cost electrochemical filtration carbon membrane prepared from coal via self-bonding. *Chemical Engineering Journal*, 385, 123928.
- Pelegrine D.H.G, Gasparetto C.A. (2006). A comparative study between ovalbumin and b - lactoglobulin fouling in a tube hot surface, 73, 394–401.
- Persson A., Jönsson A., Zacchi G. (2003). Transmission of BSA during cross-flow microfiltration: influence of pH and salt concentration, 223, 11–21.
- Peyravi, M., Jahanshahi, M., & Khalili, S. (2017). Fouling of WO₃ nanoparticle-incorporated PSf membranes in ultrafiltration of landfill leachate and dairy a combined wastewater: An investigation using model. *Chinese journal of chemical engineering*, 25(6), 741-751.

- Phuruangrat, A., Wannapop, S., Sakhon, T., Kuntalue, B., Thongtem, T., & Thongtem, S. (2023). Characterization and photocatalytic properties of BiVO₄ synthesized by combustion method. *Journal of Molecular Structure*, 1274, 134420.
- Pi, X., Zhang, S., Wang, L., Li, H., Hei, Y., Zheng, Z., ... & Luo, L. (2021). BiVO₄ photo-catalyst with controllable wettability and its improved visible light catalytic activity for degradation of 17 α -Ethinylestradiol. *Journal of the Taiwan Institute of Chemical Engineers*, 127, 140-150.
- Qazi, J. I., Nadeem, M., Baig, S. S., Baig, S., & Syed, Q. (2011). Anaerobic fixed-film biotreatment of dairy wastewater. *Middle-East Journal of Scientific Research*, 8(3), 590–593.
- Raghunath, B. V., Punnaaiarasi, A., Rajarajan, G., Irshad, A., Elango, A., & Mahesh Kumar, G. (2016). Impact of dairy effluent on environment—a review. *Integrated Waste Management in India: Status and Future Prospects for Environmental Sustainability*, 239-249.
- Ramasundaram S., Son A., Seid M.G., Shim S., Lee S.H., Chung Y.C, Hong S.W. (2015). Photocatalytic applications of paper-like poly (vinylidene fluoride)–titanium dioxide hybrids fabricated using a combination of electrospinning and electrospraying. *Journal of Hazardous Materials*, 285(2015) 267–276.
- Ramasundaram S., Seid M.G., Choe J.W, Kim E.J, Chung Y.C., Cho K., Hong S.W. (2016). Highly reusable TiO₂ nanoparticle photocatalyst by direct immobilisation on steel mesh via PVDF coating, electrospraying, and thermal fixation. *Chemical Engineering Journal*, 306. 344–351.
- Ratova, M., Redfern, J., Verran, J., & Kelly, P. J. (2018). Highly efficient photocatalytic bismuth oxide coatings and their antimicrobial properties under visible light irradiation. *Applied Catalysis B: Environmental*, 239, 223-232.
- Ravi, J., Othman, M. H. D., Tai, Z. S., El-badawy, T., Matsuura, T., & Kurniawan, T. A. (2021). Comparative DCMD performance of hydrophobic-hydrophilic dual-layer hollow fiber PVDF membranes incorporated with different concentrations of carbon-based nanoparticles. *Separation and Purification Technology*, 274, 118948.
- Ren, G., Li, R., Zhao, M., Hou, Q., Rao, T., Zhou, M., & Ma, X. (2022). Membrane electrodes for electrochemical advanced oxidation processes: Preparation, self-cleaning mechanisms and prospects. *Chemical Engineering Journal*, 138907.
- Riaz, S., & Park, S. J. (2020). An overview of TiO₂-based photocatalytic membrane reactors for water and wastewater treatments. *Journal of industrial and engineering chemistry*, 84, 23-41.
- Ruigómez, I., González, E., Rodríguez-Gómez, L., & Vera, L. (2022). Fouling control strategies for direct membrane ultrafiltration: Physical cleanings assisted by membrane rotational movement. *Chemical Engineering Journal*, 436, 135161.
- Sadeghzadeh-Attar, A. (2020). Boosting the photocatalytic ability of hybrid BiVO₄-TiO₂ heterostructure nanocomposites for H₂ production by reduced graphene oxide (rGO). *Journal of the Taiwan Institute of Chemical Engineers*, 111, 325-336.

- Sarkar B., Chakrabarti P.P., Vijaykumar A., Kale V. (2006). Wastewater treatment in dairy industries - possibility of reuse. *Desalination*, 195(1-3), 141–152.
- Schulze, A., Went, M., & Prager, A. (2016). Membrane functionalization with hyperbranched polymers. *Materials*, 9(8), 706.
- Selvaraj, M., Hai, A., Banat, F., & Haija, M. A. (2020). Application and prospects of carbon nanostructured materials in water treatment: A review. *Journal of Water Process Engineering*, 33, 100996.
- Shaban M., Ashraf A.M., AbdAllah H. & Abd El-Salam H.M. (2018). Titanium dioxide nanoribbons/multi-walled carbon nanotube nanocomposite blended polyethersulfone membrane for brackish water desalination. *Desalination*, 444 (2018) 129–141.
- Sharma D. (2014). Treatment of dairy wastewater by electro coagulation using aluminium electrodes and settling, filtration studies. *International Journal of Chem. Tech Research*, 6(1), 591–599 (2014).
- Sharma, H. K., Sharma, S. K., Vemula, K., Koirala, A. R., Yadav, H. M., & Singh, B. P. (2021). CNT facilitated interfacial charge transfer of TiO₂ nanocomposite for controlling the electron-hole recombination. *Solid State Sciences*, 112, 106492.
- She, Q., Tang, C. Y., Wang, Y. N., & Zhang, Z. (2009). The role of hydrodynamic conditions and solution chemistry on protein fouling during ultrafiltration. *Desalination*, 249(3), 1079-1087.
- Shete, B. S., & Shinkar, N. P. (2013). Comparative study of various treatments for dairy industry wastewater. *IOSR J Eng*, 3, 42-47.
- Shi, X., Tal, G., Hankins, N. P., & Gitis, V. (2014). Fouling and cleaning of ultrafiltration membranes: A review. *Journal of Water Process Engineering*, 1, 121-138.
- Silva, F. L., Zin, G., Rezzadori, K., Longo, L. C., Tiggemann, L., Soares, L. S., ... Luccio, M. Di. (2019). Changes in the physicochemical characteristics of a protein solution in the presence of the magnetic field and the consequences on the ultrafiltration performance. *Journal of Food Engineering*, 242(February 2018), 84–93.
- Sim, S. T. V., Taheri, A. H., Chong, T. H., Krantz, W. B., & Fane, A. G. (2014). Colloidal metastability and membrane fouling—Effects of crossflow velocity, flux, salinity and colloid concentration. *Journal of Membrane Science*, 469, 174-187.
- Sisay, E.J.; Veréb, G.; Pap, Zs; Gyulavári, T.; Ágoston, Á.; Kopniczky, J.; Hodúr, C.; Arthanareeswaran, G., Krishnan, G.A.S.; László, Zs. (2022) Visible-light-driven photocatalytic PVDF-TiO₂/CNT/BiVO₄ hybrid nanocomposite ultrafiltration membrane for dairy wastewater treatment. *CHEMOSPHERE* 307:1. 135589,
- Sisay, E.J., Kertész, Sz., Fazekas, Á., Jákói, Z., Kedves, E.Z. Gyulavári, T., Ágoston, Á., Veréb, G., and László, Zs. (2023). Application of BiVO₄/TiO₂/CNT Composite Photocatalysts for

Membrane Fouling Control and Photocatalytic Membrane Regeneration during Dairy Wastewater Treatment" Catalysts 13, no. 2: 315.

- Slavov, K. A. (2017). Pregled općih svojstava i mogućih postupaka obrade otpadnih voda mljekarske industrije. Food Technology and Biotechnology, 55(1), 14-28.
- Song H., Shao J., He Y., Liu B. & Zhong X. (2012). Natural organic matter removal and flux decline with PEG–TiO₂-doped PVDF membranes by the integration of ultrafiltration with photocatalysis. Journal of Membrane Science, 405-406(2012)48–56.
- Souza, N. M. D., & Mawson, A. J. (2005). Membrane cleaning in the dairy industry: A review. CRC Cri. Rev. Food Sci, 45(2), 125-134.
- Srinivasan, N., Anbuezhayan, M., Harish, S., & Ponnusamy, S. (2022). Efficient catalytic activity of BiVO₄ nanostructures by crystal facet regulation for environmental remediation. Chemosphere, 289, 133097.
- Srivastava, H. P., Arthanareeswaran, G., Anantharaman, N., & Starov, V. M. (2011). Performance of modified poly (vinylidene fluoride) membrane for textile wastewater ultrafiltration. Desalination, 282, 87-94.
- Steinhauer, T., Marx, M., Bogendörfer, K., & Kulozik, U. (2015a). Membrane fouling during ultra- and microfiltration of whey and whey proteins at different environmental conditions: The role of aggregated whey proteins as fouling initiators. Journal of Membrane Science, 489, 20-27.
- Steinhauer T., Hanély S., Bogendörfer K., Kulozik U. (2015b). Temperature dependent membrane fouling during filtration of whey and whey proteins. Journal of Membrane Science, 492, 364–370.
- Sun, J., Wang, T., Gu, Z., Lu, C., Chen, Z., Wu, Y., & Hu, C. (2022). Fundamentals of electrochemical membrane technology. In Electrochemical Membrane Technology for Water and Wastewater Treatment (pp. 43-80). Elsevier.
- Tang, C. Y., Chong, T. H., & Fane, A. G. (2011). Colloidal interactions and fouling of NF and RO membranes: a review. Advances in colloid and interface science, 164(1-2), 126-143.
- Tang C.Y., Kwon Y., Leckie J.O. (2007). Fouling of reverse osmosis and nanofiltration membranes by humic acid – Effects of solution composition and hydrodynamic conditions, 290, 86–94. (2007).
- Tang, C. M., & Li, X. L. (2013). Separative capability of γ -Al₂O₃ porous ceramic membrane modified by ZIF-8. Korean Journal of Chemical Engineering, 30(5), 1119-1124.
- Thebo, K. H., Qian, X., Wei, Q., Zhang, Q., Cheng, H. M., & Ren, W. (2018). Reduced graphene oxide/metal oxide nanoparticles composite membranes for highly efficient molecular separation. Journal of materials science & technology, 34(9), 1481-1486.

- Thereza M., Rosa M.G., Guimarães D.H.P., Arce P.F. (2019). International Journal of Heat and Mass Transfer Experimental measurements and simulation of the fouling phenomena of natural proteins. *International Journal of Heat and Mass Transfer*, 129, 1075–1085. (2019).
- Tokunaga, S., Kato, H., & Kudo, A. (2001). Selective preparation of monoclinic and tetragonal BiVO₄ with scheelite structure and their photocatalytic properties. *Chemistry of Materials*, 13(12), 4624-4628.
- Tong T., Zhao S., Boo C., Hashmi S.M., Elimelech M. (2017). Relating Silica Scaling in Reverse Osmosis to Membrane Surface Properties. *Environmental Science & Technology*, 51(8), 4396–4406. (2017).
- Trapalis A., Todorova N., Giannakopoulou T., Boukos N., Speliotis T., Dimotikali D., Yu J. (2016). TiO₂/Graphene Composite Photocatalysts for NO_x Removal: A Comparison of Surfactant-stabilized Graphene and Reduced Graphene Oxide. *Applied Catalysis B: Environmental*, 180, 637-647. (2016).
- Vanangamudi A., Saeki D., Dumée L. F., Duke M., Vasiljevic T., Matsuyama H., & Yang X. (2018). Surface-Engineered Biocatalytic Composite Membranes for Reduced Protein Fouling and Self-Cleaning. *ACS Applied Materials & Interfaces*, 10(32) (2018) 27477–27487.
- Vatanpour, V., Yekavalangi, M. E., & Safarpour, M. (2016). Preparation and characterization of nanocomposite PVDF ultrafiltration membrane embedded with nanoporous SAPO-34 to improve permeability and antifouling performance. *Separation and Purification Technology*, 163, 300-309.
- Vatsha, B., Ngila, J. C., & Moutloali, R. M. (2014). Preparation of antifouling polyvinylpyrrolidone (PVP 40K) modified polyethersulfone (PES) ultrafiltration (UF) membrane for water purification. *Physics and Chemistry of the Earth, Parts A/B/C*, 67, 125-131.
- Velpula S., Umapathy K.S., Thyarla A., Srikanth K., Saraff S. (2017). Dairy Wastewater Treatment by Membrane Systems-A Review, *Int. J. Pure App. Biosci.* 5(6), 389-395. (2017).
- Vourch, M., Balannec, B., Chaufer, B., & Dorange, G. (2008). Treatment of dairy industry wastewater by reverse osmosis for water reuse. *Desalination*, 219(1-3), 190-202.
- Wang, Y., & Serventi, L. (2019). Sustainability of dairy and soy processing: A review on wastewater recycling. *Journal of Cleaner Production*, 237, 117821.
- Wang Q., Wang X., Wang Z., Huang J. & Wang Y. (2013). PVDF membranes with simultaneously enhanced permeability and selectivity by breaking the trade-off effect via atomic layer deposition of TiO₂. *Journal of Membrane Science*, 442. (2013) 57–64.
- Wang, Z., Ma, J., Tang, C. Y., Kimura, K., Wang, Q., & Han, X. (2014). Membrane cleaning in membrane bioreactors: A review. *Journal of Membrane Science*, 468, 276–307. <https://doi.org/10.1016/j.memsci.2014.05.060>

- Wang, S., Liang, S., Liang, P., Zhang, X., Sun, J., Wu, S., & Huang, X. (2015). In-situ combined dual-layer CNT/PVDF membrane for electrically-enhanced fouling resistance. *Journal of Membrane Science*, 491, 37-44.
- Wang, J. J., Lin, T. A. N. G., Zeng, G. M., Zhou, Y. Y., Deng, Y. C., Fan, C. Z., ... & Liu, Y. N. (2017). Effect of bismuth tungstate with different hierarchical architectures on photocatalytic degradation of norfloxacin under visible light. *Transactions of Nonferrous Metals Society of China*, 27(8), 1794-1803.
- Wang S., Mu C., Xiao K., X. Zhu, X., Huang. (2020). Surface charge regulation of reverse osmosis membrane for anti-silica and organic fouling. *Science of The Total Environment*, 715, 137013. (2020).
- Xiao K., Wang X., Huang X., Waite T.D., Wen X. (2011). Combined effect of membrane and foulant hydrophobicity and surface charge on adsorptive fouling during microfiltration. *Journal of Membrane Science*, 373(1-2), 140-151.
- Xie, M., Shon, H. K., Gray, S. R., & Elimelech, M. (2016). Membrane-based processes for wastewater nutrient recovery: Technology, challenges, and future direction. *Water research*, 89, 210-221.
- Yalçın, E., & Dükkancı, M. (2022). Ternary CuS@ Ag/BiVO₄ composite for enhanced photocatalytic and sono-photocatalytic performance under visible light. *Journal of Solid State Chemistry*, 313, 123319.
- Yan, L., Li, Y. S., Xiang, C. B., & Xianda, S. (2006). Effect of nano-sized Al₂O₃-particle addition on PVDF ultrafiltration membrane performance. *Journal of Membrane Science*, 276(1-2), 162-167.
- Yan, M., Wu, Y., & Liu, X. (2021). Photocatalytic nanocomposite membranes for high-efficiency degradation of tetracycline under visible light: An imitated core-shell Au-TiO₂-based design. *Journal of Alloys and Compounds*, 855, 157548.
- Yang, W., Cicek, N., & Ilg, J. (2006). State-of-the-art of membrane bioreactors: Worldwide research and commercial applications in North America. *Journal of Membrane Science*, 270(1-2), 201-211.
- Yang, H. W., Liu, W. J., Wang, X. M., & Xie, Y. F. (2015). Filterability and structure of the fouling layers of biopolymer coexisting with ferric iron in ultrafiltration membrane. *Journal of Membrane Science*, 495, 81-90.
- Yang S.F., Niu C.G., Huang D.W., Zhang H., Liang C., Zeng G.M. (2017). SrTiO₃ nanocubes decorated with Ag/AgCl nanoparticles as photocatalysts with enhanced visible-light photocatalytic activity towards the degradation of dyes, phenol and bisphenol A. *Environmental Science: Nano*, 4(3), 585-595.

- Yang, Y., Li, Y., Cao, L., Wang, Y., Li, L., & Li, W. (2021). Electrospun PVDF-SiO₂ nanofibrous membranes with enhanced surface roughness for oil-water coalescence separation. *Separation and Purification Technology*, 269, 118726.
- Yogarathinam, L. T., Gangasalam, A., Ismail, A. F., Arumugam, S., & Narayanan, A. (2018). Concentration of whey protein from cheese whey effluent using ultrafiltration by combination of hydrophilic metal oxides and hydrophobic polymer. *Journal of Chemical Technology & Biotechnology*, 93(9), 2576-2591.
- Yu, L. Y., Xu, Z. L., Shen, H. M., & Yang, H. (2009). Preparation and characterization of PVDF-SiO₂ composite hollow fiber UF membrane by sol-gel method. *Journal of Membrane Science*, 337(1-2), 257-265.
- Yu Y., Lee S., Hong S. (2010). Effect of solution chemistry on organic fouling of reverse osmosis membranes in seawater desalination. *Journal of Membrane Science*, 351(1-2), 205-213.
- Yu, W., Graham, N., & Liu, T. (2017). Effect of intermittent ultrasound on controlling membrane fouling with coagulation pre-treatment: Significance of the nature of adsorbed organic matter. *Journal of Membrane Science*, 535, 168-177.
- Yu, F. P., Pan, Z. L., Li, L., Song, C. W., & Wang, T. H. (2022). Preparation and performance of electrocatalytic carbon membranes for treating micro-polluted water. *New Carbon Materials*, 37(3), 615-624.
- Yue Z., Liu A., Zhang C., Huang J., Zhu M., Du Y., Yang P. (2017). Noble-metal-free hetero-structural CdS/Nb₂O₅/N doped-graphene ternary photocatalytic system as visible-light-driven photocatalyst for hydrogen evolution. *Applied Catalysis B, Environmental*, 201, 202-210.
- Žerjav G., Džinović P., Pintar A. (2018). TiO₂-Bi₂O₃/(BiO)₂CO₃-reduced graphene oxide composite as an effective visible light photocatalyst for degradation of aqueous bisphenol A solution. *Catalysis Today*, 315, 237-246.
- Zhao D., & Yu S. (2014). A review of recent advance in fouling mitigation of NF/RO membranes in water treatment: pretreatment, membrane modification, and chemical cleaning. *Desalination and Water Treatment*, 55(4) (2014) 870-891.
- Zhao, Y., Li, R., Mu, L., & Li, C. (2017). Significance of crystal morphology controlling in semiconductor-based photocatalysis: a case study on BiVO₄ photocatalyst. *Crystal Growth & Design*, 17(6), 2923-2928.
- Zhao, D., Qiu, L., Song, J., Liu, J., Wang, Z., Zhu, Y., & Liu, G. (2019). Efficiencies and mechanisms of chemical cleaning agents for nanofiltration membranes used in produced wastewater desalination. *Science of The Total Environment*, 652, 256-266.
- Zhou, Z., Meng, F., Lu, H., Li, Y., Jia, X., & He, X. (2014). Simultaneous alkali supplementation and fouling mitigation in membrane bioreactors by on-line NaOH backwashing. *Journal of membrane science*, 457, 120-127

- Zoubeik M., Mohamed I., Amgad S., Amr H. (2017). New Developments in Membrane Technologies Used in the Treatment of Produced Water: A Review, *Arabian Journal for Science and Engineering* 43(5), 2093–2118.
- Zouzelka, R., Kusumawati, Y., Remzova, M., Rathousky, J., & Pauporté, T. (2016). Photocatalytic activity of porous multiwalled carbon nanotube-TiO₂ composite layers for pollutant degradation. *Journal of Hazardous Materials*, 317, 52-59.
- Zularisam, A. W., Ismail, A. F., & Salim, R. (2006). Behaviours of natural organic matter in membrane filtration for surface water treatment—a review. *Desalination*, 194(1-3), 211-231.

Appendices

Appendix 1. Regression results of total resistance (RT) for CNT based coated membranes

RT	Coef.	St.Err.	t-value	p-value	[95% Conf	Interval]	Sig
: base	0	
Replication~1							
Relication_2	1.067e+11	1.668e+11	0.64	.537	-2.651e+11	4.784e+11	
Replication_3	-6.000e+10	1.668e+11	-0.36	.727	-4.317e+11	3.117e+11	
: base PVDF	0	
C-PT100	1.133e+13	2.359e+11	48.03	0	1.081e+13	1.186e+13	***
C-PTC2	2.664e+13	2.359e+11	112.90	0	2.611e+13	2.716e+13	***
C-PTC5	7.483e+12	2.359e+11	31.72	0	6.958e+12	8.009e+12	***
C-PTC10	1.293e+12	2.359e+11	5.48	0	7.676e+11	1.819e+12	***
C-PTC15	4.113e+13	2.359e+11	174.31	0	4.060e+13	4.165e+13	***
Constant	1.623e+13	1.926e+11	84.27	0	1.581e+13	1.666e+13	***
Mean dependent var	308955555555555.		SD dependent var		15148588838266.		
	551				410		
R-squared	1.000		Number of obs		18		
F-test	6672.741		Prob > F		0.000		
Akaike crit. (AIC)	1006.527		Bayesian crit. (BIC)		1013.649		

*** p<.01, ** p<.05, * p<.1

Appendix 2. Regression results of irreversible resistance (Rirr) for CNT based coated membranes

Rirr	Coef.	St.Err.	t-value	p-value	[95% Conf	Interval]	Sig
: base	0
Replicatio~1							
Relication_2	-3.127e+11	1.956e+11	-1.60	.141	-7.485e+11	1.232e+11	
Replication_3	-1.765e+11	1.956e+11	-0.90	.388	-6.123e+11	2.593e+11	
: base PVDF	0
C-PT100	-3.430e+11	2.766e+11	-1.24	.243	-9.594e+11	2.734e+11	
C-PTC2	2.670e+12	2.766e+11	9.65	0	2.054e+12	3.287e+12	***
C-PTC5	2.773e+11	2.766e+11	1.00	.34	-3.390e+11	8.937e+11	
C-PTC10	-9.787e+11	2.766e+11	-3.54	.005	-1.595e+12	-3.623e+11	***
C-PTC15	2.165e+12	2.766e+11	7.83	0	1.548e+12	2.781e+12	***
Constant	4.646e+12	2.259e+11	20.57	0	4.143e+12	5.149e+12	***
Mean dependent var	511477777777.7		SD dependent var		1396730996693.4		
	77				16		
R-squared	0.965		Number of obs		18		
F-test	39.848		Prob > F		0.000		
Akaike crit. (AIC)	1012.253		Bayesian crit. (BIC)		1019.376		

*** p<.01, ** p<.05, * p<.1

Appendix 3. Regression results of total resistance (RT) for BiVO₄ based coated membranes

RT	Coef.	St.Err.	t-value	p-value	[95% Conf	Interval]	Sig
: base	0	
Replication~1							
Relication_2	5.214e+11	3.394e+11	1.54	.15	-2.180e+11	1.261e+12	
Replication_3	3.457e+11	3.394e+11	1.02	.328	-3.937e+11	1.085e+12	
: base PVDF	0	
C-PT100	1.167e+13	5.184e+11	22.51	0	1.054e+13	1.280e+13	***
C-PTB2	5.100e+13	5.184e+11	98.38	0	4.987e+13	5.213e+13	***
C-PTB5	4.528e+13	5.184e+11	87.36	0	4.415e+13	4.641e+13	***
C-PTB10	3.304e+13	5.184e+11	63.74	0	3.191e+13	3.417e+13	***
C-PTB15	3.378e+13	5.184e+11	65.16	0	3.265e+13	3.491e+13	***
C-PB100	7.077e+12	5.184e+11	13.65	0	5.947e+12	8.206e+12	***
Constant	1.596e+13	4.156e+11	38.40	0	1.506e+13	1.687e+13	***
Mean dependent var	42227619047619.047		SD dependent var		18767949782744.488		
R-squared	0.999		Number of obs		21		
F-test	2183.191		Prob > F		0.000		
Akaike crit. (AIC)	1207.265		Bayesian crit. (BIC)		1216.666		

*** p<.01, ** p<.05, * p<.1

Appendix 4. Regression results of irreversible resistance (Rirr) for BiVO₄ based coated membranes

Rirr	Coef.	St.Err.	t-value	p-value	[95% Conf	Interval]	Sig
: base	0
Replicatio~1							
Relication_2	4.214e+09	2.207e+11	0.02	.985	-4.766e+11	4.851e+11	
Replication_3	-1.333e+11	2.207e+11	-0.60	.557	-6.141e+11	3.476e+11	
: base PVDF	0
C-PT100	-3.430e+11	3.371e+11	-1.02	.329	-1.078e+12	3.915e+11	
C-PTB2	-4.483e+12	3.371e+11	-13.30	0	-5.218e+12	-3.748e+12	***
C-PTB5	-3.360e+12	3.371e+11	-9.97	0	-4.095e+12	-2.626e+12	***
C-PTB10	-4.483e+12	3.371e+11	-13.30	0	-5.218e+12	-3.748e+12	***
C-PTB15	-4.483e+12	3.371e+11	-13.30	0	-5.218e+12	-3.748e+12	***
C-PB100	-1.022e+12	3.371e+11	-3.03	.01	-1.757e+12	-2.878e+11	**
Constant	4.526e+12	2.703e+11	16.74	0	3.937e+12	5.115e+12	***
Mean dependent var	1886619047619.0		SD dependent var	1985015333094.1			
	48			92			
R-squared	0.974		Number of obs	21			
F-test	56.286		Prob > F	0.000			
Akaike crit. (AIC)	1189.193		Bayesian crit. (BIC)	1198.594			

*** p<.01, ** p<.05, * p<.1

Appendix 5. Regression results of flux recovery ratio (FRR) of CNT based coated membranes

FRR	Coef.	St.Err.	t-value	p-value	[95% Conf	Interval]	Sig
: base 0
Replication~1							
Relication_2	-.035	4.138	-0.01	.993	-9.256	9.185	
Replication_3	-4.595	4.138	-1.11	.293	-13.816	4.625	
: base PVDF 0
C-PT100	37.741	5.852	6.45	0	24.701	50.781	***
C-PTC2	35.544	5.852	6.07	0	22.504	48.584	***
C-PTC5	19.522	5.852	3.34	.008	6.482	32.562	***
C-PTC10	29.794	5.852	5.09	0	16.755	42.834	***
C-PTC15	37.538	5.852	6.41	0	24.498	50.578	***
Constant	61.163	4.778	12.80	0	50.516	71.81	***
Mean dependent var	86.310		SD dependent var	15.092			
R-squared	0.867		Number of obs	18			
F-test	9.339		Prob > F	0.001			
Akaike crit. (AIC)	127.406		Bayesian crit. (BIC)	134.529			

*** p<.01, ** p<.05, * p<.1

Appendix 6. Regression results of flux recovery ratio (FRR) of BiVO₄ based coated membranes

FRR	Coef.	St.Err.	t-value	p-value	[95% Conf	Interval]	Sig
: base 0		
Replication~1							
Relication_2	-1.628	.971	-1.68	.119	-3.742	.487	
Replication_3	-.387	.971	-0.40	.697	-2.502	1.727	
: base PVDF 0		
C-PT100	12.649	1.482	8.53	0	9.419	15.879	***
C-PTB2	35.639	1.482	24.04	0	32.409	38.87	***
C-PTB5	45.959	1.482	31.00	0	42.729	49.189	***
C-PTB10	44.072	1.482	29.73	0	40.842	47.302	***
C-PTB15	35.767	1.482	24.13	0	32.537	38.997	***
C-PB100	35.751	1.482	24.12	0	32.521	38.981	***
Constant	49.638	1.189	41.76	0	47.048	52.228	***
Mean dependent var	78.943		SD dependent var		16.287		
R-squared	0.993		Number of obs		21		
F-test	199.662		Prob > F		0.000		
Akaike crit. (AIC)	90.895		Bayesian crit. (BIC)		100.295		

*** p<.01, ** p<.05, * p<.1

Appendix 7. Regression results of total resistance (RT) for CNT based blended membranes

RT	Coef.	St.Err.	t-value	p-value	[95% Conf	Interval]	Sig
: base	0	
Replication~1							
Relication_2	4.633e+11	6.052e+11	0.77	.462	-8.852e+11	1.812e+12	
Replication_3	-3.000e+10	6.052e+11	-0.05	.961	-1.378e+12	1.318e+12	
: base PVDF	0	
B-PT100	-1.633e+13	8.559e+11	-19.08	0	-1.823e+13	-1.442e+13	***
B-PTC2	-2.320e+13	8.559e+11	-27.10	0	-2.510e+13	-2.129e+13	***
B-PTC5	-1.468e+13	8.559e+11	-17.16	0	-1.659e+13	-1.278e+13	***
B-PTC10	-1.143e+13	8.559e+11	-13.36	0	-1.334e+13	-9.526e+12	***
B-PTC15	-2.172e+13	8.559e+11	-25.38	0	-2.363e+13	-1.982e+13	***
Constant	4.673e+13	6.988e+11	66.87	0	4.518e+13	4.829e+13	***
Mean dependent var	32316111111111.		SD dependent var		7912537437055.8		
	109				56		
R-squared	0.990		Number of obs		18		
F-test	136.944		Prob > F		0.000		
Akaike crit. (AIC)	1052.915		Bayesian crit. (BIC)		1060.038		

*** p<.01, ** p<.05, * p<.1

Appendix 8. Regression results of irreversible resistance (Rirr) for CNT based blended membranes

Rirr	Coef.	St.Err.	t-value	p-value	[95% Conf	Interval]	Sig
: base	0	
Replicatio~1							
Relication_2	9.580e+11	6.529e+11	1.47	.173	-4.967e+11	2.413e+12	
Replication_3	3.090e+11	6.529e+11	0.47	.646	-1.146e+12	1.764e+12	
: base PVDF	0	
B-PT100	-9.403e+12	9.233e+11	-10.18	0	-1.146e+13	-7.346e+12	***
B-PTC2	-2.003e+13	9.233e+11	-21.69	0	-2.209e+13	-1.797e+13	***
B-PTC5	-1.194e+13	9.233e+11	-12.93	0	-1.400e+13	-9.883e+12	***
B-PTC10	-1.137e+13	9.233e+11	-12.31	0	-1.343e+13	-9.313e+12	***
B-PTC15	-1.361e+13	9.233e+11	-14.74	0	-1.567e+13	-1.155e+13	***
Constant	2.302e+13	7.539e+11	30.54	0	2.134e+13	2.470e+13	***
Mean dependent var	12387833333333.		SD dependent var		6203974601248.8		
	330				78		
R-squared	0.980		Number of obs		18		
F-test	71.674		Prob > F		0.000		
Akaike crit. (AIC)	1055.643		Bayesian crit. (BIC)		1062.766		

*** p<.01, ** p<.05, * p<.1

Appendix 9. Regression results of total resistance (RT) of BiVO₄ based blended membranes

RT	Coef.	St.Err.	t-value	p-value	[95% Conf	Interval]	Sig
: base	0	
Replicatio~1							
Relication_2	2.463e+11	4.573e+11	0.54	.599	-7.346e+11	1.227e+12	
Replication_3	6.338e+11	4.573e+11	1.39	.187	-3.471e+11	1.615e+12	
: base PVDF	0	
B-PTB25	-1.869e+13	7.468e+11	-25.03	0	-2.029e+13	-1.709e+13	***
B-PTB50	-2.777e+13	7.468e+11	-37.18	0	-2.937e+13	-2.617e+13	***
B-PTB75	-1.876e+13	7.468e+11	-25.13	0	-2.036e+13	-1.716e+13	***
B-PB100	-2.690e+13	7.468e+11	-36.03	0	-2.850e+13	-2.530e+13	***
B-PTCB25	-2.542e+13	7.468e+11	-34.04	0	-2.702e+13	-2.382e+13	***
B-PTCB50	-3.122e+13	7.468e+11	-41.81	0	-3.282e+13	-2.962e+13	***
B-PTCB75	-1.267e+13	7.468e+11	-16.97	0	-1.427e+13	-1.107e+13	***
Constant	4.289e+13	5.904e+11	72.65	0	4.162e+13	4.416e+13	***
Mean dependent var	23003333333333.		SD dependent var		9720917234708.7		
	328				68		
R-squared	0.995		Number of obs		24		
F-test	287.143		Prob > F		0.000		
Akaike crit. (AIC)	1397.177		Bayesian crit. (BIC)		1408.957		

*** p<.01, ** p<.05, * p<.1

Appendix 10. Regression results of irreversible resistance (Rirr) of BiVO₄ based blended membranes

Rirr	Coef.	St.Err.	t-value	p-value	[95% Conf	Interval]	Sig
: base	0	
Replicatio~1							
Relication_2	1.761e+11	1.111e+11	1.58	.135	-6.222e+10	4.145e+11	
Replication_3	1.137e+11	1.111e+11	1.02	.323	-1.246e+11	3.521e+11	
: base PVDF	0	
B-PTB25	-1.452e+13	1.815e+11	-80.00	0	-1.491e+13	-1.413e+13	***
B-PTB50	-1.613e+13	1.815e+11	-88.87	0	-1.652e+13	-1.574e+13	***
B-PTB75	-1.590e+13	1.815e+11	-87.60	0	-1.629e+13	-1.551e+13	***
B-PB100	-1.651e+13	1.815e+11	-90.98	0	-1.690e+13	-1.612e+13	***
B-PTCB25	-1.744e+13	1.815e+11	-96.10	0	-1.783e+13	-1.705e+13	***
B-PTCB50	-1.934e+13	1.815e+11	-106.59	0	-1.973e+13	-1.895e+13	***
B-PTCB75	-1.430e+13	1.815e+11	-78.81	0	-1.469e+13	-1.391e+13	***
Constant	2.260e+13	1.435e+11	157.53	0	2.229e+13	2.291e+13	***
Mean dependent var	842950000000.0		SD dependent var	5720294306809.8			
	00			98			
R-squared	0.999		Number of obs	24			
F-test	1691.304		Prob > F	0.000			
Akaike crit. (AIC)	1329.273		Bayesian crit. (BIC)	1341.054			

*** p<.01, ** p<.05, * p<.1

Appendix 11. Regression results of flux recovery ratio (FRR) of CNT based blended membranes

FRR	Coef.	St.Err.	t-value	p-value	[95% Conf	Interval]	Sig
: base 0
Replication~1							
Relication_2	-.559	.689	-0.81	.436	-2.094	.976	
Replication_3	-1.068	.689	-1.55	.152	-2.602	.467	
: base PVDF 0
B-PT100	14.306	.974	14.69	0	12.136	16.477	***
B-PTC2	44.745	.974	45.93	0	42.574	46.916	***
B-PTC5	15.355	.974	15.76	0	13.184	17.526	***
B-PTC10	10.67	.974	10.95	0	8.499	12.84	***
B-PTC15	7.316	.974	7.51	0	5.145	9.486	***
Constant	19.862	.795	24.97	0	18.09	21.635	***
Mean dependent var	34.719		SD dependent var		14.510		
R-squared	0.996		Number of obs		18		
F-test	357.765		Prob > F		0.000		
Akaike crit. (AIC)	62.858		Bayesian crit. (BIC)		69.981		

*** p<.01, ** p<.05, * p<.1

Appendix 12. Regression results of flux recovery ratio (FRR) of BiVO₄ based blended membranes

FRR	Coef.	St.Err.	t-value	p-value	[95% Conf	Interval]	Sig
: base	0	
Replication_1							
Relication_2	-.087	.18	-0.48	.635	-.474	.299	
Replication_3	-.225	.18	-1.25	.233	-.612	.162	
: base PVDF	0	
B-PTB25	17.174	.295	58.31	0	16.542	17.805	***
B-PTB50	40.2	.295	136.50	0	39.569	40.832	***
B-PTB75	32.597	.295	110.68	0	31.965	33.229	***
B-PB100	12.711	.295	43.16	0	12.08	13.343	***
B-PTCB25	20.347	.295	69.08	0	19.715	20.978	***
B-PTCB50	33.937	.295	115.23	0	33.305	34.569	***
B-PTCB75	19.983	.295	67.85	0	19.351	20.615	***
Constant	17.481	.233	75.08	0	16.981	17.98	***
Mean dependent var	39.495		SD dependent var		12.443		
R-squared	0.999		Number of obs		24		
F-test	3039.379		Prob > F		0.000		
Akaike crit. (AIC)	26.228		Bayesian crit. (BIC)		38.009		

*** p<.01, ** p<.05, * p<.1

Appendix 13. Regression results of flux recovery ratio (FRR) of BiVO₄ based blended membranes. PVDF-BiVO₄ membrane as control.

FRR	Coef.	St.Err.	t-value	p-value	[95% Conf	Interval]	Sig
: base 0		
Replication~1							
Relication_2	-.064	.207	-0.31	.764	-.515	.388	
Replication_3	-.222	.207	-1.07	.305	-.673	.229	
: base B-PB100 0		
B-PTB25	4.462	.316	14.10	0	3.773	5.152	***
B-PTB50	27.489	.316	86.86	0	26.799	28.178	***
B-PTB75	19.886	.316	62.84	0	19.196	20.575	***
B-PTCB25	7.635	.316	24.13	0	6.946	8.325	***
B-PTCB50	21.226	.316	67.07	0	20.536	21.915	***
B-PTCB75	7.272	.316	22.98	0	6.582	7.961	***
Constant	30.183	.254	118.95	0	29.631	30.736	***
Mean dependent var	42.655		SD dependent var		9.704		
R-squared	0.999		Number of obs		21		
F-test	1565.723		Prob > F		0.000		
Akaike crit. (AIC)	26.036		Bayesian crit. (BIC)		35.437		

*** p<.01, ** p<.05, * p<.1